Renewable H_2 via Pressure Swing Adsorption from waste gasification

A techno-economic analysis

Nicholas Parissi

TU Delft

Renewable H_2 via Pressure Swing Adsorption from waste gasification

A techno-economic analysis

Thesis report

by

Nicholas Parissi

to obtain the degree of Master of Science
at the Delft University of Technology
to be defended publicly on October 25, 2023 at 13:00

Thesis committee:

Chair:	Prof.dr.ir Wiebren de Jong
Supervisors:	Dr. Luis Cutz
	Dr. Elyas M. Moghaddam
External examiner:	Prof.dr.ir Wiebren de Jong
	Dr.ir. Mahinder Ramdin
Place:	Faculty 3mE department Process and Energy, Delft
Project Duration:	January, 2023 - October, 2023
Student number:	5625424

Faculty of Electrical Engineering, Mathematics and Computer Science at Delft University of Technology

Preface

I would like to express my gratitude to the following individuals who have played an important role in the successful completion of this master's thesis:

I am grateful to Dr. Luis Cutz and Dr. Elyas M. Moghaddam for their guidance, insights, and patience throughout the research and writing process. Your expertise, dedication, and mentorship have been valuable in shaping this thesis.

I extend my sincere thanks to Avikar Saberwal, whose constant support and encouragement kept me on track especially in the end of my experience.

I would like to express my appreciation to Prof.dr.ir Wiebren and Dr.ir. Mahinder Ramdin for their willingness to participate in the my thesis committee, read and assess this thesis. Your knowledge and critical feedback are pivotal to the improvement of this work and the forthcoming thesis defense.

I wish to acknowledge the individuals who generously offered their time and expertise during consultations, contributing significantly to the development of this thesis. Therefore I thank: Antonio Tripodi, Dobrin Toporov, Gioele Di Marcoberardino, Marco Binotti, Timothy Mosselmans, Nivya Uday Kodimaniyanda and Helmert van Rheenen.

I would like to express my heartfelt thanks to my family, who have always provided me the opportunities to pursue everything. When it comes to the important moments in my life, I know they will be there by my side.

I am also incredibly grateful to my friends, the ones in Italy and the ones in Delft, who have shown genuine interest in my journey and have always been there to lend a listening ear and support me in the best way possible. A special thanks to:

Daniel Jimenez Pelarda and Matéo Bouillez, for patiently waiting for me to join them. Lorenzo Mancini and Francesco Caioni, who came directly from Italy to explore the Netherlands with me. Ziad Ashqar, who has been a source of comfort since our first encounter in the Delft SEA association. To my dear friend Pablo Cecchini, who provides me insights to live outside the box since day one.

And to Céleste Isabelle Alice Marie Richard, the travel mate who embarks on every road trip and journey with me.

Thank you and I hope you enjoy reading my work.

Nicholas Parissi

17/10/2023

Abstract

This work deals with the techno-economic assessment of Hydrogen production from waste-derived syngas coming from a large-scale gasifier. This research was developed for the purpose of converting non-recyclable waste using a patented gasification technology to meet the demand for cleaner fuels, reducing global carbon emissions in line with the concept of a circular economy. A market analysis is conducted to identify the primary drivers and building blocks involved in the development of a Waste to Hydrogen scheme within the European context. Subsequently, a process route is designed and successfully implemented within Aspen Tech software to treat the raw syngas from the HTW gasifier, featuring a syngas adjustment and purification unit, a Pressure Swing Adsorption system, and a Combined Heat and Power unit. The system design achieves a Hydrogen recovery of 63% and purity around 99.5 vol%. The Hydrogen's quality aligns with the requirements for use in refineries, ammonia and methanol production, and for various heat-related applications. The economic analysis demonstrated the profitability of the plant, with a return on investment at a rate of 9.7 %. The levelized cost of Hydrogen at 7.35 €/kg substantiates the competitiveness of the Waste to Hydrogen model in comparison to steam methane reforming and electrolysis routes. The project's results offer a promising outlook for future research, indicating a sustainable approach to waste management and a viable pathway for reducing carbon emissions in the industry and transportation sectors.

Keywords: Waste to Hydrogen; Aspen Tech; Hydrogen separation; Pressure Swing Adsorption; Techno-Economic analysis

Contents

Nomenclature

List of Abbreviations

$\dot{F}$	Flow rate [mol/s]
CH_4	Methane
CO_2	Carbon Dioxide
C	Concentration
C_0	Concentration of the feed
C_{Acc}	Concentration accumulated in the bed
C_{in}	Intlet Concentration
C_{out}	Outlet Concentration
H_2	Hydrogen
NO_x	Nitrogen Oxides
O_{2frac}	Oxygen fraction [-]
SO_x	Sulphur Oxides
t_b	Break point time [s]
A_{cs}	Cross sectional area [m^2]
A_{AC}	Face area of the bed[m^2]
C_f	Characteristic packing factor [-]
C_P	Purchase Cost
c_s	Heat capacity of the solid [kJ/kg K]
c_{fac}	Correction factor [-]
$C_{b_{AC}}$	Bulk concentration in the Activated Carbon layer [kmol/kg]
$C_{b_{Zeo5A}}$	Bulk concentration in the Zeolite 5A layer [kmol/kg]
c_{pg}	Specific heat capacity of the gas [kJ/kg K]
COM	Cost of Manufacture
Cp	Specific heat capacity at constant pressure [J/(K·kg)]
$CTCI$	Total Capital Investment
$CTPI$	Total Permanent Investment
Cv	Specific heat capacity at constant volume [J/(K·kg)]
cv	Control valve specification [- or kmol/(s bar)]
D	Diameter[m]
F_P	Packing factor [1/m]
$F_{H2O,CleanedSyngas}$	Water in Cleaned Syngas stream [kg/h]
$F_{H2O,CO2Product}$	Water in CO_2 Product stream [kg/h]
$F_{H2O,Makeup}$	Water Makeup Flow stream [kg/h]
$F_{H2O,SyngasFeed}$	Water in Syngas Feed stream [kg/h]
$F_{MDEA,CleanedSyngas}$	MDEA in Cleaned Syngas stream [kg/h]
$F_{MDEA,CO2Product}$	MDEA in CO_2 Product stream [kg/h]
$F_{MDEA,Makeup}$	MDEA Makeup stream [kg/h]
Fac_p	Penetration factor [-]
$FISF$	Investment Site Factor
g_C	Conversion factor 2
G_{in}	Gas phase molar flow rate [kmol/h]
H	Bed height[m]
HD_C	Heat Duty Consumed [kW]
HD_G	Heat Duty Generated [kW]
k	Ratio of specific heat capacities [-]
k_1	Isotherm parameter [kmol/kg]
k_2	Isotherm parameter [kmol/kg K]
k_3	Isotherm parameter[1/bar]
K_4	Parameter in Fig. 11.44
k_4	Isotherm parameter [K]

k_f	Mass transfer coefficient [1/s]
L	Length[m]
L_{min}	Liquid phase molar flow rate [kmol/h]
$LCOH$	Levelized Cost of H_2 [EUR/kg]
M_{imp}	Amount of impurity adsorbed during cycle time [mol]
M_{solute}	Solute mass flow rate [kg/s]
M_G	Gas mass flow rate [kg/s]
M_L	Liquid mass flow rate [kg/s]
M_{air}	Mass of air required for combustion [kg/s]
M_{LPsteam}	Mass of low-pressure steam [ton/h]
M_{AC}	Required amount of adsorbent[kg]
Mw_{air}	Molecular weight of air [kg/kmol]
n	Number of compressor stages [-]
NHD	Net Heat Duty [kW]
NPR	Net Power Requirement [kW]
O_{2_j}	Oxygen required for component j combustion [kmol/s]
$O_{2_{\text{Tot}}}$	Total molar flowrate of oxygen for all components [kmol/s]
p	Pressure[bar]
p_f	Final pressure [bar]
p_H	High pressure [bar]
p_I	Intermediate pressure [bar]
p_i	Initial pressure [bar]
p_L	Low pressure [bar]
P_{out}	Recoverable electrical power output [kW]
p_{fi}	Final pressure after n stages [bar]
PBP	Payback Period
$Power\_C$	Power Consumed [kW]
$Power\_G$	Power Generated [kW]
q_j^*	Saturation concentration of component j [mol/kg]
q_j	Concentration of component j [mol/kg]
Q_v	Gas flow rate[m^3/s]
Q_v	Inlet flow rate [m^3/s]
Q_{out}	Recoverable thermal power output [kW]
ROI	Return on Investment
T	Temperature[°C or K]
T_1	Initial temperature [°C or K]
T_2	Temperature after compression [°C or K]
t_{ads}	Adsorption time [s]
t_{blow}	Blow-down time [s]
t_{press}	Pressurization time [s]
TFC	Total Fixed Cost
TVC	Total Variable Cost
v	Velocity [m/s]
V_m	Gas mass flow rate [kg/m^2 s]
V_{AC}	Adsorbent volume requirement[m^3]
WC	Working Capacity [mol/kg]
x	Compression rate [-]
z	1-D spatial dimension [m]
Ar	Argon
$C_{10}H_8$	Naphthalene
$C_{17}H_{34}O_2$	Methyl Palmitate
$C_{19}H_{34}O_2$	Methyl Linoleate
$C_{19}H_{36}O_2$	Methyl Oleate
$C_{19}H_{38}O_2$	Methyl Stearate
C_2H_4	Ethylene
C_2H_6	Ethane
C_3H_8	Propane
C_4H_{10}	Butane
C_6H_6	Benzene
CoMo	Cobalt-Molybdenum
COS	Carbonyl sulfide
H_2S	Hydrogen Sulfide

HCN Hydrogen cyanide

N_2 Nitrogen

NH_3 Ammonia

ZnO Zinc Oxide

ADS Adsorption

BD Blow Down

CAPEX Capital Expenditure

CCE Carbon Conversion Efficiency

CCF Capital Charge Factor

CeO_2 Cerium dioxide

CEP Circular Economy Package

CEPCI Chemical Engineering Plant Cost Index

CGC Cold gas clean-up

CGE Cold Gas Efficiency

CHP Combined Heat and Power

CO Carbon Monoxide

Cu-Zn Copper-Zinc

D Column Diameter [m]

db dry basis[-]

DSL Dual Site Langmuir

ED1 First Depressurization

ED2 Second Depressurization

EIA Energie-investeringsaftrek

EP1 First Pressurization

EP2 Second Pressurization

EU European Union

ExL Extended Langmuir isotherm

Fe-Cr Iron Chromium

GHG Greenhouse Gas

h Hours

H_2O Water

HGC Hot gas clean-up

HT-WGSR High temperature WGS reactor

HTW High Temperature Winkler

HYDRO Hydrolysis reactor

IAS Ideal Adsorbed Solution Theory

IEA International Energy Agency

J Conversion factor 1

K Equilibrium constant [-]

KPI Key Performance Indicators

L/D length-diameter ratio [-]

LargeBtH Large scale Biomass to H_2

LargeBtH Steam Methane Reforming with Carbon Capture and Storage

LargeWtH Small scale Waste to H_2

LCA Life Cycle Assessment

LDF Linear Driving Force

LHV Low Heating value

LT-WGSR Low temperature WGS reactor

MBT Mechanical Biological Treatment

MDEA Methyldiethanolamine

MPS Medium pressure steam

MRF Material Recovery Facilities

MSW Municipal Solid Waste

MTZ Mass-Transfer Zone

OPEX Operational and Maintenance Expenditure

P/F Purge to Feed ratio [-]

PG Purge

PSA Pressure Swing Adsorption

RDF Refuse Derived Fuel

Re Reynolds number [-]

RP Feed Pressurization

SmallBtH Small scale Biomass to H_2

SmallWtH Large scale WtH

SmallWtH Small scale WtH

SMR	Steam Methane Reforming
SMRwCCS	Small scale Waste to H_2
SRF	Solid Recoverd Fuel
TRL	Technology readiness level
TSA	Temperature Swing Adsorption
WGC	Warm gas clean-up
WGS	Water Gas Shift
wt	weight [-]
WtE	Waste to Energy
WtH	Waste to Hydrogen
x	mole fraction of solute in the liquid phase[-]
y	Year
y	mole fraction of solute in the gas phase[-]

Constants

π	Pi

List of Symbols

ΔG	Gibbs Free Energy
ΔH	Enthalpy
ΔS	Entropy
η_j	Conversion or separation efficiency for component j [-]
η_p	Polytropic efficiency [-]
μ_L	Dynamic viscosity of liquid [Ns/m^2]
ν_j	Stoichiometric coefficient for component j [-]
ρ_{Ad}	Adsorbent density[kg/m^3]
ρ_b	Bulk density [kg/m^3]
ρ_G	Density of gas [kg/m^3]
ρ_L	Density of liquid [kg/m^3]
ε	Void fraction [-]

List of Figures

List of Tables

1

Introduction

In recent decades, there has been a substantial increase in waste generation worldwide and this trend is expected to reach a total of 3.4 billion metric tons by 2050 [1]. Population growth, urbanization, economic development and consumer behavior are the major drivers for this phenomenon. The volume of waste that people produce each year is a major concern for authorities. From all the waste that is received annually in the waste processing facilities worldwide, less than 20% of waste is recycled, 70% is deposited in landfills and 10% utilized in Waste to Energy (WtE) schemes [1, 2]. A WtE business model can simultaneously address issues related to energy demand, waste management, and greenhouse gas (GHG) emissions [2]. Unfortunately, more than 90% of WtE plants use incineration as a guideline practice to process waste causing the release of harmful chemicals and pollutants (e.g. particulate matter and heavy metals) [3]. Nowadays, in the Netherlands WtE plants contribute to 10% of the country's "renewable" energy mix [4]. The continuous accumulation of waste and lack of sustainable solutions not only poses environmental challenges (e.g. soil degradation and air pollution) but also presents an untapped resource for renewable energy production.

Typical feedstocks for WtE purposes are non-recyclable materials, especially metals, due to the fact that they cause damage to the sorting equipment of waste processing facilities. This waste can be converted into refuse derived fuel (RDF) or solid recovered fuel (SRF), which are highly energy dense fuels ready to be used as feedstocks in WtE plants. In the Net Zero Scenario defined by the International Energy Agency (IEA), 2/3 of total energy supply in 2050 will be provided by wind, solar, bioenergy, geothermal, and hydro [5]. Consequently, the electricity demand will primarily be supplied by solar and wind power, with batteries serving as a short-term form of energy storage to balance eventual mismatches. In this context, the utilization of hydrogen (H_2) derived from waste presents a promising avenue for addressing long-term energy storage challenges. The current production of H_2, which contributes to 2.5% of global final energy consumption [6], is primarily from fossil-based sources, and is responsible for more than 900 million metric tons of CO_2 emissions, with most of it released into the atmosphere [7]. Conversely, the production of H_2 from waste derived syngas encounters challenges associated with impurity elimination and H_2 separation. Impurities contained in the syngas (e.g tar, Nitrogen and Sulphur compounds) have detrimental effects on downstream processing steps and catalytic reactions. Consequently, it mandates the integration of various operational units into a complex interconnected system to remove the impurities and separate a pure H_2 stream.

The existing academic literature lacks investigation concerning the systematic design of a H_2 production plant utilizing syngas obtained from existing industrial facilities. Thus, most of the research remains at lab or prototype scale. Further research is needed on large-scale system to generate knowledge to scale-up these technologies. The High Temperature Winkler (HTW) gasification process has been proven on a large scale to convert waste streams like RDF and waste wood into syngas. Therefore, the significance of this study resides on getting a deeper understanding from a process simulation view regarding the use of Pressure Swing Adsorption (PSA) process for H_2 production from waste-derived syngas of HTW gasification systems. The HTW gasification process has been proven on a large scale to convert waste streams like RDF and waste wood into syngas. The process simulation starts with a typical output syngas from HTW Gasification system, and then adheres to industry standards for the subsequent downstream process units. The novelty of this study lies in the development of user guideline to simulate a PSA unit in the Aspen Tech environment including Aspen Adsorption for a syngas coming from a large-scale gasifier.

This project serves as a valuable resource for scholars and analysts in the field. The present work aims to reveal the potential impact H_2 generation from waste-derived syngas as an alternative route towards decarbonization of sectors where emissions are hard to abate, namely industry and transportation. Such an approach contributes significantly to environmental sustainability and energy security, carrying social and economic implications. By integrating Waste to Hydrogen (WtH) systems, local communities can benefit from reduced waste disposal costs, job creation, and improved environmental quality. Ultimately, as global demand for clean energy rises, research in this field drives innovation and economic growth.

1.1. Municipal Solid Waste

In 1997, the United Nations defined waste as follows [8]:

Materials that are not prime products (that is products produced for the market) for which the generator has no further use in terms of his/her own purposes of production, transformation or consumption, and of which he/she wants to dispose. Wastes may be generated during the extraction of raw materials, the processing of raw materials into intermediate and final products, the consumption of final products, and other human activities.

Municipal solid waste or MSW includes (bulky) household waste, solid waste from businesses, non-hazardous industrial waste and other residual streams [9]. The characteristics of MSW are largely influenced by factors such as: physical properties, geographic location and living standards [10, 11]. In Figure 1.1, it is possible to see how the production of waste has increased over the 15 years period during the years 2006 and 2021. It is relevant to state that variations reflect differences in consumption patterns and economic wealth, but also depend on how municipal waste is collected and managed among the different countries in the EU. Therefore, current and future generation of MSW is difficult to predict [10].

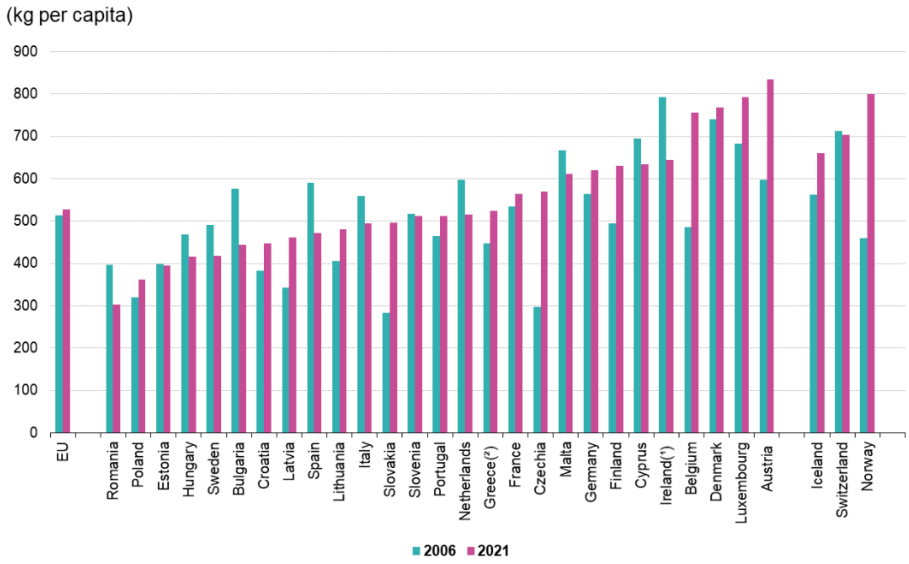

Figure 1.1: MSW Generation in EU between 2006-2021 [12].

1.2. MSW management: Policies, Incentives and Framework

1.2.1. MSW management: Policies

Even though waste management is appointed as a delicate financial and political topic as local authorities are in charge of its collection, the EU has adopted a set of legislation, over the past two decades, aiming at supporting/guiding national policies towards a more efficient waste management infrastructure. Landfills, open dumping, and incineration have been traditional methods of disposing of solid waste for centuries. To limit those practices, at the end of the 1980s, the EU presented for the first time the ”Waste Hierarchy”. The environmental impacts of landfilling and incineration were soon recognized as a possible threat to the point where in 1995, landfills in the EU accounted for around 3% of total GHG emissions [12]. Consequently, a

series of legislation (e.g the Waste Framework Directive and the Landfill Directive) were approved, revised and expanded over the years to limit the environmental damages [13]. Data provided by Eurostat shows the trends in MSW generation and treatment in the European Union from 1995 to 2021 [12] as illustrated in Figure 1.2.

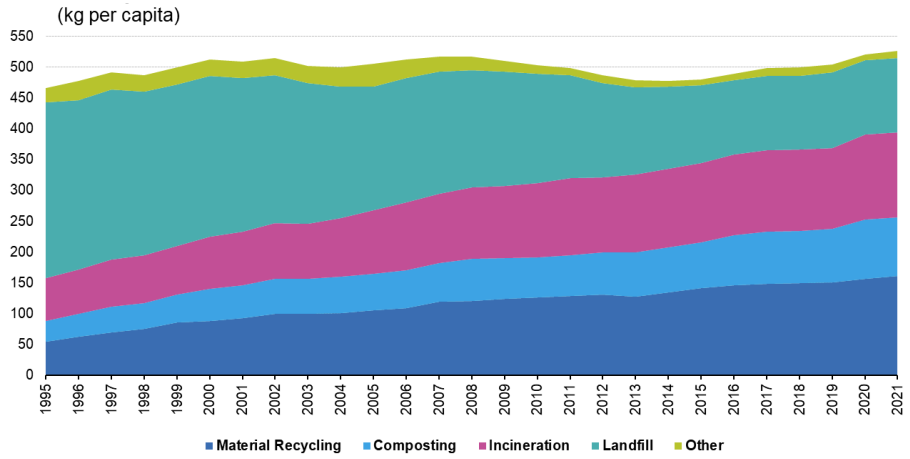

Figure 1.2: MSW Treatment in EU between 1995-2021 [12].

Even though more waste is being produced, the total amount of municipal waste landfilled has diminished. A possible correlation can be found with the directives established in those years such as [12]:

- Directive 62/1994, recovering a minimum of 50 % of all packaging put on the market by 2001.
- Directive 31/1999, reducing the amount of biodegradable municipal waste going to landfills to 75 % by 16 July 2006.

The 2008 revised version of Waste Framework Directive 2008/98/EC implemented more ambitious legislation as stated in [14]:

- Article 4 on ”Waste Hierarchy”, promoting a pyramid scheme on the principles of (a) prevention; (b) preparing for re-use; (c) recycling; (d) other recovery (e.g. energy recovery); (e) disposal.
- Article 8 on the ”Extended producer responsibility”.
- Article 10 on ”Recovery”, in which the Member States shall take the necessary measures to ensure that waste undergoes pre-treatment for re-use, recycling or other recovery operations.

Starting from 2015 until now, another step towards the promotion of WtE supply chains was made when the European Commission established the ambitious Circular Economy Package (CEP), introducing legislative and non-legislative measures for a strategic and sustainable use of waste. The CEP reduces the exploitation of natural resources and extends the focus on the entire life cycle of products. Accordingly, the CEP is setting the conditions to facilitate the EU’s 2050 climate neutrality targets [15].

1.2.2. MSW management: Framework

Waste management systems in European countries consists of essential operational units such as collection, shipping, treatment, recycling and disposal [1]. Although EU directives stand up as guidelines to shape trends on waste management, each different country adopts a specific framework [16]. For the scenario implemented, it is appropriate to perform a detailed analysis on the Dutch waste sector, with a particular focus on the main actors involved and their obligations as it was done by de Jong et al. [17]. Figure 1.3, presents the Dutch waste market, highlighting the different participants, as well as cash and material flow.

Several companies are now entering the waste to energy market to bridge the gap between ”Private Processors” and ”Industry”. In addition to that, one of the advantages for companies entering this sector, is that they receive monetary compensation to process the waste, which makes the business model attractive

[1] An overview regarding the state of the global solid waste management practices projected until 2025 is given by Hoornweg et al.[11].

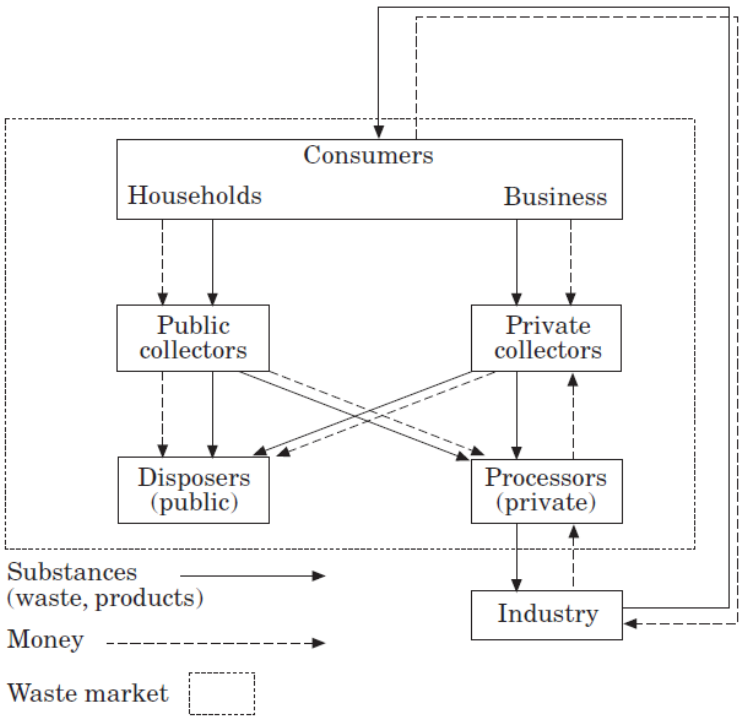

Figure 1.3: Flow of waste and money in the waste market [17].

for many investors. On the other hand, a barrier for the deployment of waste to energy schemes, could be attributed to the volatility of waste materials to process. Since the generation is difficult to predict as well the remuneration prize of collection, waste processors attempt to guarantee a sufficient flow by tying collectors to long term contracts [17].

1.3. Refuse Derived Fuel

The direct utilization of MSW is challenging due to the heterogeneous composition of the collected waste. To tackle this variability issue, it is common practice to enhance the handling characteristics, homogeneity and thermodynamic properties of MSW via thermal or mechanical pre-treatment to obtain SRF or RDF [18]. RDF is defined as fuel derived from combustible fraction of solid waste such as plastic, wood, textile and/or organic waste [2] in the form of pellets or fluff [19]. Generally, the quality of produced RDF is determined by consumers, based on their process characteristics; nonetheless, there have been attempts in Europe to define standardized RDF compositions [3]. Figure 1.4 shows the possible pathways of an incoming waste stream towards the production of RDF following the method of Mechanical Biological Treatment (MBT) [19].

The MBT acts simultaneously:

- Mechanically [4], being able to sort, separate and perform size reduction (shredder).
- Biologically, stabilizing the organic or compost streams.

Based on the requisites of RDF, the process may incorporate a drying section (in case thermal drying is privileged over natural drying); rotary trommel used for a second screening procedure (ensuring appropriate size separation); magnetic separators employed to remove traces of inerts such as metals; fans to divide light and dense materials; and pellet press (optional for the purpose of producing fuel pellets) [19, 22].

[2] The presence of organic waste dictates the type of RDF and consequently the type of pre-treatment [19].

[3] Information regarding the state of the art and trends in the use of SRF globally and, more specifically in Europe, is given by IEA [20].

[4] A typical Material Recovery Facility includes five separation/ sorting stages for recovering recyclable materials such as paper/-cardboard, metals, glass and plastics into individual streams [21].

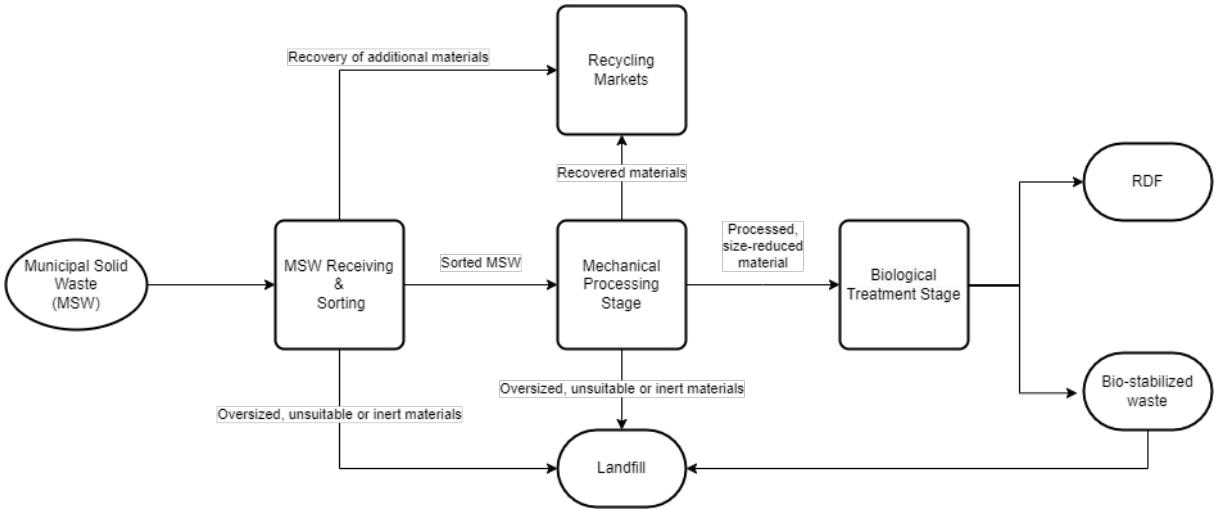

Figure 1.4: A generalised schematic flow diagram of Mechanical Biological Treatment [19].

1.4. Market analysis and Economic considerations

H_2 is the lightest and most abundant element in the universe and in its pure form is a colorless, odorless, and highly flammable gas. IEA [7] reported the most relevant physical properties of H_2, highlighting how it contains more energy per unit of mass than natural gas but a lower energy density per unit of volume. This means that larger volumes of hydrogen must be moved to meet identical energy demands as compared with other fuels. The demand for H_2 has grown steadily starting from 1975, with oil price uncertainties and petroleum shortages. In the 1990s, concerns about climate change led to an increase in studies on H_2, with a particular focus on carbon capture and storage, peaking with the announcements of the Kyoto Protocols. By the early 2000s, these concerns had begun to translate into renewed policy action aimed at the decarbonization of the transportation sector. Figure 1.5 illustrates the trend of global annual demand for H_2 from 1975-2018 [7], peaking at around 70 million tonnes per year (MtH_2/y).

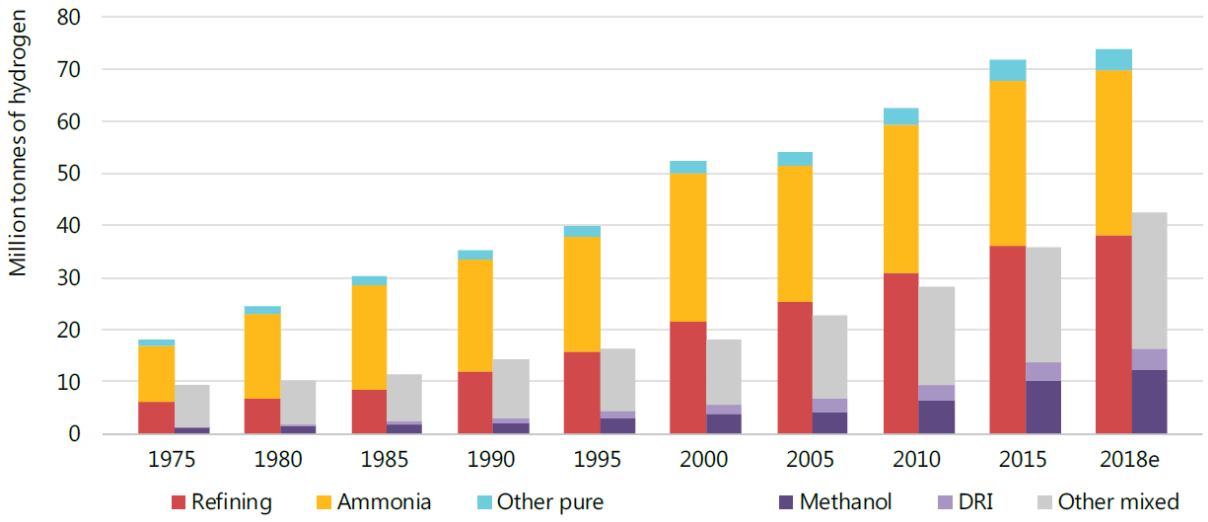

Figure 1.5: Global annual demand for H_2 from 1975-2018 [7].

Figure 1.5 showcases some quantitative values for the volume of end use application of H_2. Nevertheless, it would be appropriate to assess the complete H_2 value chain, starting from the most common sources for H_2 production, up to the final end use application. IEA [7] has summed up all this information in a Sankey diagram for the year 2019 (illustrated in Figure 1.6). The diagram highlights how 98.5% of

the dedicated production of H_2 is fossil-fuel based; while the demand for pure H_2 is mainly attributed to chemicals manufacturing and industry.

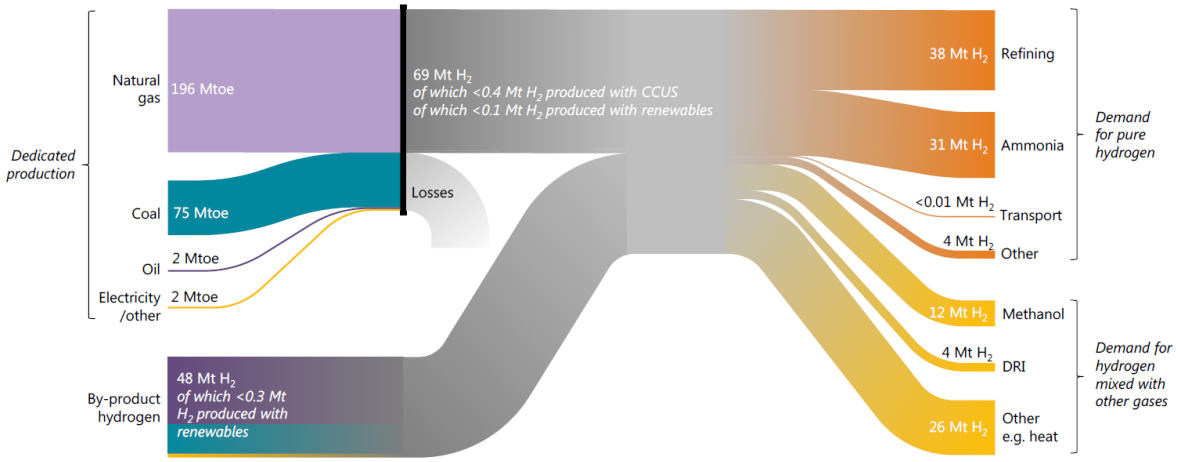

Figure 1.6: The 2019 H_2 value chains [7].

It becomes evident that assessing the main stakeholders, as well as the barriers and opportunities within the H_2 market, is essential to gain the complete overview of both current and potential future trends.

1.4.1. Market barriers and opportunities

The main technical challenges in business models involving the thermo-chemical conversion of waste for the production of H_2 are related to the waste feed composition [23]. The heterogeneous nature of waste causes issues for material recovery facilities. This issues, related to material handling and pre-treatment of waste, have led to project failures in the past [23]. Figure 1.7 shows the trend in waste management.

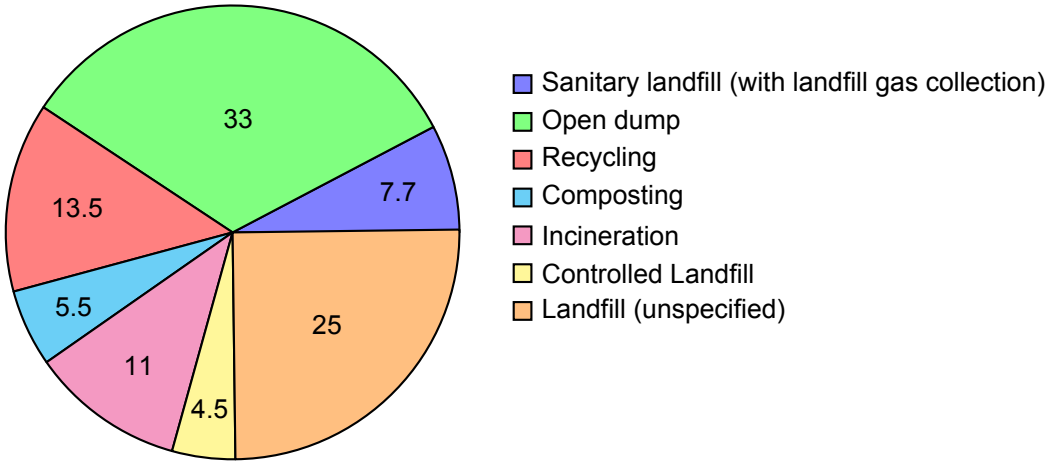

Figure 1.7: Trend in Waste Management [24].

Other barriers for the conversion of waste into H_2 could be imputed to:

- Securing the waste feedstock supply.
- Evaluate and arrange long term commitments with H_2 buyers. H_2 projects based on gasification require purification steps, heavy to sustain in terms of investments, which will translate to a higher H_2 price compared to H_2 from fossil fuels. Current waste gasification models are targeting the chemicals market due to their higher value and more mature off-takers.

- Bureaucracy slowing down the implementation of policy frameworks and incentives to make the price of H_2 competitive.

Despite challenges and barriers, the production of H_2 via waste gasification is hindering great opportunities [7, 20, 25, 26]. The most relevant are summarized below:

- Gasification is a commercial solution ready to be scaled-up to abate the final H_2 price. In a future scenario in which the price of emitting CO_2 in the atmosphere will increase, the waste to H_2 scheme could be a potential cost-efficient solution in the energy transition context.
- The lifecycle GHG emissions of waste to H_2 projects are expected to be significantly lower than the current emissions profiles of fossil fuels (natural gas, coal and petcoke).
- Residual wastes are available globally and converting waste to H_2 can be undertaken in locations that do not have indigenous resources of fossil fuels or abundance of solar and wind potential.

1.4.2. Economics and Incentives

Finally, qualitative considerations regarding potential stakeholders, financial schemes and economic incentives are necessary to sustain the WtH business model. In Figure 1.8, a stakeholder mapping is presented to get a visual representation of all the parties who can influence a project and how they are connected. The order of the stakeholders is based on the level of interest (x axis) and their influence (y axis); moreover, it is shown how the different stakeholders are grouped in 4 categories.

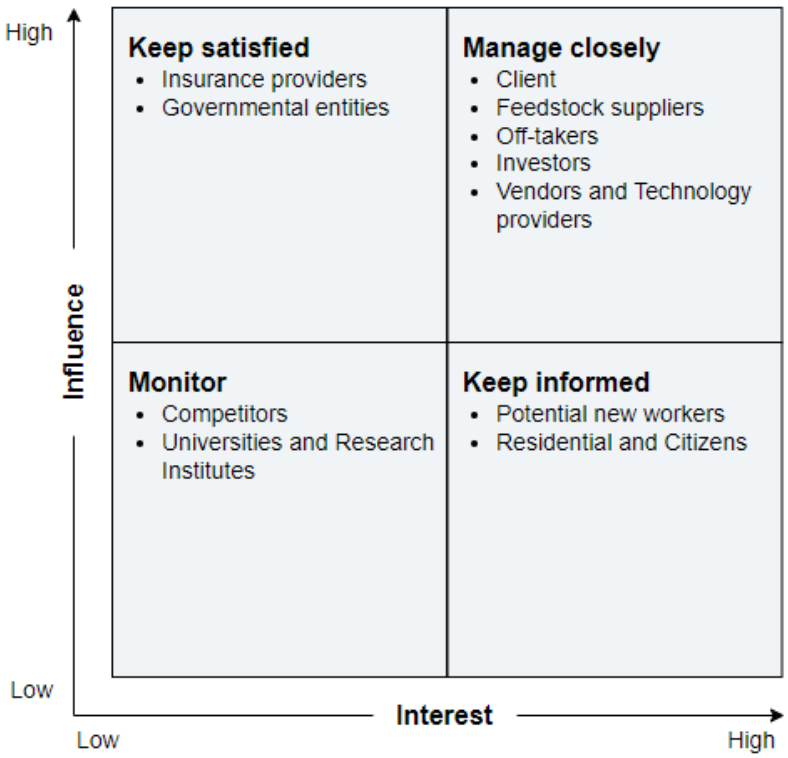

Figure 1.8: Stakeholder mapping.

Financial schemes may differ based on the process configurations, agreements and investment support. Even though some business cases can be taken as reference (e.g. FUREC [27], ENERKEM [28] ...), it is more appropriate to list some of the resources in terms of economic incentives. In the EU, the Innovation Fund Programme aims to support innovative projects related to industrial electrification and H_2 production and utilization. This support is in line with the 2030 renewable H_2 targets set out in the REPowerEU Action Plan and is designed to reduce dependency on imported fossil fuels [29]. Specifically for the Netherlands,

over the time period between 2015-2017, a boost of subsidies towards bioenergy implementation, were introduced. In just 2 years, the subsidies for using solid biomass in energy production increased from 29 to 117 million € [30]. In 2023, the Dutch Enterprise Agency has allocated a budget of 249 million € for the EIA (Energie-investeringsaftrek), for companies active in sustainable energy projects [31].

1.5. Research Formulation

H_2 can be obtained from different processes such as steam methane reforming (SMR), electrolysis, gasification and others. Thus, the generation of H_2 carries different challenges depending on the conversion technology. For instance, biomass gasification has a higher exergetic efficiency compared to competing technologies. Nevertheless, the operational variables and feedstock type significantly impact syngas quality and downstream processes if oriented to H_2 production. As a consequence, it is a common business practice to remove impurities (e.g. Tar, Nitrogen and Sulphur compounds...) from syngas prior the separation of pure H_2 from the mixture [18]. Subsequently, the syngas obtained must be subjected to separation methods, which are mainly classified as physical adsorption and chemical absorption methods. The former includes adsorption techniques such as Pressure Swing Adsorption, cryogenic distillation and membrane separation, while the latter involves a solvent based method [32]. The main disadvantages of solvent absorption methods are related to solvent recovery and operating cost, alongside lower degree of purity achieved. On the other hand, membranes (such as Palladium) show promising results in terms of operating conditions (higher H_2 temperature and pressure which reduces cost for compression) but are limited by their technology readiness level (TRL) [33]. Barriers for cryogenic processes are namely the extremely low temperatures and the dissatisfaction of end-use H_2 purity standards [18, 32]. Regarding the PSA process, the potential advantages are the absence of any thermal energy duty during the regeneration step as well as being the main post-treatment technique for large scale applications [34]. Over 85% of current global H_2 production units use PSA technology for achieving purification standards [35].

This study is conducted using HTW as the base case for gasification technology due to its maturity and commercial availability. The HTW gasification unit can be utilized to produce valuable products such as advanced biofuels for use in the road transport, marine and aviation sectors, helping these sectors to reduce their carbon emissions and become more sustainable. The project taken into exam focuses on addressing a critical research gap:

Research Gap

The existing body of research lacks comprehensive investigation into the utilization of PSA process for H_2 production from waste-derived syngas, particularly in the context of syngas generated at a large-scale system High Temperature Winkler gasifier.

Therefore, in order to fill this knowledge gap, a research objective has been formulated and quantitatively assessed by answering the following research questions:

Research Objective

The primary objective of this research project is to evaluate, technically and economically, the production of H_2 from blends of woody biomass and MSW-driven (e.g. RDF) waste streams.

Research Question 1

What is the process route for the sequence of purification steps prior to the PSA to achieve the highest quality of gas in terms of H_2 content?

Research Question 2

Are the available computational tools valid for simulating the Waste to H_2 process route?

Research Question 3

What would be the price comparison between different H_2 production routes (e.g. electrolysis, SMR, among others)?

The significance of this study lies in its potential WtH businesses, specifically in the context of producing advanced biofuels, a critical endeavor for both environmental sustainability and energy security. These findings hold immense value for several waste to energy companies, as they offer a pathway to enhance the flexibility of waste to energy processes. Moreover, this study's comprehensive approach, which involves developing, explaining and integrating each modeling step and equation into Aspen Plus and Aspen Adsorption, sets a benchmark for future large-scale gasifier projects and serves as a valuable resource for scholars and analysts in the field.

The relevance of this project extends to techno-economic assessment by providing a comprehensive overview of both the technical and economic performance of the evaluated system. This holistic approach equips decision-makers with the necessary insights to assess the viability of WtH projects. Additionally, the inclusion of a price comparison for H_2, adds a crucial dimension to profitability measurements, enabling stakeholders to make informed choices when comparing their operations to other businesses. The study's alignment with simulation tools further enhances its relevance, as it bridges the gap between theoretical research and practical implementation in the field.

1.6. Structure of the Report

The structure of the report is as follows. Chapter 2 conducts a comprehensive literature review. Chapter 3, establishes the fundamental material and methods used as tools to approach the study. Next, Chapter 4, delves into model development. Chapter 5 presents the technical outcomes of the study. Chapter 6 offers an evaluation of the economic performance of the system. Finally, Chapter 7 encapsulates the study's conclusions and offers insightful recommendations.

2

Literature Review

In this chapter the theoretical concepts and relevant findings concerning conceptual design and simulation tools are presented. The introductory discussion presented in Chapter 1 serves as a critical foundation for delineating a process flowchart tailored to the WtH business model under investigation. The flowchart encompasses key components, including a HTW gasification unit, syngas adjustment and purification unit, a PSA system which anticipates a H_2 production line and a Combined Heat and Power (CHP) unit. Figure 2.1 shows a general block flow diagram for a typical Waste to Hydrogen process.

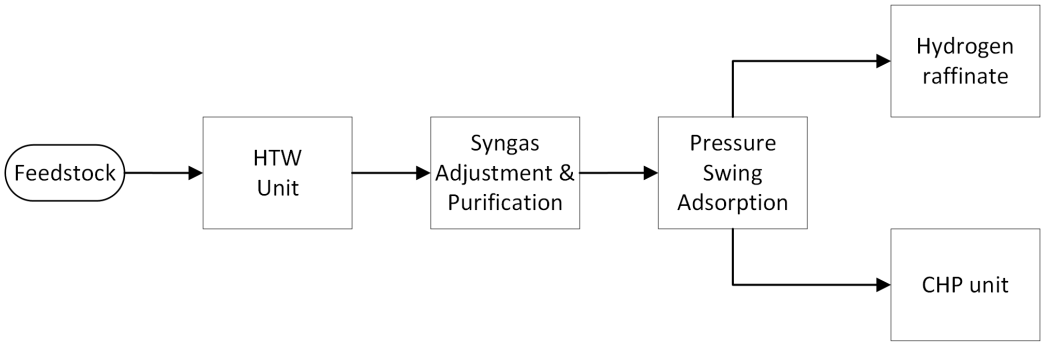

Figure 2.1: General block flow diagram.

2.1. Gasification: Concepts and Technology

The waste to H_2 conversion methods can be divided into thermochemical and biochemical mechanisms differing by the energy requirements, operating conditions, feedstock inputs, efficiencies, reaction times and final yields. In general, the thermochemical processes (gasification and pyrolysis), showed higher H_2 yields, conversion efficiencies and shorter reaction times. The selection of gasification technologies offers advantages not only from technical and economic standpoints but also in terms of side product recovery and adaptability to the chemical production markets

Gasification is the process of converting carbonaceous feedstocks into a combustible synthesis gas, or syngas, by partial oxidation. The synthesis gas is mainly a mixture of H_2 and CO but may also contain CO_2, CH_4, tar, H_2O and other light hydrocarbons. the gasification process is sub-divided into four stages, which are:

1. Drying
2. Pyrolysis
3. Partial combustion of volatile matter
4. Gasification of decomposed products

Sajid et al. [36] report that co-gasification demonstrates substantial enhancements in gas yield, Cold Gas Efficiency (CGE) and Carbon Conversion Efficiency (CCE) when compared to individual gasification

processes. This study provides valuable empirical evidence, including a table detailing different feedstock types, gasifier configurations, operating conditions and performance metrics for co-gasification systems using waste[1]. Among the many operating variables to control a gasification unit, the most important ones typically include:

- Operating temperature and pressure.
- Physical and chemical composition of the feedstock (moisture and ash content, and particle feed size among the many).
- Gasifying medium and equivalence ratio.

A review of the process description, critical factors affecting conversion and the state of the art can be found in many articles [18, 38, 39]. Regarding the gasification medium, Sajid et al. [36] documented that the utilization of steam as a gasification agent is favored due to its capacity to promote increased H_2 production via the Water Gas Shift (WGS) reaction. Furthermore, a study on steam gasification using different blends of waste biomass revealed that the CGE is dependent on gasification temperature and the steam to carbon ratio.

Commercially speaking, there are three main technology classifications into which most of the commercially available gasifiers fall. These categories comprehend: Fixed-bed gasifiers, Entrained-flow gasifiers and Fluidized-bed gasifiers [40]. A fixed-bed reactor, has a slow moving solid state with respect to the gas phase and can be configured in an updraft or a downdraft configuration, which have a co-current and counter-current flow, respectively. The downdraft configuration reduces the amount of tar, but also has a lower flexibility than the updraft configuration. The fixed-bed reactor has a high conversion per reactor volume, although they are usually limited to temperatures below 1000 °C. The entrained-flow reactor is the most flexible and produces the lowest amount of tar. The feed, which is a fine powder, and gasifying agent both enter from the top of the reactor and react at an operating temperature between 1200 and 1600 °C. These higher temperatures result in a higher conversion. Finally, a fluidized-bed reactor is usually operated between 800 and 1000 °C. In this configuration feedstock and gasifying agent are entering from the bottom. Fluidized-bed reactors have better heat and mass transfer, due to better mixing within the reactor [41].

This study primarily focuses on the High-Temperature Winkler gasification process, with detailed documentation provided by Toporov [42]. The HTW technology offers several advantages such as: its exceptional flexibility in handling diverse feedstock compositions and sizes, its low oxygen consumption owing to moderate temperatures, its robust partial load behavior spanning a wide performance range and its operation at high pressure, which significantly enhances the overall performance [42]. Additionally, HTW can operate using municipal solid waste as demonstrated by the demonstration plant at Berrenrath (Germany) and Niihama (Japan) [43].

2.2. Syngas Adjustment and Purification

H_2 production from co-gasification requires further gas conditioning and cleaning before the end-use application. Woolcock et al. [44] confirm the fact that contaminants formation in the syngas is influenced by feedstock composition, operational conditions and reaction involved withing the gasifier. In Appendix A, a table evaluating impurities and their implication for syngas applications is given. Moving on, several comparative studies for different syngas cleaning techniques and their basic functional principle have been studied to find a general patter for syngas cleaning systems. An overlook at the main commercial syngas cleaning units is collected in these recent studies [45, 46, 47]. After categorizing syngas cleaning techniques into three temperature-based regimes: hot gas clean-up (HGC), cold gas clean-up (CGC) and warm gas clean-up (WGC), Woolcock et al. [44] concluded that several well-established technologies are available for removing impurities. However, dealing with particulate matter, tar and sulfur presents challenges, necessitating a careful balance between maintaining high thermal efficiencies, minimizing activity losses, and considering economic factors when designing the cleaning unit. Asadullah [48] observed that most projects employ a combination of high and low temperature cleaning methods, facilitating the removal of the impurities.

[1] For completeness of the analysis, the overview of large scale waste gasification technologies (with summary information regarding pre-treatment of feedstocks, reactor capacity and products) is given by Lee et al. [37].

In the context of the designed process, the incorporation of fundamental principles pertaining to the Water Gas Shift reaction and gas absorption and adsorption process is imperative.

2.2.1. Water Gas Shift Reaction

The Water Gas Shift reaction is a chemical reaction, typically carried out in the presence of a catalyst to convert the carbon contained in the CO to CO_2, while maximizing the H_2 content. The balanced chemical equation for the water gas shift reaction is as follows:

$$CO + H_2O \rightleftharpoons CO_2 + H_2 \tag{2.1}$$

Moreover, the valuable operating alternatives for the CO conversion unit are listed here below:

- High Temperature CO shift at about 300-450°C to reach approximately a conversion of 2.5% CO on dry basis (db).
- Medium temperature isothermal shift at 220-270°C down to approximately 0.5% CO on db.
- Low temperature CO shift at about 180-250°C down to approximately 0.2 % CO on db.

Regarding the thermodynamics, the WGS is a mildly exothermic reversible reaction. Hence, its equilibrium constant decreases with temperature, and high conversions are favoured by low temperatures and excess quantity of steam injected, but is unaffected by difference in pressure.

For industrial implementations, it is common to perform the CO shift in two steps to have a better control on the products and the equipment. This is a consequence of the mildly exothermic nature of the reaction, which requires an inter-cooling system. Condensation has to be absolutely avoided, as it can be harmful to the catalyst: for this reason, the lower temperature limit is 200°C [49].

The position of the WGS reactor in the process configuration depends on the characteristics of the syngas exiting the gasifier and its intended final applications. When sulfur compounds are present in the syngas, the WGS reaction is referred to as the 'sour shift'. Conversely, when the WGS is performed on syngas that has been desulfurized, it is termed the 'sweet shift'. The choice between the sour or sweet shift implies the use of different catalysts as well as operating conditions [49].

An extensive review of the thermodynamics and kinetics of the reaction for different catalyst can be found in many sources [35, 50, 51]. It is business practice to use iron-chromium (Fe-Cr) and copper-zinc (Cu-Zn) catalysts to facilitate the reaction at high and low temperatures sweet shift, respectively. Pal et al. [51] state how the current research trend is directed towards Cerium based catalysts (CeO_2) due to the ability to switch between the oxidized and reduced states. Nevertheless, in the summary table provided, it is clear how the use of novel based catalysts for large scale applications is not yet feasible due to low CO conversion, selectivity and stability.

2.2.2. Gas Absorption Process

In the process of absorption, a gas mixture comes into contact with a liquid substance, typically referred to as the absorbent or solvent. The objective is to selectively dissolve specific components from the gas into the liquid. These components that migrate from the gas phase to the liquid phase are commonly termed solutes or absorbates. Gas absorption processes can be classified based on the interaction between the absorbent and absorbate into three main types [52]:

- Physical solution, in which the component to be separated exhibits higher solubility in the liquid absorbent than other gases present. There is no chemical reaction between the component and the absorbent.
- Reversible reaction, involving a chemical reaction between the gaseous component and a liquid-phase component to form a different compound.
- Irreversible reaction, in which an irreversible reaction takes place between the component to be absorbed and a liquid-phase.

Typically, the option of physical absorption is privileged when the feed gases are present at high pressure and the component to be absorbed is in high concentration. In contrast, chemical absorption is preferred when the components to be separated in the feed are at low partial pressures. It is common practice to operate absorption processes counter-currently. In this configuration, the solvent enters the

vertical vessel from the top, while the gas mixture is introduced from the bottom. The absorbed substance is washed out by the lean solvent and exits as a liquid solution from the bottom. This process is usually conducted at a pressure higher than atmospheric to benefit from the pressure-dependent gas solubility. The loaded solvent is often reclaimed through a subsequent stripping or regeneration step as described in Figure 2.2.

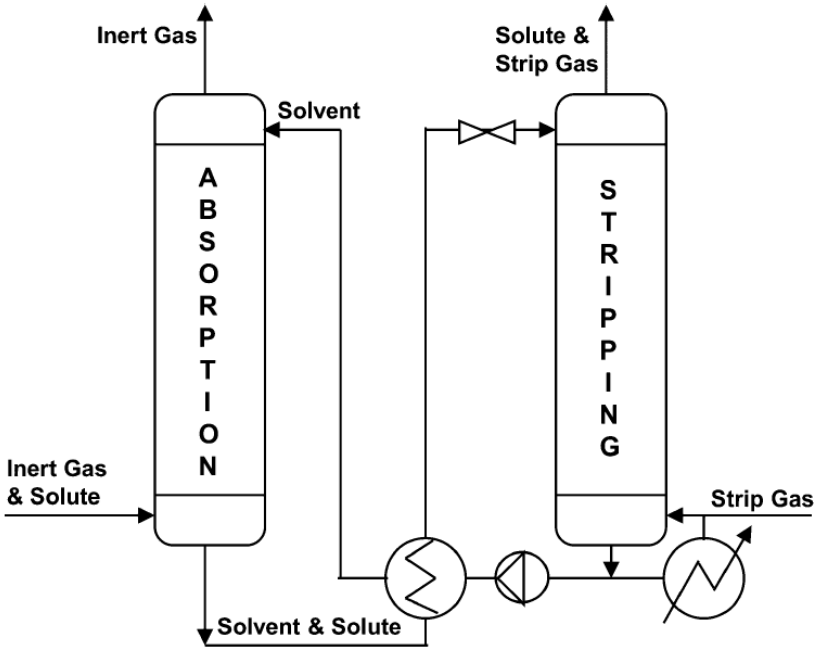

Figure 2.2: Basic scheme of an absorption installation with stripping for regeneration [52].

Desorption, the reverse process of absorption, is performed in several ways, such as pressure reduction, reboiling or stripping with an inert gas or steam. The dimensions of the absorption and desorption equipment are dictated by the difference between the partial pressure of the absorbed key component over the regenerated solution and the purified gas. The lean solvent, now free of gas, undergoes heat exchange, recovering some of the required heat for heating the rich solvent. It is then cooled to the desired temperature and returned to the absorption column. Occasionally, a small amount of fresh solvent (known as make up stream) may be added to compensate for losses during desorption, including evaporation and irreversible reactions within the system.

Operating Conditions in Industrial Applications
In industrial gas absorption applications, typical operating conditions encompass a broad range of temperatures and pressures. The selection of these conditions depends on the solubility characteristics of the target gas components. A list of the main parameters for industrial gas absorption is provided below [52, 53, 54]:

- Temperature, moderate to low temperatures are often preferred to reduce energy consumption. However, higher temperatures can be advantageous in cases where increased solubility is required.
- Pressure, operating at elevated pressures can enhance gas solubility and absorption rates.
- Trade-off between minimum solvent flow rate and number of counter-current equilibrium contacts between the gas and liquid phases.
- Column specifications, including dimensions, design and type (packing or tray configuration) of the absorption column, significantly influence the available surface area for gas-liquid contact. This, in turn, affects absorption efficiency.

2.3. Gas Adsorption Process

The investigation of solid-gas ab/ad sorptivity began in the late 1700s, but it was not until the early 1900s that any industrial application was found. Over the years, engineers filed patents on the major gas-adsorptive separations we know today, such as hydrogen sulfide removal, oxygen/nitrogen separation and some drying applications. Later on, refinements to these technologies have appeared, and numerous authoritative textbooks have consolidated the scientific knowledge of the subject [49, 55, 56, 57].

Adsorption is a separation process in which certain components of a fluid phase are transferred to the surface of a solid adsorbent. Adsorption processes may be classified as purification (considerably less than 10 wt% of a stream must be adsorbed) or bulk separations (10 wt% or more of a stream), depending on the concentration in the feed fluid of the components to be adsorbed [52]. Usually, for large scale industrial applications, the fluid is passed continuously through the bed until the solid is nearly saturated and the desired separation can no longer be achieved. The flow is then switched to a second bed until the saturated adsorbent can be replaced or regenerated [53].

Regarding notations, the adsorbed species in the fluid bulk are called adsorbate while the porous solids are called adsorbents or substrates. The adsorption phenomenon is caused by several types of inter-molecular forces (charge and concentration differences, chemical reactions and shape or size effects to name few), either strong or weak [53, 55]. The adsorption mechanism can be distinguished between [58, 59]:

- Physical adsorption or Physisorption, involving the attraction of adsorbates driven by Van der Waals forces with a lower energy release (10-40 kJ/mol).
- Chemical adsorption or Chemisorption, involving the formation of chemical bonds with consequent higher energy release (80-200 kJ/mol).

The complete review of the main differences between Chemisorption and Physisorption is provided by Ruthven [60].

2.3.1. Adsorption Thermodynamics and Equilibrium

From a thermodynamic point of view, the concentration of a substance from the vapor phase onto a solid surface corresponds to a reduction in freedom of motion of molecules and thereby to a loss in system entropy ΔS. As such, the attraction of species to a solid surface translates typically into an exothermic interaction, which corresponds in a negative sign of ΔH, to maintain a favorable free-energy driving force ΔG. The explanation of ΔH < 0 is found in the energy level of solid and fluid (bulk) phases. Since the molecules located on the surface of the solid do not have all their bonds occupied by the neighboring molecules, they are at a higher energy level and tend to attract species from lower energy state coming from the bulk [61]. In the correlation below, it is possible to evaluate the effect of enthalpy and entropy on the driving force:

$$\Delta G = \Delta H - T\Delta S \tag{2.2}$$

The sign of ΔG is dependent on the dominant mechanism in the adsorption process.

- $\Delta S > \Delta H$, species prefer to be in the bulk (desorbed state).
- $\Delta S < \Delta H$, species tend to be adsorbed.

It is clear how a reduction in temperature will favour the adsorption of species and vice versa. It results that temperature represents a key parameter to control the Gibbs free energy difference and the tendency of the system towards adsorption/desorption. Therefore, when a vapor is adsorbed onto a previously unoccupied solid surface or its pore space, the amount of the vapor adsorbed is proportional to [58]:

- Solid mass.
- Temperature.
- Equilibrium of the vapor partial pressure.
- The nature of the solid and vapor.

Theoretical design of these processes requires numerical integration of rigorous, non-isothermal, and non-isobaric process models using boundary conditions for the process steps [35]. Nevertheless, many

theoretical models are applied under the condition of fixed temperature (T). The adsorbed quantity per unit mass of the solid is then only a function of the pressure (p). The relation between the adsorbed quantity and p at a given T is called adsorption isotherm [58]. The adsorption isotherm is the dynamic equilibrium relationship between the concentration in the fluid phase and the concentration in the adsorbent particles at a given T.

For pure gases, experimental physical adsorption isotherms, in amount adsorbed with respect to the partial pressure or concentration have shapes that are classified into five types by Brunauer, in which the amount adsorbed is reported with respect to the concentration as it can be noted in Figure 2.3. It stands out how isotherm type I is a typical example of favorable isotherm because a relatively high solid loading can be achieved with moderate concentration in the fluid. An isotherm that is concave upward is called unfavorable because relatively low solid loadings are obtained and because it leads to quite long mass-transfer zones in the bed (type III). Both types I and II are desirable isotherms, exhibiting strong adsorption, even at lower concentrations. Nevertheless, it is relevant to point out that there is a possibility of obtaining a limiting case of a very favorable isotherm: irreversible adsorption, where the amount adsorbed is independent of concentration down to very low values that might be problematic in case of a regeneration step [53, 52].

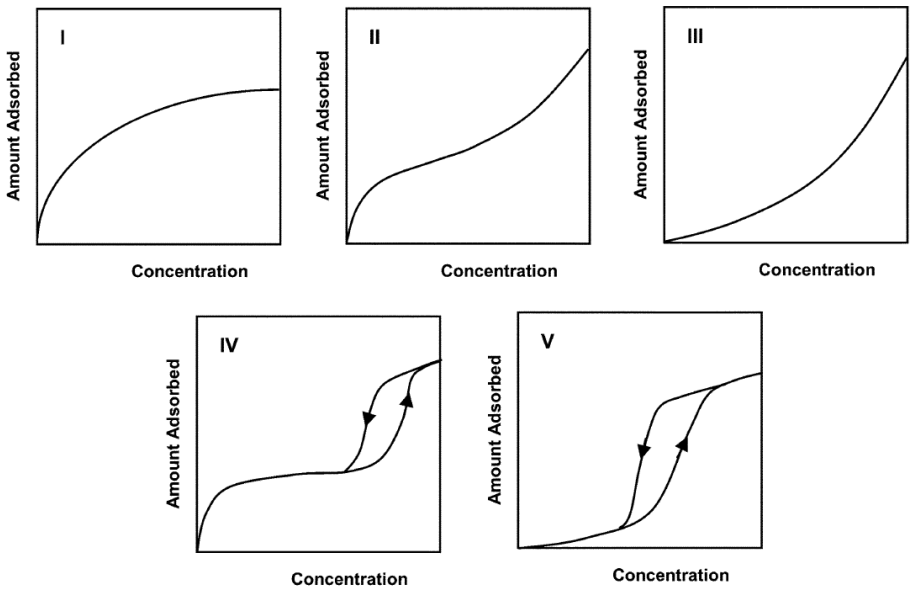

Figure 2.3: The Brunauer classification of adsorption isotherms [52].

2.3.2. Kinetics

The rate of physical adsorption is usually controlled by diffusion limitations. Therefore, the adsorption of a chemical species onto a porous solid surface forecasts four main steps:

1. External mass transfer of the impurity from the bulk fluid through a thin film or boundary layer, to the outer solid surface of the adsorbent.
2. Internal mass transfer of the impurity by pore diffusion from the outer surface of the adsorbent to the inner surface of the internal pore structure.
3. Surface diffusion along the internal pore structure
4. Adsorption onto the porous surface

During regeneration of the adsorbent, the reverse of the four steps occurs. However, under most practical conditions, the internal mass transfer step is ruling over adsorption/desorption mechanisms due to the fact that the external film resistance is rarely rate limiting [52]. The representation of the different regions treated in the present study is shown in Figure 2.4 [55]:

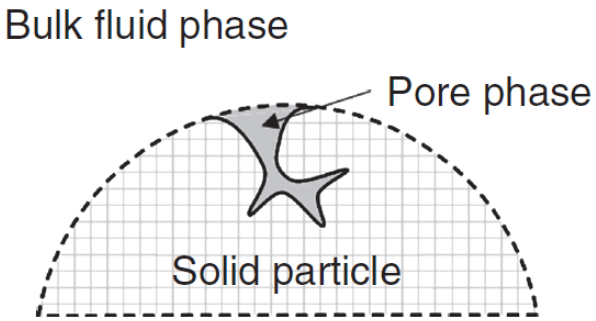

Figure 2.4: The phases involved in the adsorption process [55].

2.3.3. Adsorption equipment

A typical system used for adsorption foresees the placement of adsorbents particles in a packed or fixed bed configuration. The systems are usually designed in such a way that there is always a column that is accepting feed gas, in order to have a continuous flow of purified gas, while the other columns are being regenerated. The size of the adsorbent bed is function of the flowrate and cycle time. Ideally, a long bed is preferred because increases the adsorption cycle and capacity. On the other hand, large size beds lead to higher pressure drop and capital cost.

In fixed-bed adsorption, the concentrations patterns in the fluid and solid phase vary according to time and space of the bed as shown in Figure 2.5. Assuming a bed completely regenerated, most of the mass transfer takes place near the inlet of the bed. It can be noted that at t_1, the concentration in the fluid relative to that in the feed (C/C_0) drops exponentially. Moreover, in the second time-frame t_2, the solid near the inlet is nearly saturated, and most of the mass transfer takes place further from the inlet [53]. The reason for the 'S' shaped concentration gradient is related to external and internal mass transfer resistance and axial dispersion [52].

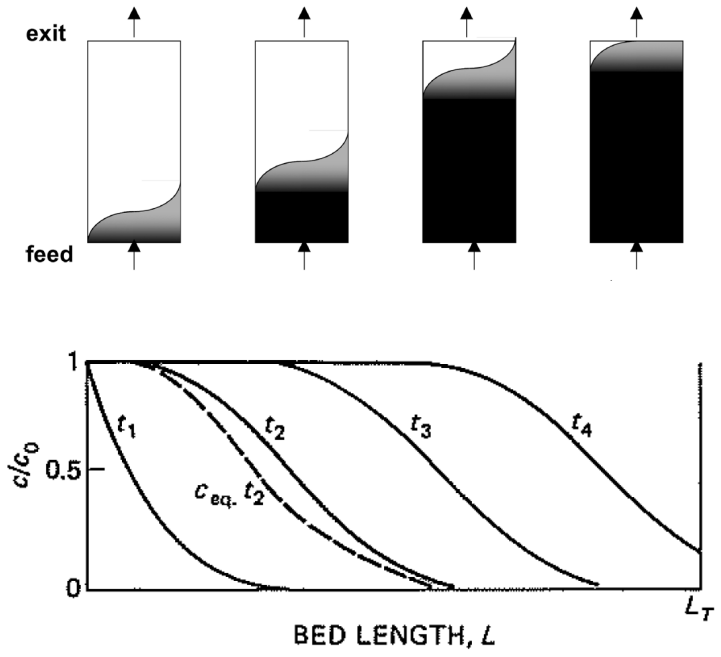

Figure 2.5: Concentration profiles along the bed (top) [52]. Concentration profiles based on different time-frames in fixed bed adsorption (bottom) [53].

However, these profiles can be predicted and used in calculating the curve of concentration with respect to time for fluid leaving the bed, also called "Breakthrough curve". At the inlet of the bed, during the instants

t_1 and t_2, the adsorbent has become saturated and in equilibrium with the adsorbate in the inlet fluid. As presented in Figure 2.6, the exit concentration is zero because the bed is still in the loading phase. Starting from t_3, the exit concentration is increasing until the instant t_b also referred as the break-point time, in which the flow is redirected to a fresh adsorbent bed. The break point is often taken as a relative concentration of 0.05 or 0.10. In case the bed is not switched, the concentration rises sharply to C/C_0 = 0.5 and more slowly towards a saturation point (C/C_0 = 1) in which no mass transfer is happening since the bed is not able to accept the species in the fluid. The region between t_b and saturation point is the Mass-Transfer Zone (MTZ), where adsorption takes place. The width of the MTZ is expressed as a function of the mass transfer rate, flow rate and shape of the equilibrium curve [53].

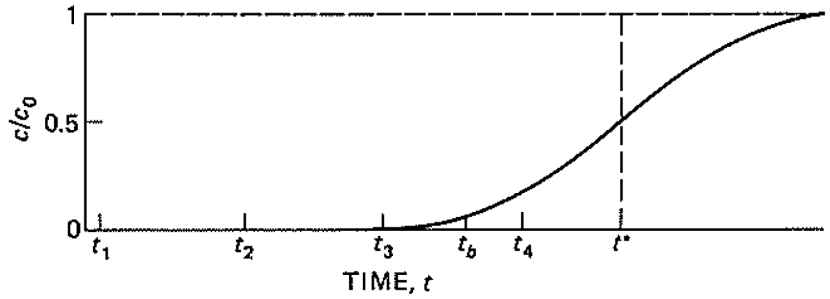

Figure 2.6: Breakthrough curve for fixed bed adsorption [53].

Clearly, Figure 2.5 and 2.6 appear to be nearly symmetrical. Some of the reason which might cause asymmetry are: mass transfer resistance in the column (e.g. diffusion of species through outer/inner layers before landing on the solid), dispersion or diffusion effects due to change in temperature and adsorption kinetics. From Figure 2.6 it is possible to evaluate the quantity that will exit the bed and most importantly the capacity of the bed at any given point in time and space of the bed. Equations 2.3 and 2.4 are used as an example of computation for capacity out and accumulated of the bed at the break point time:

$$C_{out} = \dot{F} \int_0^{t_b} C \, dt \tag{2.3}$$

$$C_{Acc} = C_{in} - C_{out} = \dot{F} C_0 t_b - \dot{F} \int_0^{t_b} C \, dt \; = \dot{F} \int_0^{t_b} (C_0 - C) \, dt \tag{2.4}$$

Cycle time and consequently selecting the right break point time will govern the adsorption capability and size of the bed. The break point time separates the capacity of used (left) and unused bed (right) as shown in Figure 2.6. To back up this statement, designing an early break point time will guarantee a higher purity of the product; on the other hand, the unused capacity will be higher as well, necessitating a larger bed to achieve the same degree of separation.

Nevertheless, with regards to high-purity hydrogen production from a gas mixture, PSA processes has become the state of the art technology in the chemical and petrochemical industries. To confirm this statement, a 2010 study has shown that over 85% of current global H_2 production units use PSA technology for H_2 purification [35]. Furthermore, for continuous PSA separation processes, the idea is to operate the beds using at least two steps [55]:

- Adsorption, during which the adsorbent selectively retains the adsorbed species from the feed. Typically, for large scale applications, the flow is switched when a bed is saturated.
- Regeneration, happening when the adsorbent releases the retained species and thus regenerating the adsorbent for use in the next cycle.

As there are only a limited number of methods that accomplish the release in the regeneration phase usually done by either changing the pressure (PSA) or the temperature (Temperature Swing Adsorption or TSA) [55, 62]. As seen in Equation 2.2, temperature and pressure revealed to be key parameters for adsorption and regeneration. PSA is, overall, more common than TSA especially for continuous operations due to the fact that PSA can be accomplished much more quickly than TSA. In addition to that, TSA in

general has a higher energy energy requirement and according to Golmakani et al. [63], it results more efficient in case there is a source of waste heat nearby to exploit. Nevertheless, advantages for TSA appear during regeneration step of strongly adsorbed species, since the increase in temperature is more effective than pressure to to release species or phases [55].

2.3.4. PSA systems: Basic operating sequence

A PSA plant consists of the adsorber vessels containing the adsorbent material, tail gas drum(s), valve skid(s) with interconnecting piping, control valves and instrumentation and a control system for control of the unit. The PSA process has the following elementary process steps [35, 55, 64, 65, 66]:

Adsorption
Adsorption of impurities is carried out at the highest pressure of the system being determined by the pressure of the feed gas (between 10-40 bar [64]). The feed gas flows through the adsorber vessels in an upward direction and highly pure H_2 exits the adsorber vessel at top.

Co-current depressurising/Pressure equalisation
The adsorption bed is co-currently depressurised to an intermediate pressure level between the high and the low pressure. A H_2-rich stream is withdrawn from the product end and is passed to another adsorption bed undergoing a complementary pressurising pressure equalisation step. According to [65], 1-4 of pressure equalization steps are performed in order to minimize H_2 losses and increase the product recovery rate because H_2 is still present in the void space of the adsorbent material.

Co-current providing purge
The adsorption bed is co-currently depressurised to an intermediate pressure level. A pure H_2 stream is obtained from this step, ready to purge or regenerate another bed.

Counter-current blowdown
The adsorption bed is counter-currently depressurised to prevent break-through of impurities at the top of the adsorber. In this step the lowest pressure of the PSA cycle is achieved (around 1-3 bar [64]). An outgoing stream is extracted at the feed end containing a portion of the desorbed impurities.

Counter-current purge
Desorption of the bed at the lowest pressure by a H_2-rich stream, withdrawn from another bed. Desorbed impurities follow the tail gas line.

Counter-current pressurising/Pressure equalisation
Before restarting adsorption, the regenerated adsorber must be pressurized again. This is accomplished in the pressure equalization step by using pure H_2 from adsorbers presently under depressurization (usually with a split stream from the H_2 product line). This sequence is operated to lower the energy consumption with regards to the pressurization system.

Counter-current product pressurisation
The adsorption bed is counter-currently pressurised to the adsorption pressure by introducing at the product end a portion of H_2 product withdrawn during the adsorption step.

Idle
The adsorption bed is disconnected from the surroundings with no gas streams flowing into or out of the bed. This step may be required for bed synchronization purposes.

The relevance of multibed systems is highlighted in a study carried out by Luberti et al. [64], in which general methods to improve H_2 PSA performance are assessed [2]. To provide continuous H_2 supply, a minimum of 4 adsorber vessels are required. Figure 2.7 encapsulates how the main process steps mutually interact with each other, exchanging pressurized streams of material, within a 4 beds configuration developed by Linde.

[2] For completeness of the analysis, the multibed criteria for PSA improvement are reported in Appendix B.

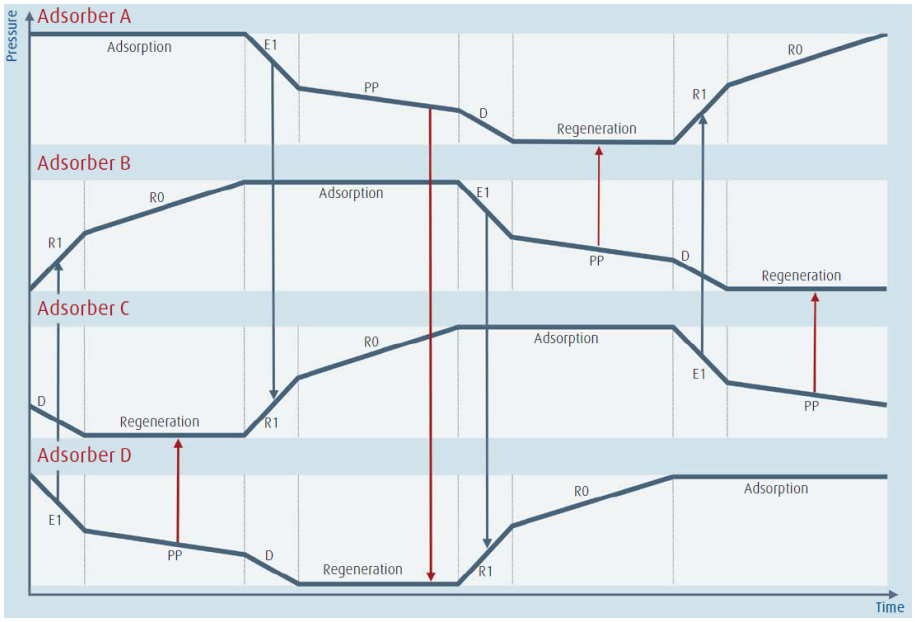

Figure 2.7: Pressure time diagram for the 4 beds system developed by Linde [65].

2.3.5. Industrial adsorbents for H_2 production in PSA units

Usually, the role of the adsorbent is to provide the selectivity and capacity required for the separation of a mixture. Since the adsorption forces reflect the nature of the adsorbing molecule and the characteristics of the substrate, different substances are adsorbed with different affinities, as shown in table 6.2 and 6.3 of the book of de Haan et al. [52]. Besides a high selectivity, the adsorption capacity represents another relevant feature of the adsorbents as anticipated in Section 2.3.1, determining the size of the bed.

While designing a PSA unit, the capacity relates directly to the size and cost of the adsorbent bed. To achieve a high adsorption capacity commercial adsorbents are made from microporous materials with a high specific area, typically in the range of 300 to 1200 m^2/g. Porous particles are usually selected for adsorption technologies, making a trade-off based on the following considerations:

- Small porous particles cover a large inner area per m^3, a higher capacity and pressure drop. Consequently, high pressure drop lead to higher pressure to apply to the system to facilitate the passage of the fluid in the packed bed and in some extreme scenario could lead to cracks in the bed.
- Large porous particles have a small inner area per m^3, a lower capacity and pressure drop. On the other hand, employing larger particles results in a lower degree of utilization.

A review on the most viable commercial gas adsorbents is illustrated by many sources [35, 52, 56]. Silica gel, activated carbon, molecular sieve zeolite and activated alumina were proven to be the most effective for large scale applications from a technical and economic point of view.

Abdeljaoued et al. [67] suggest that PSA units typically present a first layer, acting as a guard bed, composed of alumina or silica gel to essentially adsorb H_2O; the second is composed of activated carbon, which adsorbs CH_4, CO, CO_2 and traces of sulfur components; and as a third layer, zeolites are used for improved adsorption of CO, N_2 and other trace components. It is relevant to highlight the fact that strongly adsorbed species on porous materials could be difficult to desorb during regeneration cycles, such as CO_2 in zeolites. Table 2.1 presents qualitative adsorption features for different industrial adsorbents [64]:

2.4. Combined Heat and Power

Combined Heat and Power plants can deliver concurrent production of electricity and useful thermal energy from a common fuel. CHP units are generally classified by the type of application, in particular: heating and/or cooling of buildings and industries, power generation at a reasonable price with the availability of back-up and top-up power. Since CHP plants are usually sized to meet heat demand, any excess

Table 2.1: Difficulty of impurity removal per adsorbent in H_2 PSA systems [64].

	Silica gel	Activated carbons	Zeolites
H_2O	Very easy	Very difficult	Very easy
C_2H_4	Easy	Very easy	Very easy
C_4H_{10}	Easy	Very easy	Very easy
C_3H_8	Easy	Easy	Very easy
C_2H_6	Moderate	Easy	Very easy
CO_2	Moderate	Easy	Very easy
CH_4	Moderate	Easy	Moderate
CO	Moderate	Moderate	Easy
N_2	Difficult	Difficult	Moderate
Ar	Difficult	Difficult	Difficult
H_2	Very difficult	Very difficult	Very difficult

electricity can be sold back to the grid or supplied directly to another customer via a distribution system [68]. From a technical standpoint, CHP plants consist of four basic elements: a prime mover (engine or drive system), an electricity generator, a heat recovery system and a control system. Nevertheless, it is relevant to note that the energy conversion device, alongside with its requirements, dictates the gas that can be fed in it [69, 70].

The general idea is to run the CHP engine autonomously. However, due to fluctuations in the market it could be advantageous to cover any additional electricity and heat needs at the site respectively with the grid and stand-by boilers or boost heaters. Therefore, in accordance with the project strategies, it will be necessary to integrate the CHP unit within an optimal distance with the energy supply and demand stations, promoting an abatement of transmission losses.

Hagos et al. [70], found that syngas-fuelled engine with a direct injection system is expected to have better engine power output. Moreover, an extended literature survey for similar low heating values (LHV) biomass derived syngas revealed that lean burn fuelling, variation of ignition timing and compression ratios are among the most relevant tuning parameters. It was observed that the increase in H_2 content in the syngas is proportional to higher brake thermal efficiency, Nitrogen Oxides (NO_x) emissions, as well as LHV. In summary, reduction of torque was reported in most of research with syngas as compared to their fossil-based counterparts. Consequently, higher volume of gas to produce equal amount of power are demanded. Final process and technology selections are based on a trade-off between technical and economic aspects. Below, some of the parameters that influence design choices:

- Oxidant injection in the gasifier which will vary syngas composition and therefore the LHV and the acceptability in engines.
- Environmental impact of pollutants (especially NO_x and SO_x) and the feasibility of flue gases procedures to respect emission regulations.
- Auxiliary storage mechanisms to counter-act market fluctuations.

2.5. Simulation Tools: Aspen Plus and Aspen Adsorption

In this study, two packages of the industry-standard simulation tools Aspen Tech were utilized (Aspen Plus and Aspen Adsorption) to model and analyze the renewable H_2 production coming from a waste derived syngas. It is relevant to point out that there is a lack of in depth analysis regarding the Aspen Adsorption package. In this section, an extensive analysis will be carried out, to understand and summarize the most important features of Aspen Adsorption. Nevertheless, for completeness sake, a general description of the Aspen Plus package will be provided as well as the relevant literature concerning Aspen Plus simulation for syngas cleaning and purification units.

2.5.1. Aspen Plus

Aspen Plus is a widely used process simulation software developed by Aspen Technology. It is renowned for its versatility in simulating various chemical processes, particularly those involving separation, reaction and thermodynamics. Aspen Plus provides a comprehensive platform for designing and optimizing process flowsheets, enabling engineers to perform detailed mass and energy balances, as well as assessing the performance of different unit operations. In this work, Aspen Plus was utilized to model the syngas adjustment and purification as well as the combined heat and power unit, enabling the prediction of the overall process behavior and technical performance.

Francois et al. [71], implemented an Aspen Plus® model with Fortran sub-models to predict the performance of CHP biomass gasification plant. The results obtained were compared with the current state of the art plant, giving relevant insights for the purpose of a techno-economic study.

Nicolaou [72] developed a tar removal system using biodiesel in Aspen Plus® based on wet-model theories. Two validation experiments were conducted to confirm Aspen Plus® accuracy. Methyl-palmitate oil was used instead of biodiesel in the scrubber due to similar properties. Since tar solubility and absorption data in biodiesel were limited, a simulation predicted their theoretical solubility. The wet model was tested using data from Synvalor and Guessing plants, and the simulation results were compared with the actual plant cleaning systems.

[73, 74] are two useful sources with regards to step by step approach for an amine based absorption plus stripping columns. In particular, the former is a reference book for process modellers in ProMax, Aspen Plus®, Aspen HYSYS and Invensys Pro/II environments. On the other hand, the latter reference, aims to develop a H_2 production unit model evaluating in detail the absorption based methyldiethanolamine (aMDEA) process in the attempt of minimizing energy consumption for solvent regeneration while obtaining a 90% carbon removal.

Pellegrini et al. [75], analyzed a state of the art steam methane reforming plant aimed at producing 100,000 m^3/h of H_2 via PSA. The resulting tail gas, once carbon dioxide was removed, was directed to the burners of the SMR unit. The primary focus of this research was the design of units to treat the PSA tail gas, utilizing an aqueous solution of MDEA. Simulations were conducted using the ASPEN Plus® considering various column configurations for the absorber and regenerator.

Costa et al. [46] developed a H_2 generation unit via purification and adjustment of a SMR syngas. The plant was simulated combining Aspen Plus® and MATLAB®, obtaining key insights from a process engineering standpoint and more specifically, a better understanding of the dynamic behavior of a PSA system for H_2 purification (despite the simplifying assumptions made in the model).

2.5.2. Aspen Adsorption

Aspen Adsorption is a specialized software tool also developed by Aspen Technology, tailored for the simulation and analysis of adsorption processes. This software is specifically designed to handle complex gas and liquid adsorption systems. Aspen Adsorption offers capabilities to model and optimize adsorption cycles, including the design of adsorption beds, selection of adsorbents, and prediction of breakthrough curves.

The main sequential steps for every simulation using Aspen Adsorption are illustrated in Figure 2.8 [55, 76, 77, 78]. The initial step in constructing simulation models entails incorporating components. This can be accomplished by importing components from Aspen Properties software or by utilizing custom properties, often input through FORTRAN code.

Next, two simulation modes for gas phase adsorption processes are available: the gas Dynamic and gas CSS (gCSS) simulation modes. The former is suitable for non-cyclic adsorption processes (e.g. breakthrough experiments), while the latter is tailored for cyclic adsorption processes. While these modes share functionality and configuration similarities, they enable the software to execute diverse numerical methods to solve mass, momentum and energy balances.

Moreover, creating the simulation worksheet involves using models such as: beds, tank voids, valves, gas feed and products and lastly gas interaction units. Each one has input data to define to replicate the behavior of real unit operations. All these models can be interconnected through Gas Material Connection Streams and come with initial default values for all required specifications.

The Gas Bed model facilitates the representation of the adsorption process and necessitates comprehensive input regarding the bed's properties and the underlying physical phenomena.

In case of in cyclic processes such as PSA, a Cycle Organizer is integrated in the model to delineate the specific sequence of actions the bed will undergo throughout the cycle. Initially, the number of steps in the cycle needs to be established, with each step being assigned a name. Subsequently, the manipulated variables for each step can be selected. Once each step is meticulously defined, the software must be instructed regarding the timing of transitions from one step to the next. This entails three primary options: time-driven, event-driven or step-dependent.

Partial differential equations (PDE), ordinary differential equations (ODE) and algebraic equations are utilized by Aspen to encapsulate mass, momentum and energy balances. When equipped with appropriate initial and boundary conditions, they comprehensively describe the adsorption process. The Aspen Adsorption Reference Guide [79] to enhance accuracy, stability and simulation time. In addition to that, discretization methods and solver options in both simulation modes are configurable features in Aspen Adsorption. Different approaches for non-linear solvers (e.g. Newton and Fast Newton) and integrators (e.g. Implicit and Explicit Euler) should be tested, with tolerances and step sizes adjusted to optimize results.

Once the problem is fully defined, and numerical methods are selected, the simulation can be initialized and run. Upon completion, the simulation results can be extracted and presented. Results can be visualized through time series plots or profile plots.

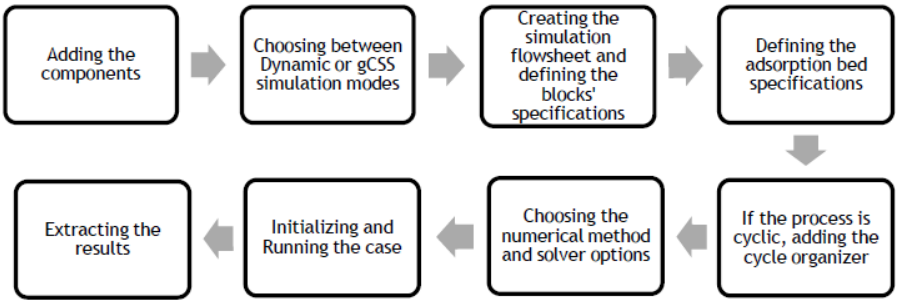

Figure 2.8: Flow diagram for the main steps for a simulation in Aspen Adsorption [76].

In this research, Aspen Adsorption was employed to simulate and analyze the adsorption process, facilitating the study of adsorbent characteristics, breakthrough behavior and overall process performance. Table 2.2 presents the feedstock type and composition, PSA model and the adsorbents utilized in the relevant literature that served as benchmarks for this study.

Table 2.2: Summary of references with regards to Aspen Adsorption simulation of PSA.

Ref.	Feedstock	Model	Adsorbents	Description
[80]	Coal gas (H2/CO2/CH4/CO/N2 = 38/50/1/1/10 vol%)	2 beds PSA with 6 steps	Activated carbon and Zeolite 5A	The model's accuracy was validated through experimental data comparison. A sensitivity analysis was performed with regards to adsorbents height ratio to optimize purity, recovery and productivity.
[81]	Biogas (CH4/CO2 = 55/45 mol%)	6 dual-bed PSA with 6 steps	Carbon Molecular Sieve (CMS-3K)	After completing a verification study, indication with regards to bed design were illustrated. In this case the sensitivity analysis is extended to feed flowrate, adsorption time and pressure with respect to H_2 purity.
[82]	Steam methane reforming syngas (H2/CH4/CO/CO2 = 72.9/3.6/4.5/19 mol%)	2 beds PSA with 6 steps	Activated carbon and Zeolite 5A	Detailed information are provided regarding cycle definition. The analysis revealed that feed composition as well as purge to feed (P/F) ratio have significant consequence on purity and recovery.
[83]	Syngas (H2/CO = 70/30 mol%)	1 bed PSA with 5 steps and 2 beds PSA with 6 steps	Zeolite 5A	A study of the temperature profiles of the single bed configuration in comparison with the experimental data anticipates the parametric study.
[67]	Bio-Ethanol reformed gas (H2/CO2/CH4/CO = 73/25/1/1 mol%)	4 beds PSA with 12 steps	Activated carbon	After revising the experimental section, in depth justification for Aspen Adsorption parameters are evaluated (specifically, regarding isotherm selection and discretization methods).
[84]	Steam reforming and Autothermal reforming Biogas (CH4/CO2/CO/H2/H20/N2 = Variable in mol%)	4 beds PSA with 10 steps	Activated carbon and Zeolite 5A	The 4 beds interaction is clearly expressed in terms of cycle time, scheduling and pressure gradients.

3

Material and Methods

In this chapter, the methods and tools used for the project development are explained, with a particular focus on the stoichiometry and equations expressed valid for the techno-economic assessment.

3.1. Process route Mapping

The process map provides insights into technology selection and justification, as well as the market alternatives. Figure 2.1 illustrates the main block for the WtH chain: Syngas Adjustment, Syngas Purification, Pressure Swing Adsorption and Combined Heat and Power units.

During the initial conceptual phase of the plant design, rigorous specifications were identified based on a comprehensive review of existing literature, reference projects, and input from potential vendors. As depicted in Figure 3.1, a decision tree flow chart was conceived to guide the design process.

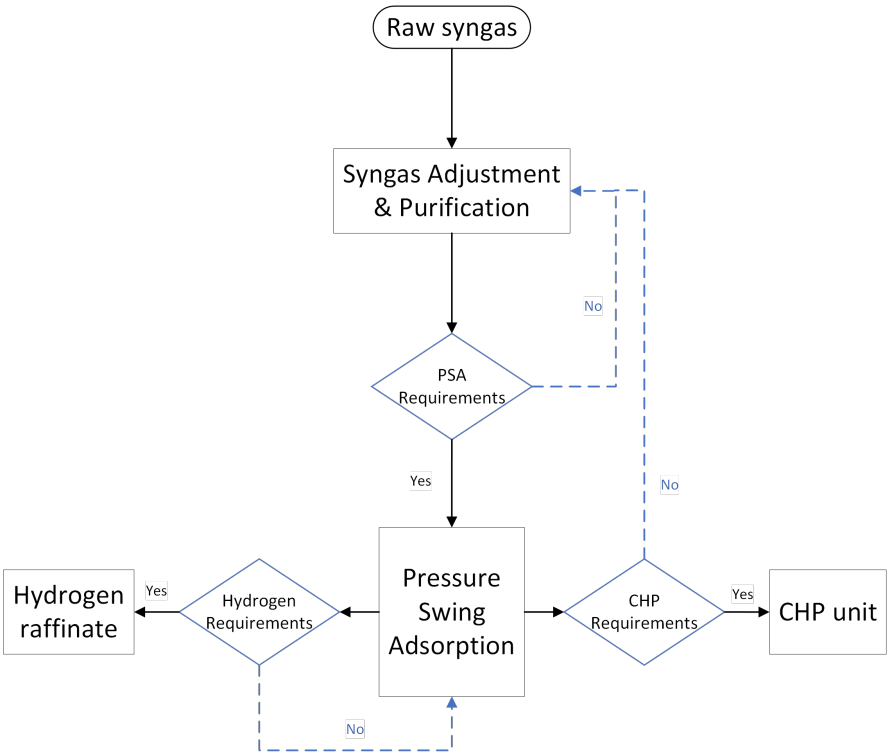

Figure 3.1: Decision tree flowchart for the conceptual phase. Black arrows = the process stream, blue dotted arrows = iterative steps

Upon acquiring data for a typical raw syngas stream from a HTW Gasification process, it became

evident that the implementation of a syngas adjustment and purification unit was necessary to eliminate specific contaminants prior to the PSA process. It should be noted that if the requirements for the PSA, H_2 raffinate, and CHP generation units are not met as per the established criteria, the design process necessitates iterative adjustments and adaptations to ensure compliance with the specified standards and operational objectives. This iterative approach is essential to achieve the desired performance and efficiency in the plant's operation (black arrows = the process stream, blue dotted arrows = iterative steps). Table 3.1 provides information on the type of equipment chosen by design in comparison with a market alternative.

Table 3.1: Process route mapping for technology selection.

Equipment	Selection Justification	Market Alternative
Sour Syngas Adjustment	The syngas adjustment unit is aimed at enhancing the H_2 composition of the syngas. It comprises: • High-Temperature WGS, to convert CO into H_2. • Hydrolysis Reactor, COS and HCN conversion. • Low-Temperature WGS, to convert CO into H_2.	Hydrolysis reaction to remove sulfur in the form of H_2S before the syngas entered the two WGS reactors. However, this approach was ultimately discarded due to: • The inclusion of a ZnO bed would have increased both capital and operational expenditures, thus rendering it less economically viable. • Comprehensive information on operational reliability from industry experts for the sour route.
Bio-Diesel Absorption column	Bio-Diesel from third generation biomass represents a valuable alternative in the optic of sustainability. C_6H_6 and $C_{10}H_8$ may cause clogs and condensation on the adsorbents of the PSA and must be removed. A stripping column operates with low pressure steam to regenerate bio-Diesel.	A two stages scrubber working with oil (for tar) and water (for NH_3) was discarded due to negative performance in simultaneous removal of impurities and solvent recovery.
Water Absorption column	High NH_3 removal efficiency [71], which needs to be separated before the PSA and in case of H_2 use in fuel cell applications.	The double stage scrubber is not able to remove the high content of water in the syngas which would have harmed the adsorbents in the PSA and required the purchase of a guard bed (e.g. based on silica gel [35]) to remove the significant amount of water.
Aqueous MDEA Absorption column	Removal of CO_2 and H_2S. Part of the CO_2 is separated due to: • Reduced column size. Retaining all CO_2 within the syngas would require each of the four beds in a PSA unit to be 8 meters tall, resulting in significant changes to system hydrodynamics, pressure drop, safety factors and overall costs. • Efficient use of the tail gas. The tail gas coming from the PSA is a mixture of CO_2, H_2 and CH_4. Its inadequate composition, would have made this stream not suitable for combustion or direct use in greenhouses.	Physical solvents such as Methanol are overlooked due to the acid gas loading curve with respect to pressure [85].

3.2. Methodology

The development of a techno-economic analysis for a H_2 plant model necessitates a precise delineation of optimal operating conditions, key performance indicators, equipment sizing and utility consumption. The approach adopted reflects (partially) the methodology carried out by Alamia et al.[86] and comprises two distinct phases: a data analysis phase and process simulation phase.

During the data analysis phase, experimental data is assimilated into the mass and energy balance equations to compute the input variables (associated with their uncertainties) needed to be imported in the simulator. These derived parameters are dependent by boundary conditions provided by vendors [87, 88] or literature. Conversely, in the process simulation phase, the input variables are fed into the Aspen Tech environment. This is the phase where all the assumptions are put into action. Subsequently, process simulation results are obtained (associated with their uncertainties) ready to be analysed from a technical and economic point of view. Figure 3.2 presents the two distinct phases described above.

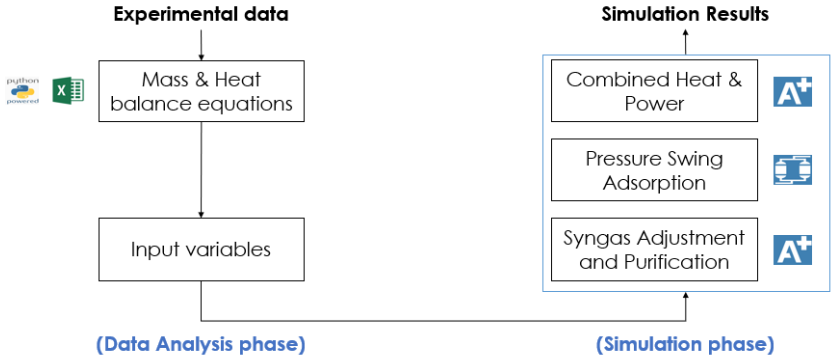

Figure 3.2: Methodology for utilization of the data analysis and process simulation phases.

Following the conceptual flowchart of Figure 2.1 the feedstock, composed by 75% RDF and 25% waste wood is directed towards the HTW-unit. The HTW-unit is a complex technology as it includes process units dedicated to performing the gasification of the feedstock, cooling down the syngas, removing solid particles and conducting an initial gas cleaning step. Dust is removed by a combination of filters and scrubbers, whilst the gas cleaning step is a caustic soda wash that aims at removing all chlorine, part of sulfur, NH_3 and HCN. It is out of the scope of this thesis to model the entire HTW-unit. Instead, the starting point for this study is the product stream of the HTW-unit. Table 3.2 provides input specification for raw syngas stream.

Table 3.2: Saturated raw syngas specifications.

Specification	**Value**
Temperature [°C]	141.2
Pressure [bara]	12.6
Mole Flow [kmol/h]	1951.32
Composition	**[mol%]**
H_2	24.6
CO	19.73
CO_2	19.64
CH_4	4.88
N_2	0.2
Traces	30.95

3.3. Syngas adjustment unit

The adjustment of the syngas composition involves 3 primary units: the High Temperature Water Gas Shift Reactor (HT-WGSR), the Hydrolysis reactor and the Low Temperature Water Gas Shift Reactor (LT-WGSR). The sizing of the first 2 reactors is determined based on the flow rate of the reactors used in similar industrial units, ensuring that they can effectively catalyze the desired chemical reactions. However, particular attention is directed towards the LT-WGSR, which is sized using the Ergun equation (Equation 3.1). In this context, the Ergun equation is used to calculate the height of the LT-WGSR, comprising a Cobalt-Molybdenum (CoMo) catalyst. The equation is inverted to determine the required vessel height, with the assumption of a targeted pressure drop of 0.6 bar. Additionally, pertinent vessel data are extracted from a reliable source [89]. Appendix C provides the typical physical properties of a sour shift catalyst.

$$H = \frac{\Delta_p \cdot d_p^2 \cdot \epsilon^3}{150 \cdot (1-\epsilon)^2 \cdot \mu \cdot u + (1.75 \cdot \rho \cdot u^2 \cdot (1-\epsilon) \cdot d_p)} \tag{3.1}$$

The stoichiometry with regards to the WGS reaction is provided in Equation 2.1 while the 2 hydrolysis reaction are documented in Equations 3.2 and 3.3.

$$COS + H_2O \rightarrow H_2S + CO_2 \tag{3.2}$$

$$HCN + H_2O \rightarrow NH_3 + CO \tag{3.3}$$

3.4. Syngas purification unit

This unit is dedicated to the purification of syngas prior to the PSA and consists of the following elements: the bio-Diesel absorption and stripping columns, the water absorption column and the aqueous MDEA absorption and stripping columns. Appendix D provides all the data required to validate this section's equations.

3.4.1. Bio-Diesel Absorption column

The bio-Diesel absorption column is based on a black-box approach, which calculates three main parameters necessary for the purpose of the techno-economic assessment: the minimum bio-Diesel solvent flow rate, the tar removal efficiency and the column sizing. The minimum flow rate of bio-Diesel L_{min}, operating at 50 °C and 1 bar, is computed through a mass balance applied to the entire absorber system, assuming that equilibrium is achieved between the incoming gas G, y_{in} and the outgoing liquid at the bottom L, x_{out} of the column, as illustrated in Figure 3.3.

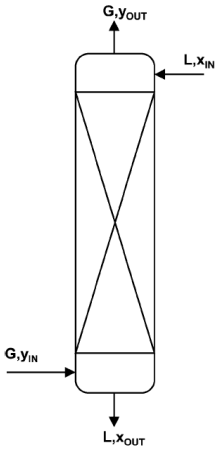

Figure 3.3: Continuous, steady-state operation in a counter-current column [52].

The overall mass balance across the column, under the equilibrium conditions depicted above in which is given by Equation 3.4 provided in the book of de Haan et al. [52]:

$$L_{\text{min}} = \frac{G_{\text{in}} \cdot (y_{\text{in}} - y_{\text{out}})}{x_{\text{max}} - x_{\text{in}}} = \frac{G_{\text{in}} \cdot (y_{\text{in}} - y_{\text{out}})}{\frac{y_{\text{in}}}{K} - x_{\text{in}}} \tag{3.4}$$

Where:

- x_{in} and x_{max}: mole fraction of component(s) to be absorbed (solute) in the liquid phase respectively in and out (theoretically highest possible concentration) the column.
- y_{in} and y_{out}: mole fraction of component(s) in the gas phase respectively in and out the column.
- K: equilibrium constant.

It is relevant to note that in case of the minimum bio-Diesel flow rate, a correction factor of 1.5 was accounted in accordance with the book of de Haan et al. [52]. The composition of the bio-Diesel implemented within the simulator, originates from Wet Spirulina sp. and is obtained through a One-Step Extraction-Transesterification process based on the procedures outlined by Pradana et al. [90]. Table 3.3 presents the results of GC-MS analysis of the bio-Diesel produced from Spirulina sp.

Table 3.3: Fatty acid composition of bio-Diesel derived from Spirulina sp. [90].

Component	Chemical Formula	Yield [wt %]
Methyl Palmitate	$C_{17}H_{34}O_2$	41.03
Methyl Linoleate	$C_{19}H_{34}O_2$	8.34
Methyl Oleate	$C_{19}H_{36}O_2$	45.10
Methyl Stearate	$C_{19}H_{38}O_2$	5.54

With regards to columns sizing, each one is conceived following the same method and computed according to a set of equations below for the column diameter and hydraulic check calculation. First, the diameter of the column is determined, followed by a subsequent assessment of the column's flooding percentage through a hydraulic check as reported below.

Column diameter calculations

$$\frac{L'}{G'}\frac{G}{L} = \frac{M_{\text{L}} + M_{\text{solute}}}{M_{\text{G}}}\left(\frac{\rho_{\text{G}}}{\rho_{\text{L}}}\right)^{0.5} \tag{3.5}$$

$$\frac{L'}{G'}\frac{G}{L} \rightarrow \text{Fig. 6.34 of [91]} \rightarrow \frac{(G')^2 C_f (\mu_L)^{0.1} J}{\rho_G(\rho_L - \rho_G) g_C} \tag{3.6}$$

$$\frac{(G')^2 C_f (\mu_L)^{0.1} J}{\rho_G(\rho_L - \rho_G) g_C} \rightarrow G' \tag{3.7}$$

$$A_{\text{cs}} = \frac{M_{\text{G}}}{G'} \tag{3.8}$$

$$D = \left(4 \cdot \frac{A_{\text{cs}}}{\pi}\right)^{0.5} \tag{3.9}$$

Hydraulic check calculations

$$\frac{L'}{G'}\frac{G}{L} \rightarrow \text{Fig. 11.44 of [92]} \rightarrow K_4, K_{4\text{flood}} \tag{3.10}$$

$$Trial_{\text{flood}} = \left(\frac{K_4}{K_{4\text{flood}}}\right)^{0.5} \cdot 100 \tag{3.11}$$

$$V_m = \left(\frac{K_4 \rho_G(\rho_L - \rho_G)}{13.1 F_P \left(\frac{\mu_L}{\rho_L}\right)^{0.1}}\right)^{0.5} \tag{3.12}$$

$$Trial_{A_{\text{cs}}} = \frac{M_{\text{G}}}{V_m} \rightarrow D_{\text{Tr}} \rightarrow D \rightarrow A_{\text{cs}} \tag{3.13}$$

$$flood\% = Trial_{\text{flood}} \frac{Trial_{A_{\text{cs}}}}{A_{\text{cs}}} \tag{3.14}$$

Appendix D includes a review of the input parameters to find all the 4 columns key specifications. The sizing is then completed by fixing the length to diameter ratio (L/D) parameter, equal to 4.5 for the Bio-Diesel absorption and stripping columns and the Aqueous MDEA absorption and stripping columns in accordance with [93].

3.4.2. Bio-Diesel Stripping column

Following the same concept derived from Figure 3.3, a similar procedure is carried out to express the minimum stripping gas flow rate of low pressure steam (G_{min}), injected at 159 °C and 6 bar, for a stripper in Equation 3.15. The input parameters for the low pressure steam flowrate necessary to strip the bio-Diesel can be found in Appendix D.

$$G_{\text{min}} = \frac{L_{\text{in}} \cdot (x_{\text{in}} - x_{\text{out}})}{y_{\text{max}} - y_{\text{in}}} = \frac{L_{\text{in}} \cdot (x_{\text{in}} - x_{\text{out}})}{K \cdot x_{\text{in}} - y_{\text{in}}} \tag{3.15}$$

3.4.3. Water Absorption column

For the water absorption column, two main chemical equations representing the reversible reaction between NH_3 and H_2O, for which in the forward reaction, hydroxide ions (OH^-) and ammonium ions (NH_4^+) are produced. The second reaction describing the reversible reaction of water splitting into OH^- and hydronium ions (H_3O^+). Equations 3.16 and 3.17 present the two stoichiometric reactions involved in the water absorption column.

$$NH_3 + H_2O \rightleftharpoons OH^- + NH_4^+ \tag{3.16}$$

$$2H_2O \rightleftharpoons OH^- + H_3O^+ \tag{3.17}$$

3.4.4. Aqueous MDEA Absorption and Stripping columns

The result of the PSA unit is a H_2 raffinate and a tail gas, constituted mainly by CO_2, H_2, CH_4, CO and N_2. During the initial stages of this study, it proved challenging to establish a market value for the tail gas produced by the PSA. In conclusion, the designed plant incorporates a CHP unit for burning tail gas from the PSA. However, as outlined by Hagos et al. [70], certain CO_2 concentration limits must be met in the tail gas for it to be combustible. Thus, an MDEA absorption unit is placed before the PSA to separate the CO_2 from the syngas (Figure 3.4). Hagos et al. [70] presented a table summarizing various syngas compositions suitable for combustion. This data proves valuable for determining the quantity of CO_2 that needs to be eliminated in the MDEA absorption column while ensuring the final low heating value of the tail gas (from the PSA) remains above 10 MJ/kg. Equilibrium calculations, executed through Aspen Plus (as represented by Equation 3.4), are employed to establish the minimum values of CO_2 removal. Figure 3.4 illustrates the iterative conceptual design process (black arrows = the process stream, blue dotted arrow = iterative steps).

The reactions for the absorption (forward direction) and stripping (backwards direction) for aqueous MDEA are presented in the Equations 3.18 to 3.23. These are based on the work done by Adams et al. [73] for an MDEA industrial plant.

$$H_2O + MDEA^+ \rightleftharpoons MDEA + H_3O^+ \tag{3.18}$$

$$H_2O + HCO_3^- \rightleftharpoons CO_3^{2-} + H_3O^+ \tag{3.19}$$

$$2H_2O + CO_2 \rightleftharpoons HCO_3^- + H_3O^+ \tag{3.20}$$

$$H_2O + HS^- \rightleftharpoons H_3O^+ + S^{2-} \tag{3.21}$$

$$2H_2O \rightleftharpoons OH^- + H_3O^+ \tag{3.22}$$

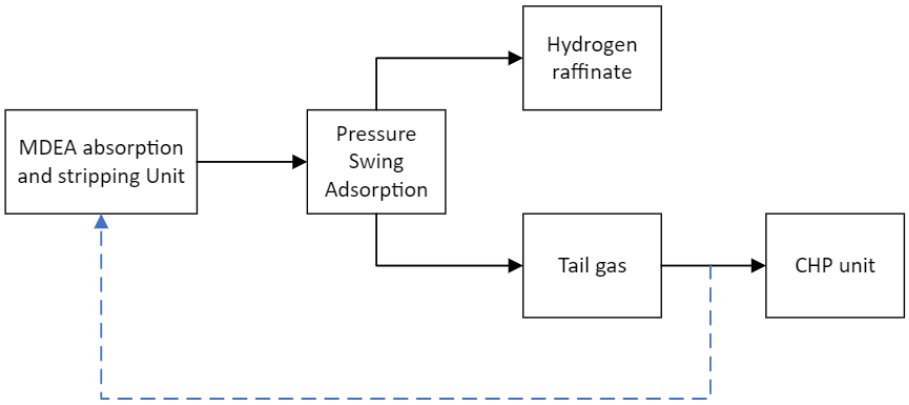

Figure 3.4: Iterative methods for the conceptual CO_2 capture.

$$H_2O + H_2S \rightleftharpoons H_3O^+ + HS^- \tag{3.23}$$

In addition, since the stripper unit does not achieve full solvent recovery efficiency, a makeup stream containing fresh solvent (water and MDEA) into the plant's configuration must be integrated (Equation 3.24 and 3.25). This assumption is in agreement with [73].

$$F_{\text{MDEA,Makeup}} = F_{\text{MDEA,CO2 Product}} + F_{\text{MDEA,CleanedSyngas}} \tag{3.24}$$

$$F_{\text{H2O,Makeup}} = F_{\text{H2O,CO2 Product}} + F_{\text{H2O,CleanedSyngas}} - F_{\text{H2O,SyngasFeed}} \tag{3.25}$$

Centrifugal compressor calculations

Before the syngas is fed to the PSA system, it must be compressed to a pressure of 15 bar for the designed application. A step by step guideline for compressor design is provided by the Engineering company INTECH GmbH [94]. First, the compression rate x must be defined so the final pressure after each stage (for n=1,...,N) can be calculated. Intech and Atlas Copco corporations offer insights into determining the optimal number of stages for a centrifugal compressor in syngas applications [94, 95]. As a result, a single-stage centrifugal compressor is considered.

$$x = n\sqrt{\frac{p_f}{p_i}} \tag{3.26}$$

$$p_{fi} = p_i \cdot x^n \tag{3.27}$$

The rise in temperature as a result of compression is a factor that also needs be taken into consideration to ensure the longevity of equipment and its ability to withstand thermal stress. Thus, the temperature evolution along the compressor is defined as:

$$T_2 = T_1 \left(\frac{p_2}{p_1}\right)^{\frac{k-1}{k}} \tag{3.28}$$

Where $k = cp/cv$ and indicates the ratio between the specific heat capacity at constant pressure divided by the specific heat capacity at constant volume. In this study the maximum allowed temperature increase is 150 °C (with attached cooling before PSA) due to material properties indicated by company Atlas Copco [95]. The compressor is assumed to be a polytropic centrifugal compressor. Mechanical efficiency is set to 90%, and the polytropic efficiency is determined using Equation 3.29 in [96], where Q_v represents the flow rate at the inlet in m^3/h:

$$\eta_p = 0.61 + 0.03\log\left(0.5885 Q_v\right) \tag{3.29}$$

3.4.5. Pressure Swing Adsorption

The design of a Pressure Swing Adsorption system comprises sizing of the columns, validating isotherm models and operational conditions, and establishing cycle schedules. These steps are described below.

Bed sizing calculations

The first design approach to size the beds and valves of a PSA was developed by Dr. Louis Theodore in 1985 and later published in 1988 [97]. Theodore's approach is re-adapted in the present work and summarized in the following steps. The input data to calculate the bed sizes can be retrieved from Appendix E.

1. Select the adsorbent type and size.
2. Choose the cycle time; estimate the regeneration time; set the adsorption time equal to the regeneration time.
3. Set the velocity v, typically between 0.15-0.5 m/s [53].
4. Obtain the adsorption working capacity (WC) from the adsorption isotherm curve at a certain defined pressure. The isotherm curve can be obtained from literature or adsorbent vendors.
5. Calculate the amount of impurity adsorbed during the cycle time, denoted as M_{imp}.
6. Calculate the required amount of adsorbent, denoted as M_{AC}, using the equation: $M_{AC} = \frac{M_{\text{imp}}}{WC}$.
7. Determine the adsorbent volume requirement, denoted as V_{AC}, using the equation: $V_{AC} = \frac{M_{AC}}{\rho_{\text{Ad}}}$, where ρ_{Ad} represents the adsorbent density.
8. Calculate the face area of the bed, denoted as A_{AC}, using the equation: $A_{AC} = \frac{Q_v}{v}$, where Q_v represents the gas flow rate.
9. Calculate the bed height, denoted as H, using the equation: $H = \frac{V}{A_{AC}}$.
10. Set the L/D ratio.
11. Calculate D using the L/D ratio, while adhering to the constraints: $D \leq 2.5$ m and $L \leq 9$ m; an L/D ratio of 2–4 is acceptable.

.

Adsorption isotherm selection

Designing adsorbers is challenging due to the lack of experimental data for mixture adsorption equilibria. As a result, a common practice in the field is to predict mixture isotherms by leveraging the data obtained from pure component isotherms. Furthermore, the Aspen Adsorption guide [78] states that even when model parameters are derived from the exact same data set, the use of different models can yield substantially distinct simulation results. Several methods for predicting mixture isotherms from pure component data are proposed in Aspen Adsorption literature [78]. Here are a few examples of typical ones ones:

- Extended Langmuir isotherm (ExL) [78]: introduces a weighting factor to account for the inter-species interactions present in mixtures. The ExL approach takes a parameter from the single-component gas isotherm and, depending on the components of the multi-component gas mixture, calculates a fitting parameter to account for the presence of other components.
- Dual Site Langmuir (DSL): which assumes that there are two kinds of adsorption sites with different adsorption energies [67, 98].
- Ideal Adsorbed Solution Theory (IAS) [78]: this model uses experimental data for pure-component adsorption equilibria at the same temperature and for the same adsorbent material. The IAS model treats the mixed adsorbate phase as an ideal solution in equilibrium with the gas phase, utilizing the Gibbs approach for vapor-liquid equilibria. Despite initial skepticism about ideal behavior in the adsorbed phase, numerous systems have exhibited robust correlations between experimental data and IAS theory predictions. These systems encompass binary and ternary mixtures adsorbed on diverse substrates such as activated carbons, zeolites, and silica gel. Notably, IAS is available as an option in Aspen Adsorption, enabling users to implement it by selecting the appropriate isotherm on the Isotherm Tab within the layer configuration form.

The efficacy of various adsorbents within a singular adsorption step is assessed in Aspen Adsorption.

The primary objective was to discern which adsorption model exhibited superior performance in maintaining H_2 purity levels at or above 99.9% over extended periods of adsorption. Longer adsorption times (for the same bed length) are indicative of increased H_2 productivity, a key factor in assessing the economic viability of the Waste to H_2 project.

To do so, four simulations are implemented for the following isotherms: Extended Langmuir 1, Extended Langmuir 2, Extended Langmuir 3 and Dual Site Langmuir. The fundamental aspects that remained invariant across the four simulations included the maintenance of the identical flowsheet and operating conditions:

- Feed temperature of 298.15 K and a pressure of 15 bar.
- Empty bed and tank voids (CH4/CO/CO2/H2 = 0/0/0/1 mol%)
- Feed composition (CH4/CO/CO2/H2 = 9/1/16/74 mol%)
- Product boundary pressure of 1.013 bar.

Such stringent adherence to consistency in operating conditions, boundary conditions, and feed composition ensures that any discernible variations in H_2 purity across the adsorbent models can be confidently attributed to the inherent characteristics of each adsorption model. The lack of relevant literature and validation studies with regards to IAS for this study's feed composition discarded the use of IAS. Table 3.4 evaluates different adsorbents and related isotherm models.

Table 3.4: Adsorbents and Isotherm Types

Ref.	Adsorbent(s)	Isotherm type
[82]	Activated Carbon and Zeolite 5A	Extended Langmuir 1 (ExL1)
[99]	Activated Carbon and Zeolite 5A	Extended Langmuir 2 (ExL2)
[80]	Activated Carbon and Zeolite 5A	Extended Langmuir 3 (ExL3)
[67]	Activated Carbon	Dual Site Langmuir (DSL)

The comparative analysis serves as an indicator for selecting the isotherm that can significantly prolong the adsorption duration, consequently enhancing H_2 productivity and its associated economic value. The choice of the adsorption isotherm is guided by the remarkable performance of the Extended Langmuir isotherm 3 of the adsorbents used by Xiao et al. [80]. At the same time, the selection process was influenced by the absence of certain species in the syngas composition based on literature, particularly the values pertaining to N_2. This absence strengthen the decision to adopt the adsorbents' isotherm studied by Xiao et al. [80], as it provided comprehensive data for the this study.

Adsorption isotherm validation

The generated adsorption model (Appendix E) is compared against an existing literature study [80] for an adsorption step using a one bed PSA. This validation process was carried out to assess the accuracy and reliability of our model when applied to a one-bed PSA system. The model uses activated carbon and zeolite 5A as adsorbents to capture the four major impurities in the syngas prior PSA. The behavior of the two adsorbents is described using the Extended Langmuir isotherm model as done by Xiao et al. [80]. Since the source of Xiao et al. [80] did not report any specifications for valves and gas tank void, the control valve specification was determined using Equation 3.30. The control valve specification c_v is equal to the flow rate divided by the pressure difference in and out of the bed. The gas tank void was left as default in Aspen Plus. The complete analysis of the flowsheet for the validation model is presented in Appendix E.

$$c_v = \frac{\dot{F}}{p_{\text{in}} - p_{\text{out}}} \tag{3.30}$$

Validation of isotherm conditions: Temperature evolution

After validating and selecting the model, it is necessary to perform a counter-check of the isotherm conditions. As discussed in Chapter 2, physical adsorption phenomena involve the release of energy. To

ensure the maintenance of isotherm conditions, a simplified mass and energy balance is formulated to calculate the temperature evolution within an empty bed during a single adsorption cycle. The formulation presents the following major assumptions:

- Heat transfer between wall and bed is neglected.
- Adiabatic column.
- Constant pressure and velocity over the reactor length.

Equation 3.31 represents the energy balance and is constituted by three terms respectively representing: the gas and solid phase enthalpy of accumulation, the gas convective term and the generation of energy term due to heat of adsorption.

$$(\varepsilon\rho_g c_{\text{pg}} + \rho_b c_s)\frac{\delta T}{\delta t} + (\varepsilon\rho_g c_{\text{pg}})v\frac{\delta T}{\delta z} + \rho_b \sum_{J=1}^{n} \frac{\delta q_j}{\delta t}\Delta H_j = 0 \tag{3.31}$$

Equation 3.31 can only be solved incorporating the mass balance of the amount of species adsorbed over the column. Therefore, Equation 3.32 is repeated for all the species (indicated by the j subscript).

$$\frac{\delta q_j}{\delta t} = k_f(q_j^* - q_j) \tag{3.32}$$

In which, the information on the type of isotherm used (Extended Langmuir model) is deconstructed in Equation 3.33.

$$q_j^* = \frac{q_j^s b_j p_j}{1 + \sum_{j=1}^{n} b_j p_j} \tag{3.33}$$

$$q_j^s = (k_1 + k_2 T) \tag{3.34}$$

$$b_j = k_3 exp(\frac{k_4}{T}) \tag{3.35}$$

The algorithm for the isothermal conditions verification is provided in Appendix E.

Cycle scheduling

Jain et al. [100] provide a guideline to conceptualize a PSA cycle. All the considerations have been adapted based on the process simulation environment. Nevertheless, a list of governing concepts and equations is listed for clarity, which reflects the information illustrated in Chapter 2.

- Selection of adsorption pressure.
- Selection of adsorption time, the adsorption time is determined by the breakthrough time. Nevertheless, it was determined based on single bed adsorption simulation in Aspen Adsorption, based on H_2 output purity (to be kept $\geq$99%).
- CO_2 penetration in the Zeolite 5A layer (to be kept $\leq$3%), avoiding the attachment in the adsorbent during depressurization.
- During the cycle, a bed might adsorb while another is purging. A pure H_2 stream from the product line is used for purging and therefore a trade-off between productivity and recovery has to be made. In this study the effect of purge to feed ratio (P/F) is parameterized with the value of 0.15.
- Pressure equalization steps are necessary to increase the recovery of H_2 and established before an intermediate level of pressure. A typical value of intermediate pressure is reported as $\frac{p_I}{p_L} = (0.5 - 0.8)\frac{p_H}{p_L}$.
- Pressurization time, the heuristic rule proposed a ratio equal to: $\frac{t_{\text{press}}}{t_{\text{ads}}} = 0.0 - 0.2$.
- Blow-down time, in which the ratio $\frac{t_{\text{blow}}}{t_{\text{ads}}} = 0.15 - 0.7$.

3.4.6. Combined Heat and Power

The tail gas separated in the pressure swing adsorption is conducted in the Combined Heat and Power unit for utilization in a combustion engine. As illustrated in Chapter 2, conventional operating procedures for syngas combustion necessitate an over-stoichiometric oxidant ratio. INNIO Jenbacher's provided data played a pivotal role in evaluating thermal and electrical outputs, as well as the operational parameters for input air. The stoichiometry is documented below.

$$CH_4 + 2O_2 \rightarrow CO_2 + 2H_2O \tag{3.36}$$

$$CO + 0.5O_2 \rightarrow CO_2 \tag{3.37}$$

$$H_2 + 0.5O_2 \rightarrow H_2O \tag{3.38}$$

Moreover, a set of equations is applied to find the quantity of air needed for burning the tail gas. The j stands for the component to be burned, namely CO, CH_4 and H_2.

$$O_{2_j} = W_j \cdot \nu_j \tag{3.39}$$

$$O_{2_{\text{Tot}}} = \sum_{j=1}^{n} O_{2_j} \tag{3.40}$$

$$M_{\text{air}} = c_{\text{fac}} \cdot \text{Mw}_{\text{air}} \cdot \left(\frac{O_{2_{\text{Tot}}}}{\text{O}_{\text{2frac}}} \right) \tag{3.41}$$

With regards to the recoverable thermal and electrical power out, a correction factor based on flow rate of the nominal engine output (JMS 420 GS-S.L co-generation unit [101]) is used. It is relevant to note that the recoverable thermal output is assumed to be used for the generation of low pressure steam.

$$P_{\text{out}} = \frac{F_{\text{Des}}}{F_{\text{INNIO}}} \cdot P_{\text{INNIO}} \tag{3.42}$$

$$Q_{\text{out}} = \frac{F_{\text{Des}}}{F_{\text{INNIO}}} \cdot Q_{\text{INNIO}} \tag{3.43}$$

$$M_{\text{LPsteam}} = \frac{Q_{\text{out}}}{c_p \cdot \Delta T} \tag{3.44}$$

The technical datasheet by INNIO Jenbacher is found in Appendx F.

3.5. Simulation phase

In accordance with Figure 3.2, the second phase entails transferring the data derived from the data analysis phase into Aspen Tech software. The initial platform employed for simulating syngas adjustment and purification was Aspen Plus. The ultimate syngas product is manually entered into Aspen Adsorption for PSA modelling. Subsequently, the PSA outputs are integrated back into Aspen Plus to simulate the CHP Unit. Finally, a comprehensive analysis, inclusive of uncertainties, is conducted on the outcomes obtained from Aspen Tech's various environments in a Techno-Economic analysis.

3.6. Techno-Economic assessment

3.6.1. Technical methodology

The technical assessment involves a comprehensive examination of various aspects related to the equipment's real-life application and explores potential alternatives for conducting sensitivity analyses. Within this assessment, significant emphasis is placed on the conceptualizationof the process and any issues or discrepancies in comparison to state of the art standards are scrutinized.

In this way, the technical assessment can be extended to three main topics:

- Conversion and separation efficiencies of the syngas adjustment and purification unit.
- PSA analysis, focused on isotherm model validation and comparison, bed and cycle analysis and Key Performance Indicators (KPI) tracking.
- Net Energy requirements of the developed system.

Conversion and separation efficiencies

The system's performance considers factors such as: conversion rates, overall process and separation efficiencies. These metrics are then compared with established market standards to gauge their competitiveness. Equation 3.45 serves to evaluate conversion and separation efficiencies for a generic chemical species j.

$$\eta_j = 1 - \frac{Out_j}{In_j} \tag{3.45}$$

Key Performance Indicators for Pressure Swing Adsorption systems

"KPI stands for key performance indicator, a quantifiable measure of performance over time for a specific objective" [102]. In this context, H_2 purity and recovery are the KPI considered for the evaluation of the PSA performances expressed in Equation 3.46 and 3.47:

$$PURITY = \frac{\int_0^{t_{\text{ads}}} x_{\text{H}_2,\text{2out}} \cdot \dot{n}_{\text{H}_2,\text{out}}\, dt}{\sum_{j=0}^{n_{\text{species}}} \int_0^{t_{\text{ads}}} x_{j,out} \cdot \dot{n}_{j,out}\, dt} \times 100 \tag{3.46}$$

$$RECOVERY = \frac{\int_0^{t_{\text{cycle}}} x_{\text{H}_2,\text{out}} \cdot \dot{n}_{\text{H}_2,\text{out}}\, dt}{\int_0^{t_{\text{cycle}}} x_{\text{H}_2,\text{in}} \cdot \dot{n}_{\text{H}_2,\text{in}}\, dt} \times 100 \tag{3.47}$$

Net Energy requirements

Before, calculating the net energy requirements of the system, a heat integration model is developed, incorporating pinch point analysis. This pinch point analysis aims to determine if it's feasible to efficiently reuse the heat generated by hot streams and is conducted based on the principles outlined in the Turton book [103].

Subsequently, an analysis of the energy requirements is investigated, deriving insights from utility consumption and output production. This comprehensive evaluation is critical in terms of highlighting system's energy demands and potential areas for internal supplement translated in Equation 3.48 and 3.49. Equation 3.48 refers to the Net Power requirement (NPR) obtained by subtracting Power generated ($Power_G$) and Power consumed ($Power_C$), while Equation 3.49 can be used to calculate the Net Heat duty (NHD) by the difference of Heat duty generated (HD_G) and Heat duty consumed (HD_C).

$$NPR = Power_G - Power_C \tag{3.48}$$

$$NHD = HD_G - HD_C \tag{3.49}$$

3.6.2. Economic methodology

The economic assessment is based on three main analysis:

- Capital expenditure (CAPEX).
- Operational and Maintenance expenditure (OPEX).
- Key Performance Indicators for the economic analysis: Return on Investment (ROI), Payback Period (PBP) and Levelized Cost of H_2 ($LCOH$).

Capital expenditure

The Total Capital Investment ($CTCI$) of a chemical plant or a chemical product manufacturing facility is a one-time expense for the design, construction, and startup of a new plant. $CTCI$ was calculated by first retrieving the purchase cost (C_P) of each individual unit. The purchase cost can be found using the correlations provided by Seider et al. [104] and are size-based. The units were either sized using Aspen

Plus, mass and heat balance correlations in the data analysis phase or by employing a flow rate ratio from a similarly sized HTW gasification unit.

Furthermore, equations listed in Appendix O calculate the costs based on reference book of Seider et al. [104] which uses 2013 pricing. To convert these to 2022 pricing, the Chemical Engineering Plant Cost Index (CEPCI) is used. The CEPCI begins with a value of 100 for 1957-1959 and is updated monthly to account for changes in price and technology. The CEPCI for 2013 is 567, while the value for June 2022 is 832.6 [105], resulting in a multiplication factor of 1.468.

Once the purchase cost of all units is calculated, the total ($C_{P_{\text{Tot}}}$) is determined. However, this value needs to be adjusted for location using the Investment Site Factor (FISF) since the calculations from [104] are based on the U.S. Gulf Coast. This factor takes into account differences in labor availability, workforce efficiency, local regulations and customs, union status, and other factors.

Subsequently, the Total Permanent Investment ($CTPI$) and $CTCI$ can be calculated using Equation 3.50 and 3.51. The factor of 1.05 in both equations accounts for equipment delivery. The Lang factors, f_{LTPI} and f_{LTCI}, are used to estimate $CTPI$ and $CTCI$. Originally based on 14 different chemical plants, these factors have been refined over the years by considering more than 150 capital cost analyses. For a this processing plant, the Lang factors are 4.28 and 5.03, respectively. $CTCI$also includes the cost of land, which is assumed to be 2% of $CTPI$.

$$CTPI = 1.05 \cdot f_{LTPI} \cdot C_{P_{\text{Tot}}} \tag{3.50}$$

$$CTCI = 1.05 \cdot f_{LTCI} \cdot C_{P_{\text{Tot}}} + C_{\text{land}} \tag{3.51}$$

The complete capital expenditure cost breakdown can be found in Appendix O.

Operational and Maintenance expenditure

Operational expenditure refers to the continuing costs associated with the operation of a chemical plant [104]. These ongoing costs comprise various components, including:

- Cost of raw materials, catalysts, adsorbents and chemicals consumed.
- Utility usage expenses.
- Labor costs.
- Maintenance expenses.
- Operating overhead.
- Taxes.
- Depreciation.

The operating expenditures are summed up and divided principally in total fixed and variable costs. The annual cost calculations are primarily based on equations and factors from Seider et al. [104]. Some specific costs, such as prices of catalysts and raw materials, are determined using data from from certain vendor specifications. The utilization of strippers unit required the definition of a general formulation for utilities requirements expressed in Equation 3.52 as:

$$Utility = Recycled + Makeup \cdot h/y \tag{3.52}$$

The cost of manufacture (COM) is obtained by the sum of the total variable cost (TVC) and the total fixed cost (TFC) as in Equation 3.53.

$$COM = TFC + TVC \tag{3.53}$$

Subsequently the amount of H_2 produced is used to calculate the sales, which are the source of an additional cost for the project defined as general expenses. Therefore the total production cost (TPC) is represented also by this quota and reported in Equation 3.54.

$$TPC = TFC + TVC + GeneralExpenses \tag{3.54}$$

The complete operational expenditure cost breakdown is presented in Appendix P.

Key Performance Indicators

Return on Investment

The return on investment (ROI) is a widely used financial metric that measures the profitability of an investment relative to its cost. It provides a way to assess the efficiency and effectiveness of an investment by calculating the return or gain generated compared to the initial investment. ROI is expressed as a percentage and is typically calculated using Equation 3.55:

$$ROI = \frac{Netearnings}{CTCI} \tag{3.55}$$

Payback Period

The payback period (PBP) is a financial metric used to assess the time it takes for an investment to generate enough cash flows to recover the initial investment cost. It helps in evaluating the risk and liquidity of an investment by indicating how quickly an investor can expect to recoup their initial capital. PBP can be evaluated as in Equation 3.56.

$$PBP = \frac{CTPI}{Netearnings + Annualdepreciation} \tag{3.56}$$

Levelized Cost of H_2

Similarly to the work carried by Di Marcoberardino et al. [84], the Levelized Cost of H_2 or $LCOH$ is calculated to assess the ultimate cost of H_2 production and then compared to typical industrial $LCOH$ values. The formulation is based on thermodynamic and economic findings, standardizing the cost of H_2 per kg generated. This cost calculation incorporates consumables, auxiliary expenses, and fixed costs, and it is defined by Equation 3.57:

$$LCOH = \frac{CTCI \cdot CCF + TFC + TVC \cdot h/y}{M_{H_2}} \tag{3.57}$$

In Equation 3.57, the plant's operational hours have been set at 7920, while the capital charge factor (CCF) has been determined as 0.16 in accordance with Di Marcoberardino et al. [84].

4

Model Development

This chapter covers the considerations for the model implementation. Each unit is described according to the simulation tool used to replicate real-life equipment, with a particular emphasis on the Pressure Swing Adsorption system due to a gap in existing literature.

4.1. Property method

Choosing an adequate physical property method is an essential first step when modeling in Aspen Plus, as it affects the accuracy of the simulation. Carlson provides a detailed guide about selecting the appropriate physical property method. Moreover, 4 factors should be considered when choosing the property method: the predictive capabilities of desired properties or results of each method, the composition of the mixture, the pressure and temperature range and the availability of parameters. Subsequently, Peng-Robinson has been chosen as the physical property method due to the non-polar nature of the input syngas for the simulation as well as the presence of real components [106].

4.2. Syngas Adjustment Unit

The simulation begins with the saturated raw syngas stream extracted from a typical HTW gasification unit. A heat network system based on stream re-circulation is implemented to elevate temperature of the raw syngas stream up to 340 °C. Medium-pressure steam (MPS) is injected in a `Mixer` alongside syngas upstream the high temperature shift reactor, which is modeled as an adiabatic equilibrium reactor using the block `REquil`. Subsequently, the process flows into the hydrolysis reactor, which is simulated with a stoichiometric `RStoic` block. The reactor operates adiabatically with a fixed conversion of HCN and COS of 99.99%. Next, a second shift reactor is used for the conversion of CO into H_2 at a lower temperature level (200 °C) modeled based on equilibrium (`REquil`). The syngas adjustment unit is modeled in Aspen Plus as illustrated in Appendix G.

4.3. Syngas Purification Unit

4.3.1. Bio-Diesel Absorption column

In the context of this study, the absorption and stripping columns are not properly modeled in Aspen Plus because it is considered outside the boundaries of the investigation. Although a more intricate approach has been proposed by Nicolaou [72], this study focuses on simulating the absorption column using a `Mixer` and a separator `Sep` block, while ensuring 99.9 % tar removal. Notably, any impacts related to energy consumption within the process of absorption in the column are disregarded in this study, as is the simulation of the stripper.

4.3.2. Water Absorption column

Based on the information provided by Carlson [106], the ELECNRTL base method in Aspen Plus is selected to simulate the water absorption column. In the Properties|Chemistry|Input|Equilibrium Constants the equilibrium constants for the 2 equilibrium reactions in Equation 3.16 and 3.17 are computed using the

same correlation (which parameters are automatically added by Aspen Plus after selecting the ELECNRTL method) formulated in Equation 4.1 as:

$$\ln(K_{\text{eq}}) = A + \frac{B}{T} + C\ln(T) + D \cdot T + E\left(\frac{p - p_{\text{ref}}}{p_{\text{ref}}}\right) \tag{4.1}$$

The water scrubber is developed using the `Radfrac` block that simulates the behaviour of absorption column. Achieving the correct limits of NH_3 removal is done by the equilibrium calculations performed by Aspen Plus, adopting a 2 equilibrium stages configuration for the volume of gas and relative impurity content. Therefore, two equal streams of water are sent above the first and the second stage of the absorption column to improve NH_3 capture efficiency. A `Design-Spec` block is added to regulate the flow of water to achieve the desired syngas output. The water coming down the column is assumed to be sent to a waste water treatment facility. The flowsheet scheme built in Aspen Plus is presented in Appendix I as well as the conditions needed for the water absorption column.

4.3.3. Aqueous MDEA Absorption and Stripping column

The aqueous MDEA system is conceived following step by step the indications of validated models reported by Adams et al. [73]. The major guidelines to build up the aqueous MDEA absorption and stripping columns are provided for clarity purposes.

In the context of Electrolyte-based models, the utilization of the Electrolyte Wizard is pivotal. This tool facilitates the inclusion of electrolyte reactions given from Equation 3.18-3.23 into the system. To initiate this process, it is key to designate the primary components actively involved in the electrolyte reactions (H_2O, CO_2 and MDEA), while H_2 ion type remains designated as H_3O^+. In the Methods|Selected Method section, the ELECNRTL method should also be present. In the simulation environment, a `Radfrac` block is added. On the configuration page, 20 stages as recommended by Adams et al. [73] are designated with no condenser or reboiler. Moving to the streams tab, it is specified that the syngas feed and the fresh solvent should be directed respectively on-stage 20 and 1. In the Pressure tab, the stage 1 pressure is configured to 7.7 bar, and no pressure drop for the rest of the column. Transitioning to the Blocks|<block name>| Specifications|Efficiencies tab, the efficiency type is designated as Murphree efficiencies, specifically opting for the ”Specify efficiencies for individual components” setting. Subsequently, within the Vapor–liquid tab, the Murphree efficiency value for CO_2 is uniformly adjusted to 33.3% across all 20 stages, in accordance with the provided instructions. The heat exchanger, connecting the absorber liquid product to the stripper bottoms, can be effectively simulated in Aspen Plus using the `HeatX` model. In this scenario, it is feasible to specify a 0.2 bar pressure drop for both the hot and cold sides, while setting the cold side outlet temperature to 110°C.

For modeling the stripper, another `Radfrac` block is employed, configuring the option for the reboiler (set to the default Kettle option) and the partial condenser. Selecting 19 equilibrium stages for the column, equivalent to 17 trays when accounting for the condenser and reboiler (stages 1 and 19) as operational stages, is recommended by Adams et al. [73]. The molar reflux ratio should be set to 0.011, and the molar boilup ratio to 0.2. Given the low-pressure operation of the stripper, a condenser pressure of 2 bar and a column pressure drop of 0.3 bar are specified in the pressure tab. The vapor product emerging from the stripper undergoes further cooling within a second partial condenser/flash drum simulated as a single flash separator `Flash2` model working under 40°C and a pressure drop of 0.1 bar. Subsequently, 2 `Mixer` blocks are added to merge the flash drum liquid product into a single solvent recycle stream and combine it with a fresh makeup solvent stream. Additionally, a `Heater` model is introduced to represent the recycle cooler, with an outlet temperature specification and no pressure drop. Finally, a `Pump` block is included with a discharge pressure specification of 7.7 bar. An efficient makeup feed stream, to input into the second mixer, should be at a temperature of 35°C and a pressure of 2 bar. Regarding the quantity, the flow rates of MDEA and H_2O must align with the flow rates of these two components lost via the CO_2 product and clean syngas streams as indicated in Equation 3.24 and 3.25.

The complete process flow sheet simulated in Aspen Plus is given in Appendix K.

4.3.4. Compression

The syngas must undergo compression to reach a pressure of 15 bar before entering the PSA system. Within Aspen Plus, the Compressor (`Compr`) block with the Polytropic model, employing the ASME method

under the Specifications|Type tab, is chosen. This selection is based on its ability to perform effectively across a broader range of compression ratios and feed compositions compared to the Polytropic model, using the GPSA method. Furthermore, in the Convergence|Valid phases tab, the Vapor-Liquid indication is enabled. This choice allows for the calculation of the two-phase state, which is essential for subsequent units such as the Heater and Flash to effectively cool down the syngas and handle any condensate that may form.

4.4. Pressure Swing Adsorption

Continuous adsorptive separation processes typically require a minimum of two sequential stages:

1. Adsorption Stage. In this step, the adsorbent selectively captures and holds onto the desired components from the incoming feed.
2. Regeneration or Desorption Stage. During this phase, the adsorbent releases the captured components, effectively renewing itself for subsequent cycles of operation.

4.4.1. Model Assumptions

The PSA model in Aspen Adsorption couples mass, momentum and energy balances across the packed bed. The following key assumptions underpin the model:

- Ideal gas behavior.
- Vertical type bed, defined in a 1-D spatial dimension. In the 1-D discretization, the spatial derivatives are evaluated in axial (flow) direction only.
- Isothermal energy balance, no cooling jackets are considered as well as no re-pressurization of the feed.
- Convection-based material balance, which assumes zero dispersion, therefore a Peclet number tending to infinity.
- Ergun equation for the momentum balance which is valid for both laminar and turbulent flow.
- Linear Driving Force (LDF) to approximate the adsorption rate.
- Multi-component Adsorption equilibrium, represented by the extended Langmuir isotherm based on partial pressure.

These assumptions collectively form the basis for the mathematical framework that elucidates the complex behavior of the PSA system. For a complete review of the assumptions, please refer to Appendix L.

4.4.2. Aspen Adsorption Flow sheet

The following Gas Dynamic blocks are used to build up the simulation flowsheet:

- A `gas_feed` and 2 `gas_product` blocks to respectively simulate the `Feed`, product (`Prod`) and `Waste`.
- 4 `gas_valves`, namely the feed valve (`VF`), product valve (`VP`), data connection valve (`VD`) and a waste valve (`VW`).
- 2 `gas_tank_void` blocks, designated to establish the boundary conditions of the bed layer, one at the bottom (`TV1`) and the other at the top (`TV2`).
- `Gas_bed` block, which is used to simulate the adsorbent layers (`BED`).
- `Gas_interaction` unit, an essential component for mimicking fictional beds (`UNI`).
- `Cycle_Organizer` block, responsible for defining the cycle scheduling.

The Aspen Adsorption flow sheet is illustrated in Figure 4.1.

The Component Set is selected to obtain more detailed simulations through the association of each component with a comprehensive list of optional parameters and physical properties. These properties are automatically derived from the Aspen property system, eliminating the need for additional user input.

Furthermore, the chosen property method for these simulations is the Peng–Robinson method, as recommended in relevant references [55, 106]. Subsequently, control over the PSA process was achieved

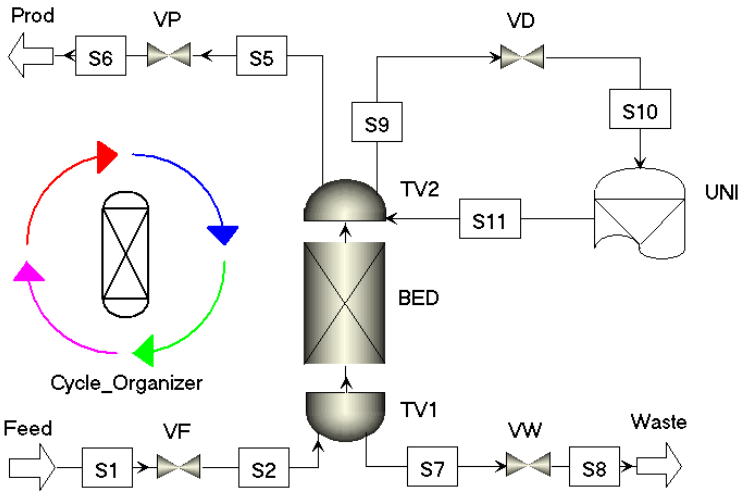

Figure 4.1: Aspen Adsorption PSA flowsheet scheme.

by setting fixed pressures and allowing the software to dynamically adjust the flow rates for the various blocks.

To fully specify the simulation, users are required to input the necessary details for the `Feed` stream, including flowrate, composition(s) in the forward direction and boundary pressure. With respect to `Prod` and `Waste`, only the boundary pressure value serves as a input. Additionally, parameters related to tank voids must be defined, and the linear features of valves should be configured using the correlation referenced in the Appendix L.

4.4.3. Adsorption Isotherm for rigorous bed definition

The adsorption rate is given by the LDF model described by Equation 3.32, where the parameter expressing the saturation capacity is strictly dependent on the type of isotherm selected. Equation 3.32 is the formal representation of the Extended Langmuir isotherm. For clarity purposes, the same equation adapted for Aspen Adsorption implementation is re-proposed in Equation 4.2.

$$q_j^* = \frac{(IP1_j - IP2_j \cdot T) \cdot IP3_j \cdot exp\left(\frac{IP4_j}{T}\right) p_j}{1 + \sum_{j=1}^{n} IP3_j \cdot exp\left(\frac{IP4_j}{T}\right) p_j} \tag{4.2}$$

The adsorption isotherm parameters for the two layers (Activated carbon and Zeolite 5A) are taken from the work of Xiao et al. [80] and re-adapted to be directly implemented in Aspen Adsorption. Table 4.1 illustrates the values for the five different chemical species.

Table 4.1: Activated carbon and Zeolite 5A isotherms parameters.

Activated Carbon					
	CH4	CO	CO2	H2	N2
MTC [1/s]	1.95E-01	1.50E-01	3.55E-02	7.00E-01	2.61E-01
IP1 [kmol/kg]	2.39E-02	3.39E-02	2.88E-02	1.69E-02	1.64E-03
IP2 [kmol/kgK]	5.62E-05	9.07E-05	7.00E-05	2.10E-05	7.30E-07
IP3 [1/bar]	3.48E-03	2.31E-04	0.01	6.25E-05	0.0545
IP4 [K]	1.16E+03	1.75E+03	1030	1.23E+03	326
Zeolite 5A					
	CH4	CO	CO2	H2	N2
MTC [1/s]	1.47E-01	6.30E-02	1.35E-02	7.00E-01	9.90E-02
IP1 [kmol/kg]	5.83E-03	1.18E-02	1.00E-02	4.31E-03	4.81E-03
IP2 [kmol/kg K]	1.19E-05	3.13E-05	1.86E-05	1.06E-05	6.68E-06
IP3 [1/bar]	6.05E-07	2.02E-02	1.58E+00	2.52E-03	5.70E-04
IP4 [K]	1.73E+03	7.63E+02	2.07E+02	4.58E+02	1.53E+03

4.4.4. The Cycle Organizer

A typical cyclic sequence for the four-bed PSA is coded, consisting of 8 steps:

1. Adsorption (ADS): adsorption takes place in one column. Part of the H2-rich product stream is used to purge the other columns counter-currently.
2. First depressurization (ED1): the column is co-currently depressurized to a lower pressure level. The depressurization stream is used to pressurize another column undergoing step (EP1).
3. Second depressurization (ED2): pressure is further reduced co-currently to a pressure level of equalization of two beds.
4. Blow down (BD): the column is counter-currently depressurized to the minimum pressure (atmospheric for PSA). The effluent gas or tail gas is directed towards the CHP unit.
5. Purge (PG): the column is purged with H_2 produced in step (1).
6. First pressurization (EP1).
7. Second pressurization (EP2) up to pressure equalization level.
8. Feed pressurization (RP): the bed is co-currently pressurized with feed entering from the bottom of the column.

For each simulation, the time step has been optimized to meet the H_2 purity requirement as well as desired pressure gradients. The cycle is scheduled according to a fictitious 2 beds PSA configuration in the Unibed approach. The visual representation of the 8 steps for the Unibed approach is presented in Figure 4.2.

In Aspen Adsorption the Cycle Organizer allows the user to rapidly create the steps that define a cyclic process. The tools available to set up the cycle are mainly related to the Cycle (such as creating and activating cycles) or the Step controls (such as defining steps, manipulation of variables and interaction between steps).

Table 4.2 reviews the manipulated variables for each step. The value for the 4 valves represents their ”Active Specification”, where Aspen Adsorption considers:

- Valve fully off = 0. The valve is completely closed.
- Valve fully on = 1. The valve is acting as a valve with high cv, fully open.
- Valve with specified Cv = 2. The valve is imposed to regulate the flow of gas with respect to the pressure drop, specifying a constant value for cv in kmol/s bar.
- Valve with specified flowrate = 3. The valve is imposed to regulate the flow of gas at a constant value set in kmol/s.

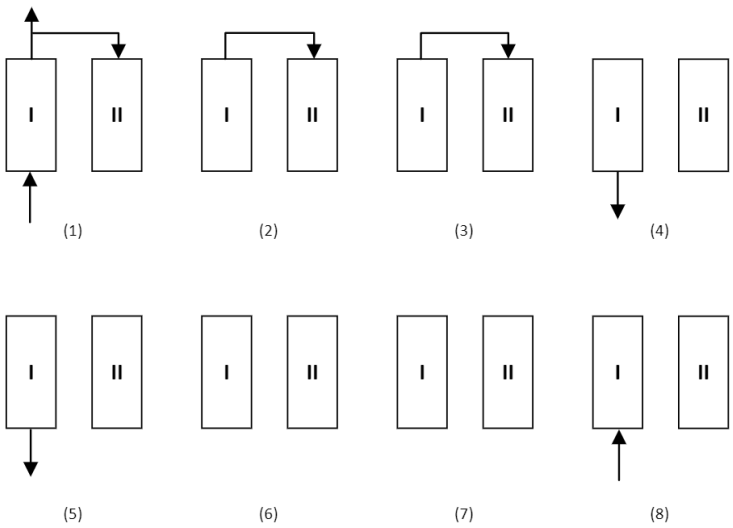

Figure 4.2: Aspen Adsorption 8 steps PSA scheduling in Unibed configuration.

Moreover, `P_Stage_Start` stands for the start pressure of the interaction unit, while `XFac` indicates the effective volume correction factor, a value used as a volume correction factor (with a typical value close to one). When the bed being interacted with is at constant pressure (acting as a very large volume tank) it should be set to a high value (e.g. 100).

Table 4.2: Manipulated variables for cycle scheduling

Step	Time [s]	VF	VD	VP	VW	UNI.P_Stage_Start [bar]	UNI.XFac
Step 1	150	2	2	2	0	1.013	100
Step 2	60	0	2	0	0	1.013	1
Step 3	60	0	2	0	0	5	1
Step 4	5	0	0	0	2	10	1
Step 5	150	0	0	0	2	15	1
Step 6	60	0	0	0	0	-	-
Step 7	60	0	0	0	0	13	100
Step 8	5	2	0	0	0	10	100

Figure 4.3 shows the interaction between the rigorously modeled bed and Unibed during the steps.

4.5. Combined Heat and Power Unit

Many literature studies decided to approach the engine modeling replicating a Brayton Joule cycle for a turbine with the addition of a calculator block, to simulate combustion and electrical and thermal power output [71, 107]. However, a simple layout is selected in Aspen Plus after consultations with the INNIO Jenbacher engine provider [101]. The results of the tail gas from the dynamic simulation in Aspen Adsorption are manually inserted back in Aspen Plus, considering average flow rate and composition. The CHP unit is simulated using an `RGibbs` reactor model operating at atmospheric pressure (1.013 bar) and imposing a Heat duty of 0 W. An over-stoichiometric quantity of ambient air is added to the system according to Equation 3.41. Subsequently, a `Heater` model serves as an exchanger between the combusted gas and a cooling block. In the Aspen Plus environment, there is no model block that simulates the behavior of an engine.

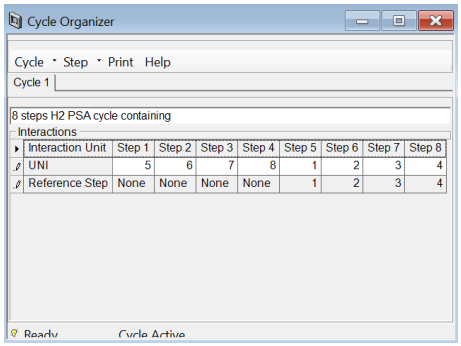

Figure 4.3: Unibed Interaction in the Cycle Organizer

4.5.1. Heat integration network

Following the completion of the simulation flowsheet in Aspen Plus, the optimization process is subsequently undertaken through the implementation of Heat Integration techniques.

Heat integration is the act of utilizing ”the energy in the high-temperature streams that need to be cooled and/or condensed to heat and/or vaporize the cold streams” [104]. Using this tactic, energy and money are saved on heating up and/or cooling down streams, since less external energy is required. Most streams that require energy input need to be cooled down, only two streams need to be heated. Nevertheless, a heat integration analysis was performed following the procedure of the Turton book [103] and using Aspen Energy Analyzer. Since no pinch is present in this system, it is found that certain streams can exchange their energy to save on externally supplied energy. The output of the HT-WGSR (1607) and Hydrolysis reactors (1610) are utilized in two `HeatX` model palettes to heat up the raw syngas stream. The `HeatX` is modeled imposing a Short-cut method (with fluids flowing counter-currently) and a pressure drop of 0.3 bar on the shell side. Finally, boiler feed water (BFW) is used for cooling, producing at the same time low-pressure steam.

Part I

Results and Discussion

5

Technical Assessment

This chapter offers a comprehensive guide to the technical assessment of the project. The system configuration is depicted in Figure 5.1. The configuration is divided into 4 units, which are as follows:

1. Syngas Adjustment system: Unit-1.
2. Syngas Purification system: Unit-2.
3. Pressure Swing Adsorption system: Unit-3.
4. Combined Heat and Power system: Unit-4.

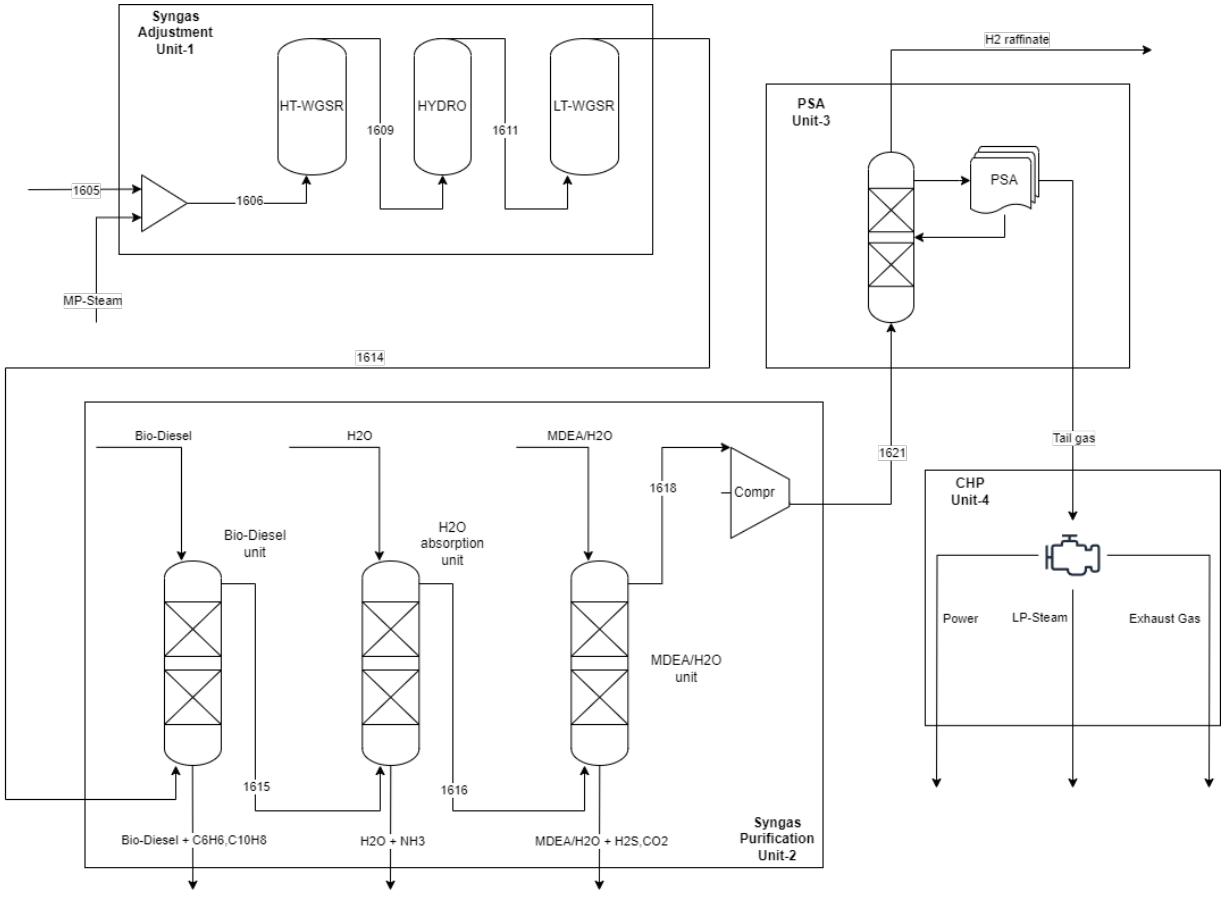

Figure 5.1: Process flowchart.

The first research question posed in Chapter 1 is repeated below for convenience.

Research Question 1

What is the process route for the sequence of purification steps prior the PSA to achieve the highest quality of gas in terms of H_2 content?

To address this question, it is essential to initially assess the performance of the designed units (syngas adjustment and syngas purification) before the PSA. Subsequently, the performance of this work, focusing on maximizing H_2, will be benchmarked against a reference plant [108], which is designed to process an input of RDF of 13 tons per hour. The RDF, is fed to the fluidized bed gasifier, which serves to generate raw syngas. Subsequently, the raw syngas is subjected to a series of treatments within a dedicated syngas treatment unit. This unit comprises particulate removal, wet scrubbing, COS and HCN hydrolysis, as well as H_2S absorption. Following this treatment stage, the gas is subjected to the Water Gas Shift reaction, and any remaining impurities are further eliminated through an acid gas removal system. In this configuration, a total of 6 adjustment and purification steps are performed to obtain syngas with a H_2 content of 70% prior the PSA. Ultimately, the shifted syngas is directed to the PSA system, yielding a total annual production of 3900 tons of H_2 [108].

Figure 5.2 compares the two process routes in terms of H_2 yield in the syngas before the Pressure Swing Adsorption system. The reference plant is represented by the yellow bar (6 steps), while the designed system is indicated by the green bar (7 steps).

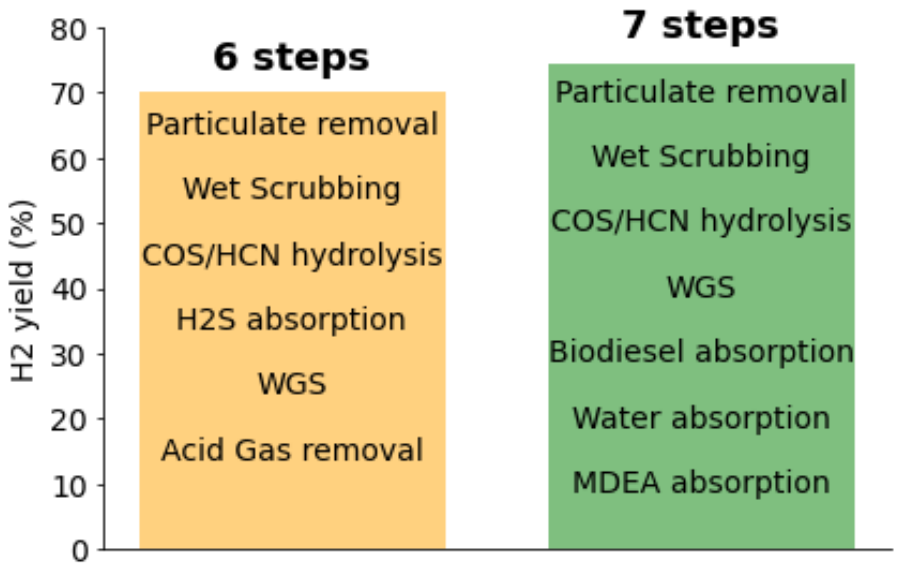

Figure 5.2: H_2 yield prior the Pressure Swing Adsorption of reference (6 steps) and design (7 steps) plant [108].

Upon comparing the two systems, the process configuration developed in this work adopts an additional purification step, which positively influences the yield of H_2. The source used as benchmark, lacks a precise description of the adopted process route. Nevertheless, given the presence of the hydrolysis unit with sulfur removal before the Water Gas Shift reaction, it suggests treatment of a sweet syngas. Furthermore, the lower efficiency of the system taken as reference might be attributed to the acid gas removal unit. In summary, following the established methodology and assumptions, the process route designed prior to PSA achieved a H_2 yield of 74.28 %, surpassing the 70 % yield of the reference plant. The designed 7 steps process configuration introduced, resulted in a improvement of 6.1 % with respect to H_2 yield.

This section is dedicated to exploring the potential real-life implications of the four units shown in Figure 5.1 and examining alternative approaches for conducting sensitivity analyses. Furthermore, it provides detailed information on the utilization of computational tools suitable for simulating the Waste to H_2 process route.

5.1. Unit-1: The Syngas Adjustment system

Following the natural process flowchart, the gas is directed towards two heat exchangers to increase its temperature. After that, the HT-WGSR is encountered, which replicates the ΔT increase in accordance with literature values [35, 109], as well as conversion efficiencies calculated following Equation 3.45.

The syngas is guided towards the hydrolysis reactor, whose conditions are replicated based on industry standards. The behavior of the reactor is idealized for the scope of this study. Nevertheless, Aspen Plus records minimal temperature increase within the hydrolysis reactor ($\leq$1°C) due to the low concentrations of COS and HCN in the gas.

Furthermore, to maximize the H_2 content, the syngas is directed to the LT-WGSR. In the context of waste gasification, the syngas typically exhibits lower quality due to a presence of impurities, notably NH_3, H_2S, $C_{10}H_8$, and C_6H_6. This content poses the risk of condensation related issues if the syngas is excessively cooled, potentially leading to machinery clogging. As articulated by Pan [49], it is crucial to maintain the inlet temperature for the LT-WGSR above the critical threshold of 200 °C, as falling below this limit could result in syngas condensation, thereby jeopardizing the integrity of the CoMo catalyst. In the Aspen Plus simulation, an inlet temperature of 198 °C is attained. However, it is important to emphasize that the designed degree of cooling is compensated by the low partial pressure of impurities and condensable species within the system. This condition remains acceptable under the specific operational parameters of the system, mitigating the risks associated with syngas condensation.

Regarding both WGS reactors, the catalyst loses its activity over time mainly due to poisoning, fouling, thermal and mechanical degradation [110]. However, in this work, catalyst deactivation is neglected from a technical point of view but considered in terms of lifetime in the economic analysis. Detailed information regarding real scale WGS reactors are treated by Mobed et al. [110]. In table 5.1 the efficiency of the CO conversion process is reported in comparison with standard efficiencies on dry basis [35].

Table 5.1: Comparison of CO Efficiency in Design Plant and State of the Art [35].

Unit	CO Efficiency Design Plant	CO Efficiency State of the Art
HT-WGSR	88.84%	84.61%
LT-WGSR	86.5%	90%

5.2. Unit-2: The Syngas Purification system

5.2.1. Bio-Diesel absorption column for Tar removal

The adjusted syngas is directed towards the bio-diesel absorption column. In the conceptual phase of this study, there was uncertainty regarding whether NH_3 or tar should be the first component to be removed. However, through the analysis of phase diagrams, it became evident that operating the bio-Diesel column as the initial step was the optimal choice, as illustrated in Appendix H [111, 112]. At the level of pressure of inlet stream (10 bar), opting for the initial removal of C_6H_6 is the more advantageous option.

As indicated by Nicolaou [72], it is of key importance to estimate the dew point of tars contaminants in the particular flow. An estimate of the dew point temperature of syngas can be retrieved from the Engineering Toolbox [113], in which the dew point temperature is provided with respect to the volume % of water vapor in a generic flue gas. The critical information, indicating a dew point of above 70 °C is taken as a reference for the given syngas composition. The notably low dew point of the tars presents an advantageous opportunity within the system. It allows for the early removal of the majority of it from the raw gas flow. This is achieved by cooling the gas to a temperature close to 80 °C (taking it 10 °C above the referenced dew point temperature for cautions reason) while simultaneously passing it through a packed bed absorption column, entering into contact with bio-Diesel at 50 °C. This might come into contrast with the fundamentals of absorption of any given reference [52]. Nevertheless, the rationale behind the moderately

elevated temperature of bio-Diesel is justified by thermodynamic principles, specifically Le Chatelier's principle, in which is understood that the solubility of $C_{10}H_8$ constitutes an endothermic dissolution process. Consequently, elevating the temperature of the solvent results in a corresponding increase in the solubility of $C_{10}H_8$. The rate of this increase in $C_{10}H_8$ solubility is intricately linked to its melting point. Notably, the melting point of $C_{10}H_8$ plays a pivotal role in governing its solubility behavior [114].

The absorption tower maintains a constant oil flow rate, which is able to efficiently capture the tars at low temperatures without the risk of oil evaporation. The used oil is subsequently recovered through a secondary system, similar to the set up developed by the pilot scale unit in the work of Müller et al. [115]. By implementing an oil recovery system, the majority of the used oil can be recirculated, thereby minimizing the operational costs associated with acquiring new oil. The indication on the stripper solvent operating conditions are hinted by the information of the "Desorber head temperature" [115]. Therefore, it is chosen to proceed with low pressure steam to regenerate bio-Diesel.

In the relevant literature, no commercial-scale application utilizing bio-Diesel for this specific purpose was identified. Therefore, the approach employed in Aspen Plus, which involves using a separator block with a fixed removal efficiency, is somewhat approximate. A more robust and rigorous method was proposed and validated by Nicolaou [72]. In Nicolaou's research, a bio-Diesel absorption column was designed in Aspen Plus. The model is then tested and validated using data from two pilot/commercialized plants: Synvalor and Guessing. A similar methodology could have been applied in the current study but was excluded as it fell outside the scope of this research. Nevertheless, in the context of conceptual modeling, the present study has provided valuable insights into the technical feasibility and operational constraints for implementing a renewable cold tar removal method using bio-Diesel from third generation biomass. Furthermore, it is important to note that the by-product tars offer the potential for energy valorization within the HTW gasifier, presenting an opportunity to enhance the overall economic feasibility of the gas cleaning process. Table 5.2 highlights the comparison of C_6H_6 and $C_{10}H_8$ removal efficiency of the designed plant against the state of the art.

Table 5.2: Comparison of C_6H_6 and $C_{10}H_8$ removal Efficiency in Design Plant and State of the Art [72, 116].

Component	Efficiency Design Plant	Efficiency State of the Art
C_6H_6	99.99%	90%
$C_{10}H_8$	99.99%	99%

5.2.2. Water absorption column for NH_3 removal

The implication of a packed bed column in real life applications for the removal of NH_3 hinders many possibilities for process improvements. Two possible design variations can be applied to the system to make it more realistic:

- Introducing a quantity of freshwater, maintained at a lower temperature (e.g. 15 °C according to Francois et al. [71]) to increase the vapor condensation in the water scrubber. Nevertheless, the system must be designed to monitor and minimize the quantity of water in the exiting gas.
- The implementation of a storage tank system located at the base of the packed column serves as a contingency for situations where process water is not required during operations. The incorporation of this system represents a potential opportunity for recycling the effluent back to the wet scrubber in a later period, thereby reducing water usage and minimizing disposal requirements.

The absorption column considered in this study is sized based on flowrate ratio of industrially available scrubbers. Nevertheless, a comparison on the inlet and exit conditions of the syngas are analysed in table 5.3.

Table 5.3: Comparison of NH_3 removal Efficiency in Design Plant and State of the Art [71].

Unit	NH_3 Efficiency Design Plant	NH_3 Efficiency State of the Art
Water Absorption column	89.83%	98.8%

5.2.3. Aqueous MDEA absorption column for H_2S and CO_2 removal

Analysing the phase diagrams revealed the feasibility of the operative conditions (35 °C and 7.7 bar) of the aqueous MDEA absorption column, as illustrated in Appendix J [117, 118]. In the H_2S and CO_2 removal section, two columns are utilized. Here, the synthesis gas enters the absorption packed column at its base, while a regenerated MDEA solution, along with additional MDEA makeup, is introduced at the upper section. This arrangement enables efficient contact between the ascending gas and descending liquid on the packed bed, while promoting the reactions (Equation 3.18 - 3.23) in the forward direction. A 2022 study conducted by Aspen Tech [85], reveals that chemical solvents are most suitable at lower pressure. Figure 5.3 showcases the comparison of effectiveness of physical and chemical solvent for a different range of pressures.

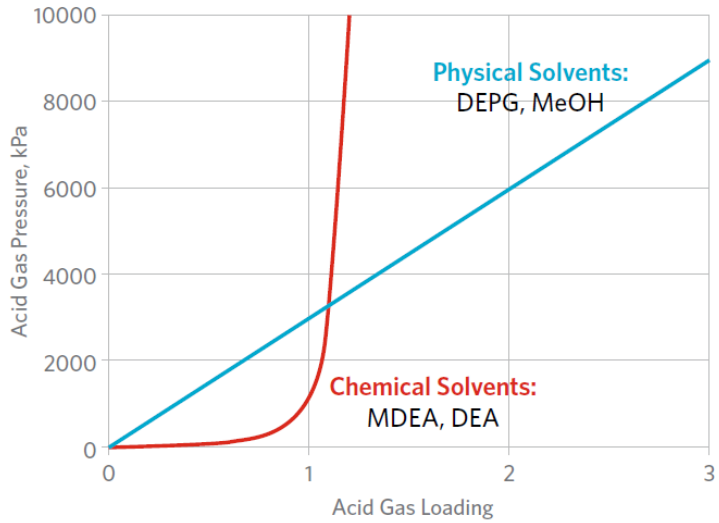

Figure 5.3: Comparison of effectiveness of physical and chemical solvent [85].

Figure 5.4 displays the heat of absorption for physical and chemical solvents. MDEA exhibits a higher heat of absorption for CO_2, emphasizing the need for energy optimization to control operating costs in chemical solvent-based processes.

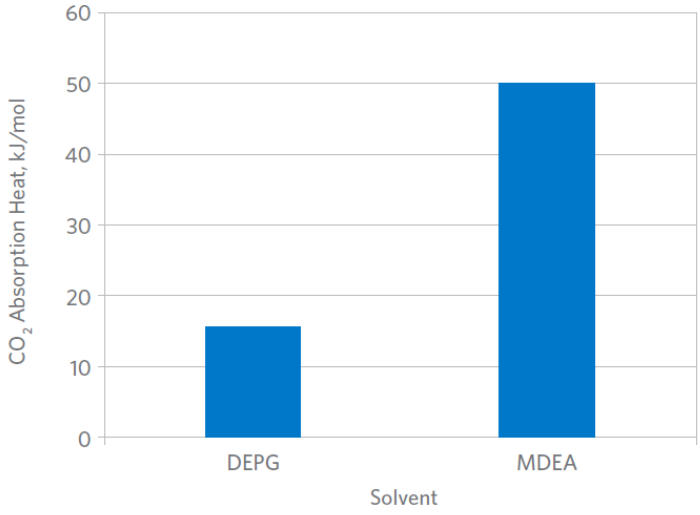

Figure 5.4: Relative magnitude of heat of absorption of physical and chemical solvent [85].

Aspen Plus incorporates the heat of absorption when evaluating the syngas outlet temperature from the MDEA absorption column, resulting in a temperature increase of 12°C. The verification is conducted by

comparing the data obtained from the Aspen Tech source [85], which represents the generation term; with the simulation results from Aspen Plus, which encompass both input and output energy flows. The energy balance equation, denoted as Equation 5.1, is expressed with the assumption of a zero accumulation term and the exclusion of any external heat sources or work.

$$\frac{dE}{dt} = E_{\text{in}} - E_{\text{out}} + E_{\text{gen}} + Q_{\text{ext}} + W_{\text{ext}} \tag{5.1}$$

The results of the verification study showed that the sum of the input and output energy terms predicted by Aspen Plus was 13 % higher than the generation term established by Aspen Tech source [85]. This discrepancy can be attributed to differences in gas composition, the amount of solvent used, and its chemical composition. However, for the purposes of this study, the verification results are considered acceptable.

Subsequently, the enriched MDEA/H_2O stream undergoes regeneration within the stripper column. In the stipulated conditions of the stripper column, the equilibrium reactions of Equation 3.18 - 3.23 proceed in the backwards direction. The desorption of CO_2 transpires under low pressures and elevated temperatures, ensuring adequate MDEA/CO_2 separation while avoiding amine degradation. The inclusion of the stripping stream for CO_2 and H_2S removal is outside the research focus. Nevertheless, Idem et al. [119] suggest that a conventional regeneration configuration utilises between 1.9-2.5 kg steam/kg of CO_2. On the other hand, for industrial applications, steam is incorporated with high volatility components such as pentane for MDEA regeneration [120]. In the current investigation, it is justifiable to focus solely on the steam quantity for the stripping process. This approach is warranted because the pentane utility consumption is minimal and does not significantly impact the overall system feasibility. Table 5.4 reports the efficiency of the CO_2 and H_2S absorption process in comparison with standard efficiencies [73].

Table 5.4: Comparison of CO_2 and H_2S absorption Efficiency in Design Plant and State of the Art [73].

Unit	CO_2 and H_2S Efficiency Design Plant	CO_2 and H_2S Efficiency State of the Art
CO_2 absorption	74.46%	75%
H_2S absorption	100%	99%

It's noteworthy to say that advance modeling of absorption and stripping columns operation is out of the scope of this study. In addition to that, the columns described work under equilibrium assumptions and are not subjected to dynamic modeling considerations, namely rate-based models. Nevertheless, the description of an aqueous MDEA absorption and stripping system for the simultaneous removal of CO_2 and H_2S is considered to be complete for the purpose of the technical and economic feasibility of this study.

5.3. Unit-3: Pressure Swing Adsorption system

This section comprises the technical feasibility of the Pressure Swing Adsorption system. Detailed information are provided for: isotherm selection and validation, bed analysis, cycle analysis and key performance indicators.

5.3.1. Isotherm model comparison

Different isotherms used in literature were evaluated in a comparative analysis [67, 80, 82, 99]. Figure 5.5 illustrates the time duration for which the H_2 purity remained consistently above 99.9 % during a single adsorption step. The isotherms under consideration exhibit variations in their mathematical expressions as noted in Appendix N. Specifically, the Extended Langmuir 1 model does not account for temperature effects. This simplification may account for its comparatively lower performance when contrasted with the other three models. In contrast, the remaining isotherms incorporate temperature as a factor with an exponential relationship, resulting in an augmented adsorption capacity. Conversely, the Dual Site Langmuir model represents a modification of the Extended Langmuir isotherm, introducing a second adsorption site (specifically, as an extension of the Extended Langmuir isotherm 2). As a result, the expected adsorption capacity is generally higher than the one predicted by the Extended Langmuir isotherm. However, it is important to note that the simulation of the DSL isotherm employs a single layer of activated carbon, which

inherently exhibits limited adsorption capacity for CO. This limitation in adsorption capacity for CO could potentially offer an explanation for the lower performance observed in the DSL model.

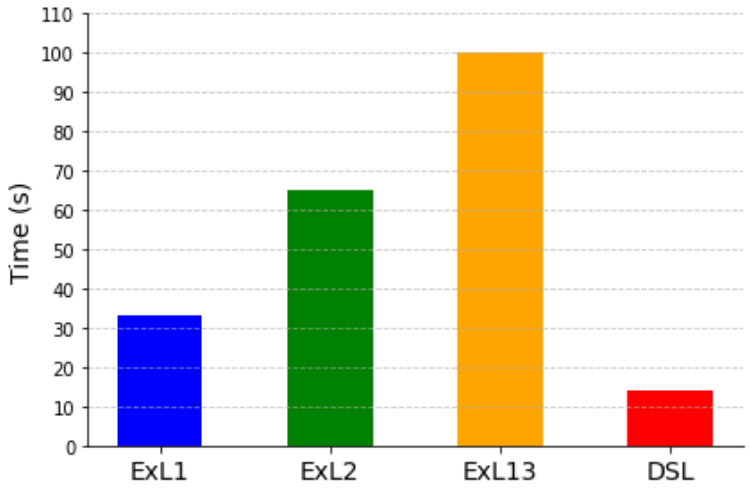

Figure 5.5: Isotherm model comparison for H_2 purity.

5.3.2. Isotherm validation

The isotherm model validation process involves replicating data from the reference source (Xiao et al. [80]). As no existing data frame is accessible, data are retrieved manually, introducing a degree of inaccuracy into the validation points. Subsequently, the actual model within Aspen Adsorption is developed based on the data originally reported [80]. The comparison of exit concentrations for the five components (referenced literature of Xiao et al. [80] = dots; replicated case = lines) is reported in Figure 5.6.

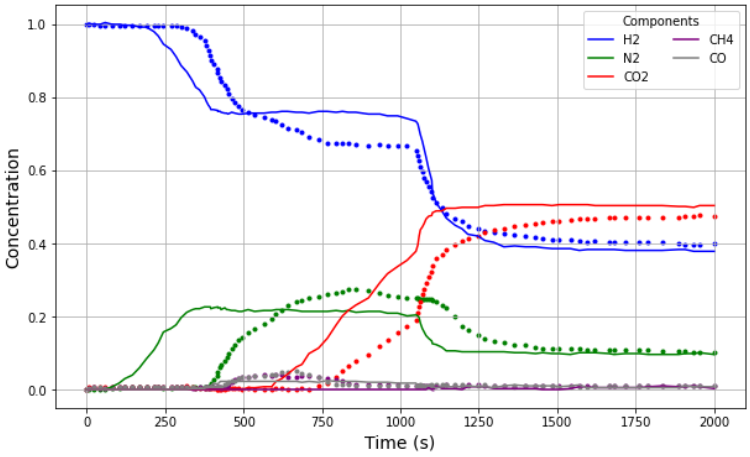

Figure 5.6: Isotherm model validation [80].

The disparity between the two models primarily arises from time delay, potentially attributed to the inherent behavior of Aspen Adsorption. Possible reasons are provided for clarification:

1. The reversible flow type with dynamic time dependency within the software impacts the internal pressure and gas velocity profiles, as it can function as both flow setters and pressure setters within the adsorption bed models. Variations in results may be attributed from control valve specifications based on flow rate or pressure, although Xiao et al. [80] does not specify the type of control valve specifications used.
2. A critical consideration is the initialization of the simulation, which requires the utilization of two tank voids before and after the bed to prevent issues arising from directly connecting blocks with

fixed or initial pressure variables. This design choice may introduce variations in the solution due to inaccuracies in the gas tank void specification.

3. The spatial discretization of the gas bed dynamic model can enhance solution accuracy by increasing the number of discretization points. Twenty discretized nodes are selected to replicate the results of the work of Xiao et al. [80], in which the parameters are not found.

Despite the notable impact of time delay on the resultant concentration, the model's validation is substantiated when considering the equilibrium state. This finding aligns with the outcomes reported by the study conducted by Xiao et al. [80]. In summary, for the objectives of this research, the simulated flowsheet is deemed validated. The selected adsorbent layers comprise activated carbon and zeolite 5A, a configuration well documented in the literature for its efficacy under conditions mirroring those in our specific context. The two-layered adsorbent setup outperforms a single adsorbent configuration due to the distinct adsorption characteristics exhibited by each material towards different components in the feed stream. This combination enhances the adsorption capacity for impurities within the feed stream. Specifically, the lower section of the column at the feed inlet houses the activated carbon layer, which predominantly adsorbs CO_2, CH_4 and CO. Conversely, the zeolite layer, situated above the activated carbon layer, is specific for N_2 and CO adsorption.

5.3.3. Isothermal conditions verification

The isotherm energy balance is formulated in Equation 3.31 for the worst possible case scenario: an empty bed. The computation is established with a bed composition of pure H_2. In this situation, the bed is able to adsorb the maximum amount of impurities for a single adsorption cycle of 150 s. As a consequence, the amount of heat released caused by adsorption is at its peak value. In Figure 5.7, it is displayed the temperature evolution of a 3 meters bed starting at a temperature of 298 K as a function of adsorption time. The final temperature registered for the worst case scenario is 304 K for a 3 m bed. The simulation can be

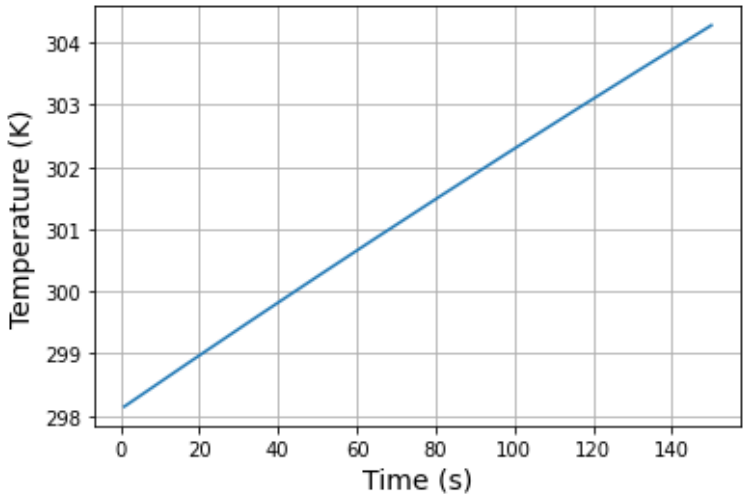

Figure 5.7: Temperature evolution caused by heat of adsorption.

adapted for a taller bed, for example 6 m. In this case, the effect on temperature difference is higher, due to the increased available adsorption working capacity, resulting in a ΔT of 12 K.

5.3.4. Bed analysis

Typically, a vertical orientation is employed for adsorption beds in order to mitigate variations in flow. Within this configuration, the attention of the technical feasibility goes to Reynolds number calculation for flow conditions and CO_2 penetration in the Zeolite 5A layer. The Reynolds equation is a fundamental equation in fluid dynamics, representing the ratio of inertial and viscous forces. Its mathematical representation is given in Equation 5.2.

$$Re = \frac{\rho v D}{\mu} \tag{5.2}$$

Given the pre-existing implementation of the correlation within Aspen Adsorption, it becomes essential to modify the bed design systematically. This modification is essential to reach the maximum permissible superficial velocity, as defined in McCabe's book [53], while adhering to the specified constraint of 0.5 m/s. Simultaneously, it avoids exceeding the minimum point of fluidization velocity. Furthermore, it is crucial to maintain a consistent gas density profile throughout the entire length of the column. The examination of the Reynolds number, as indicated by Aspen Adsorption, illustrates a consistent trend of increasing velocity throughout the spatially discretized column, aligning with the understanding that the kinematic viscosity of pure H_2 surpasses that of the gaseous mixture. Consequently, the Reynolds number experiences a decrease while retaining its laminar flow characteristics. In this context, it is noteworthy that for the number of nodes integrated into the system, all hydraulic criteria have been successfully met.

A secondary examination of the bed involves assessing the intra-particle CO_2 penetration into the Zeolite 5A layer. CO_2 penetration into the Zeolite 5A layer can introduce challenges during the desorption phase [64]. Aspen Adsorption offers valuable data for analyzing component bulk concentrations, mole fractions, and solid loading within discrete spatial elements. The CO_2 penetration factor (Fac_p) is analysed based on the first node of the spatially discretized bed and can be expressed as the ratio between the bulk concentration of CO_2 in the zeolite 5A layer and the bulk concentration of CO_2 in the activated carbon layer. Equation 5.3 provides the the relationship for calculating the penetration factor:

$$Fac_P = \frac{C_{b_{\text{Zeo5A}}}}{C_{b_{\text{AC}}}} \tag{5.3}$$

The results reveal that only 2.7% of CO_2 penetrates the zeolite layer, which is deemed acceptable within the context of this study. However, it is worth noting that a comprehensive evaluation on impurities, beyond the scope of this analysis, may hold value for future research. Such an assessment could encompass implications related to the presence of Sulphur and Nitrogen compound impurities (at the level of parts per million for this investigation) over the operational cycle and the adsorbent's longevity.

5.3.5. Cycle analysis

A PSA industrial installation comprises 4 primary components:

- Adsorber vessels constructed from carbon steel and filled with adsorbent material.
- Valve and piping skid encompassing all valves and instrumentation.
- Control system situated within a remote control room responsible for cycle controls.
- Mixing drum designed to mitigate variations in the composition of the tail gas.

Initially, the simplest model of a PSA system had to be replicated to evaluate adsorption time to prevent breakthrough of impurities. Subsequently, with a more profound grasp of the process and software employed, the design of a 2 beds PSA system was conceived. The implications of such system is mainly affecting the logistics of H_2 production line. In fact, with this layout, a vessel tank is required to store the feed during regeneration phase, being detrimental for a continuous production system. Therefore, the PSA analysis is extended towards the 4 and 8 beds system for continuous provision of H_2.

To simulate the behavior of such PSA configurations, the Unibed approach is utilized. This approach assumes that all beds undergo identical steps, necessitating the simulation of only one bed to represent the multibed cycle. This bed records mass and molar flow rates, temperature, and composition, subsequently replaying them in accordance with the cyclic sequence. In this way, the number of equations to be solved (which are discretizations of the partial differential equations) are reduced drastically. According to the Aspen Adsorption guide [78], the single bed approach retains the accuracy of the final results, more specifically same average purity and number of cycles to achieve cyclic steady state. Within this system, a pair of diminutive tanks (tank void) fulfills a dual role, encompassing both storage and the maintenance of output stream purity. These tanks, with a capacity of 0.01 m^3, corresponding to roughly 0.15 % of the bed's volume. The establishment of boundary conditions for tank pressures, alongside similar considerations for the interaction bed, is strategically undertaken to streamline the attainment of the desired final unit state following each procedural step. The analysis of the pressure gradient is necessary to check the correct functioning of the PSA. Figure 5.8 depicts a typical pressure gradient of a PSA system undergoing one cycle. Aspen Adsorption replicates the entire PSA cycle. Initially, during the adsorption phase, the pressure remains constant at the designed value of 15 bar. Once the adsorption step is completed, the system

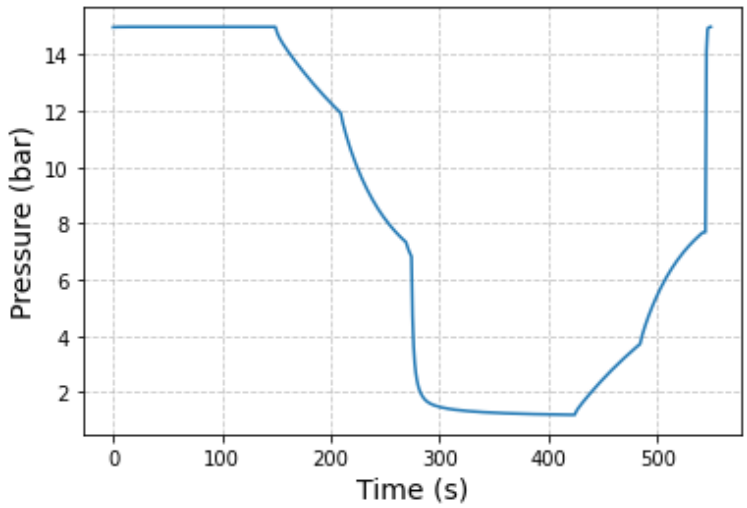

Figure 5.8: Pressure gradient of the PSA.

enters the first depressurization phase, gradually reducing the pressure to an intermediate level of around 12 bar. Subsequently, the pressure is further decreased until the beds reach a pressure equalization point at around 7.5 bar. At this stage, the blow down and purge phases are implemented in two distinct steps to optimize computational efficiency and set Unibed's pressure response conditions. After the bed is purged, no control valve specifications are provided, leaving Unibed to guide the cycle. The pressurization process to reach the bed equalization level occurs in two steps at a slightly higher pressure, approximately 7.8 bar. To conclude the cycle, the feed valve is partially opened to enable the syngas to pressurize the bed to the required adsorption pressure of 15 bar. A confirmation of similar pressure history behavior as modeled in Aspen Adsorption is supported by relevant research [82, 80]. The main difference between the cycles described in the literature and the designed case is the significant pressure gradient. The choice to use a more gradual pressure increase/decrease is justified due to convergence issues. The model developed in Aspen Adsorption occasionally encounters convergence issues during pressure equalization and purge steps. These challenges arise from changes in flow direction within the column and variations in the composition of the incoming flow. Nevertheless, such conditions can be mitigated by designing a gradual pressure gradient, initializing pressure, composition, and velocity values in the first node of the column in accordance with the specified boundary conditions.

The pressure behavior for the multiple beds configuration can not be visualized with the Unibed layout in contrast with what was shown in Figure 2.7. Nevertheless, the pressure history in the Unibed configuration flow sheet could be interpreted as follows:

- Throughout the cycle stages involving adsorption and depressurization, up to the point of pressure equalization within the rigorous designed bed in Aspen Adsorption where all conditions are precisely defined, Unibed operates as an authentic simulated bed.
- Following the equalization step and extending until the rigorous bed is re-pressurized, Unibed functions as a controlling bed that adjusts pressure levels to execute the required cycle stages for the rigorous bed.

Implication of a verification study

The column is discretized into 20 nodes, with 10 nodes allocated to each layer. This discretization spacing has been selected as the optimal compromise between computational efficiency and accuracy in accordance with Di Marcoberardino et al. [84]. On the contrary, Abdeljaoued et al. [67] examined the impact of varying the number of nodes in the simulation. The investigation involved a wide range of node counts, spanning from 10 to 120 nodes. Remarkably, the findings indicated that any increase in the number of nodes beyond 60 exhibited a marginal influence on the simulation outcomes. To sum up, a detailed verification study focusing on the number of nodes could have provided a deeper understanding of the variations observed with increasing node counts and, consequently, enhanced the precision and accuracy of the simulation results.

5.3.6. Key Performance Indicators for Unit-3

The key performance indicators are calculated to evaluate the performance of the PSA. The simulations conducted in Aspen Adsorption involve a bed that reaches equilibrium with the composition of the incoming feed, effectively simulating real operational conditions with the presence of contaminants to verify its functionality. Subsequently, the simulation reveals that a satisfactory level of purity is attained only after several cycles, typically around 9. For practical plant applications, it becomes imperative to incorporate a storage vessel to accommodate the gas until the desired market purity is achieved. Moreover, it's important to emphasize that the study's scope does not encompass the incorporation of a compressor unit for gas re-pressurization (to the 15 bar designed boundary pressure) as well as the sizing of the storage tank.

Table 5.5 reviews the KPI for the 4 and 8 beds configurations.

Table 5.5: Key Performance Indicators for 4 Beds and 8 Beds PSA.

KPI	Unit	4 Beds PSA	8 Beds PSA
H_2 Productivity	[kmol/s]	0.1628	0.1725
H_2 Purity	[%]	99.468	99.437
H_2 Recovery	[%]	61.162	62.279

As per the recommendations outlined by Luberti et al. [64], augmenting the quantity of beds within the adsorption process enables the extension of adsorption durations and the integration of additional pressure equalization, providing purge and simultaneous adsorption phases. This strategic approach is observable in the case of the 8 beds PSA, resulting in a notable enhancement of H_2 productivity and recovery compared to the 4 beds. The productivity in the 8 beds approach is increased by 6 %, resulting in a significant impact on gross earnings, totaling 4 million euros per year. This confirms that the technical performance of the system has a profound effect on the economic viability of the model. Contrarily, the 8 beds PSA system does not outperform the 4 beds counterpart in terms of H_2 purity. This disparity may be attributed to the adjustment of simulation parameters. In the case of the 4 beds system, the dimensions were customized to accommodate the syngas composition and flow rate, without using a proportional scaling factor of 2. Consequently, the differences in bed sizing between the two systems could account for the observed variations in H_2 purity. The DNV GL HyQuality study [121] provides a comprehensive overview of the precise H_2 specifications essential for various industrial processes utilizing H_2 as both a feedstock and an energy carrier. These specifications are invaluable for assessing the potential market coverage of the produced H_2. Notably, the quality of this H_2 aligns with the stringent requirements of applications in refineries, Ammonia and Methanol production, Fisher Tropsch processes, and a variety of heat related applications, ensuring its suitability for diverse industrial needs. The H_2 requirements for each application is provided in Appendix M. In terms of H_2 recovery, both configurations show promising results, consistent with findings in other literature sources [84]. Many patented works, as outlined in [35], have reported higher recovery efficiencies. Nevertheless, the rationale behind the achieved recovery efficiency can be attributed to the need for the tail gas to have a higher H_2 content, which in turn increases its lower heating value.

5.4. Unit-4: Net energy requirements

The evaluation of system performance involves the analysis of heat duties and power consumption, with data derived from the Aspen Plus model. Utility consumption values have been normalized to MW, enabling a meaningful comparison across all units. The trend in utility consumption is illustrated in Figure 5.9.

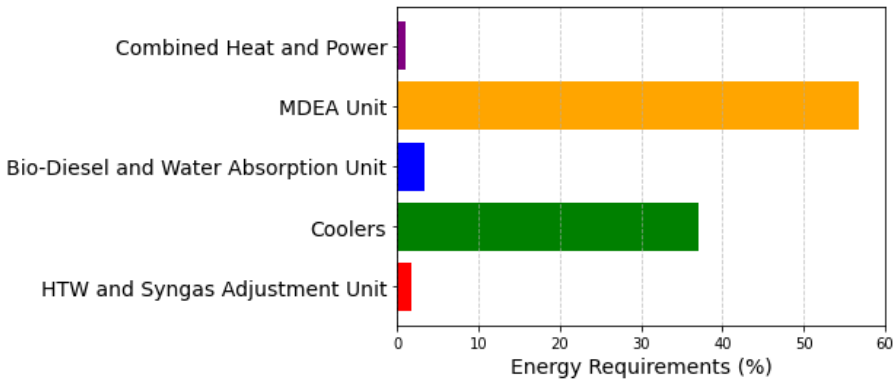

Figure 5.9: Utility consumption breakdown for the process units.

The MDEA Unit accounts for a significant portion, contributing to 56.8 % of the total utility consumption, primarily due to high-pressure steam consumption in the stripper unit. Another noteworthy contributor to utility consumption is the coolers. This is a result of the substantial amount of cooling water required to maintain the desired temperature control and ensure system efficiency.

Following technical discussions with INNIO Jenbacher, datasheets were obtained for the syngas composition feeding the Cogeneration Unit JMS 420 GS-S.L model 9 [101]. However, to assess the thermal and electrical self-sufficiency of the system accurately, estimates of heat and power were calculated based on the INNIO Jenbacher datasheets, adjusted according to flowrate. The overall results of the system are presented in Figure 5.6.

Table 5.6: Utility Consumption and Production.

Utility	Consumption	Production	Net
Electricity [MWh]	-1.9	6.2	4.3
Low Pressure steam [t/h]	-34.7	44.3	9.6

Furthermore, the assessment of heat duties and power consumption/production for each unit has revealed two critical aspects: the system operates as an electrically independent entity, and any surplus electricity generated can be sold in the electricity market. Table P.3 in Appendix P offers essential data regarding utilities consumption and production. It is worth noting that approximately 42% of the total power consumption is attributed to the HTW-unit, while the compressor accounts for 55%. This distribution aligns with expectations, given that the compressor constitutes one of the primary expenditures in the operation of a large-scale H_2 plant employing Pressure Swing Adsorption separation technology [84]. Similarly, the utilization of low-pressure steam aligns with this pattern, despite the fact that boiler feed water is procured from the market at a rate of 68 t/h.

The second research question posed in Chapter 1 is repeated below for convenience.

Research Question 2

Are the available computational tools valid for simulating the Waste to H_2 process route?

Figure 5.10 compares the efficiency of Unit-1 and Unit-2 developed in Aspen Plus with the state of the art for each individual technology. It is relevant to indicate that the efficiency is expressed specifically with regards to:

- CO conversion efficiency for the WGS reactors [35].
- HCN and COS conversion efficiencies for the hydrolysis reactor [122].
- C_6H_6 removal efficiency for the Bio-Diesel absorption column [72].
- NH_3 removal efficiency for the water absorption column [71].
- CO_2 removal efficiency for the aqueous MDEA absorption column [73].

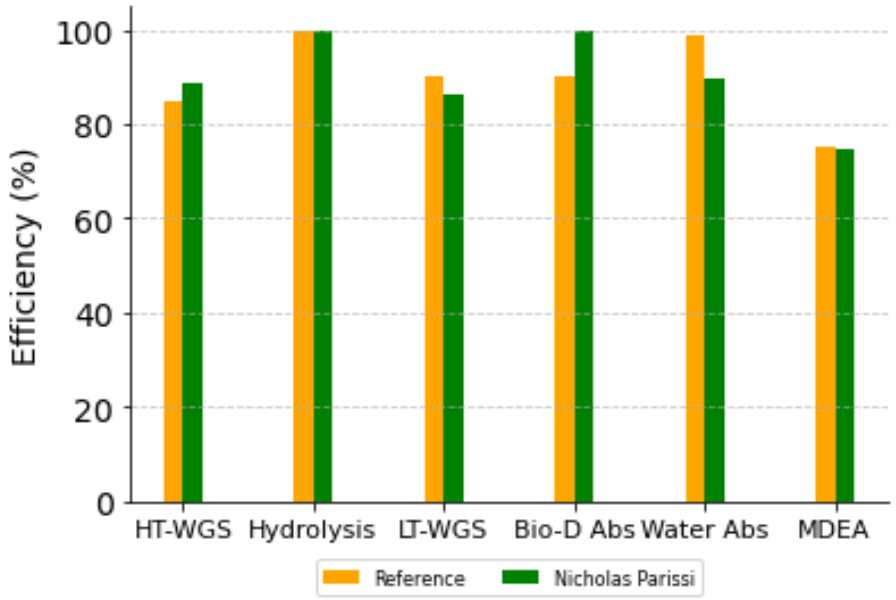

Figure 5.10: Benchmarking the efficiency of the Syngas Adjustment and Purification system with market standards.

Aspen Plus has been used to replicate the performance of the high temperature shift and hydrolysis reactors, adhering to the process conditions as found in industry standards. However, the Aspen Plus designed system, in some instances, falls short when compared to state of the art technologies, such as the low temperature WGS reactor and the water absorption column. The source used for the comparison of the CO conversion efficiency [35], pertains to typical industrial facilities. Yet, when assessing the disparity between the two water gas shift efficiency combined with the design of the plant, a relative error of only 0.4 % is obtained. Francois et al. [71] have chosen a system that aligns with the gasification to combined heat and power plant in Güssing, Austria. In this study, the entire plant is modeled in Aspen Plus, and the water scrubber exhibits a 98.8 % removal efficiency for NH_3. In the academic context, it can be argued that the under performance of the designed system may be attributed to difference in flowrate compositions as well as operating conditions. For instance, the water used for scrubbing was available at a lower temperature, which led to increased condensation of NH_3 and H_2O. In the case of the Pressure Swing Adsorption unit within the Aspen Adsorption framework, the acquired findings are consistent with industry standards. However, there is always potential for improvement, particularly in terms of cycle scheduling setup and conducting a comprehensive sensitivity analysis on critical parameters (e.g. adsorption pressure, purge to feed ratio, cycle time...). These advancements are essential to achieve ultra-pure H_2 with purity levels

surpassing 99.99%, thereby enhancing the technical feasibility of the process and expanding its economic viability across various sectors in the H_2 market, including transportation and the steel industry. Aspen Adsorption is a complex computational tool, and achieving convergence can be challenging. Moreover, another limitation of Aspen Adsorption involves sensitivity analysis of key design variables (e.g. adsorption pressure, purge to feed ratio, and cycle time), which is constrained due to manual implementation. Finally, the combined heat and power unit modeled in Aspen Plus is instrumental for gaining insights into the chemical species produced during tail gas combustion, as well as realistic temperature evolution within a combustion chamber.

Figure 5.11 shows the results of the computational tools in terms of H_2 yield with respect to the total stream flowrate in the Waste to H_2 process route. The green bars represent the H_2 yield, which starts at 24.6 % after the HTW gasification unit and gradually increasing through subsequent stages until reaching 99.4%. On the other hand, the orange bars indicate the total stream flowrate for each process unit. The flowrate values are highest after the syngas adjustment unit, but they decrease throughout the purification process. This progression suggests the effectiveness of the purification process in eliminating impurities from the gas.

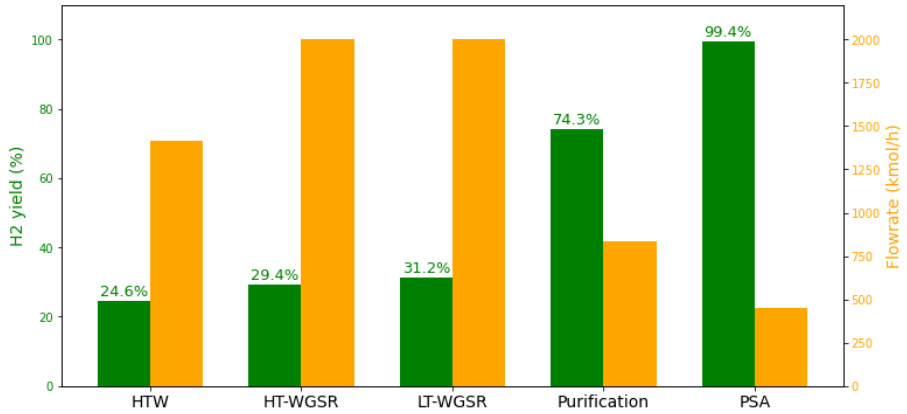

Figure 5.11: H_2 yield with respect to the total stream flowrate in the Waste to H_2 process route.

In conclusion, developing a theory-based model for equipment design and optimal input configuration is critical for accurately representing system behavior. The incorporation of Aspen Tech has proven valid for simulating the process units in the Waste to H_2 route, within the set assumptions and approximations.

6

Economic Assessment

In order to appraise the process economics of the proposed system, it is necessary to define expected costs of the project and revenues over the lifetime. As suggested by Seider et al. [104] costs can be classified into:

- Capital cost, which reflects all expenses that occur only once at the beginning of the project, including the cost of purchase and installation of equipment, site preparation, acquisition of necessary licenses or permissions.
- Operating costs, which reveal during the regular operation mode of the system after being put into production. The operating costs include the cost of raw materials and operating personnel as well tax payments and insurance. Maintenance costs, to ensure the system operational availability, were included into variable cost.
- Financial and decommissioning expenditures.

6.1. Capital expenditure

The capital expenditure is carried out by employing the methodology given in Chapter 3. All the formulas retrieved from Seider et al. [104] revealed the cost of each singular equipment. It is noteworthy to say that not all the machines necessary for a H_2 plant are reported in the cost calculations (e.g. specific packings in the absorption packed columns, buffer and storage tanks) of Appendix O. Nevertheless, the main process units are computed and each one is accounting for operating conditions implications (severe temperature and pressure gradient effects) and inflation. Figure 6.1 provides an overview of the cost distribution for equipment purchases. When assessing industrial applications, the inclusion of solvent regeneration units, such as those for bio-Diesel and MDEA, can significantly impact the initial capital expenditure required for the plant. However, this influence may not be immediately evident in Figure 6.1, since the purchase cost for columns represents less than 5 % of the total expenditure. The largest portion of the cost is attributed to the HTW gasification unit, accounting for nearly 60 % of the total expenses. Therefore, leveraging national and European funds could be an effective measure to alleviate the financial burden associated with the HTW unit.

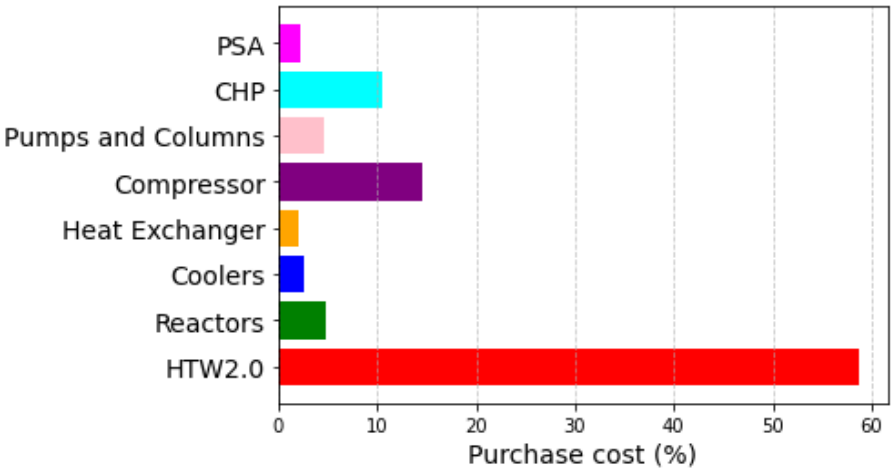

Figure 6.1: Purchase cost breakdown.

A summary of the results from the capital cost calculations can be found in Table 6.1

Table 6.1: Capital Expenditure Information.

Expenditure type	**[M$]**
Purchase cost	23.1
Corrected per location	27.75
Total Permanent Investment	124.7
Total Capital Investment	149

6.2. Operational and Maintenance expenditure

The operational expenditures are ongoing costs associated with the operation of a chemical plant. The operating expenditure consists of the cost of raw materials, catalysts, and chemicals consumed, utility usage, labor, and maintenance. Additionally, operating overhead, taxes and depreciation also need to be taken into account. Furthermore, 330 days of operation per year are assumed, meaning the plant is not running for 35 days per year. Most of the equations and factors used to calculate the annual cost are taken from Seider et al. [104]. Certain costs, such as the price of catalysts and raw materials, are calculated using data based on vendor specifications. The complete table review of assumptions formulated for OPEX establishment is provided in Appendix P. However, a special mention goes to:

- The Feedstock for HTW is pelletized waste containing RDF and waste wood. It is assumed that a monetary compensation is received for processing waste (circa 50 €/ton for RDF). This compensation is subtracted to the total material cost.
- A CO_2 stream is used for the gasification process of HTW, which is assumed to be re-circulated from the MDEA stripping column and therefore not accounted as a cost.
- The make up stream for MDEA column is bought hourly from the market, the remaining instead is considered to be a one time purchase for the 20 years of plant operation.

Figure 6.2 illustrates the cost distribution for the operational expenditures. Utilities, comprising nearly a quarter of the total operational expenses, play a key role in driving operational expenditure. This becomes evident when examining the substantial volumes of resources, such as oxygen and various grades of steam (mostly medium and high pressure), required for the operation of the HTW gasifier and the MDEA stripping column. A potential remedy to alleviate the cost imposed by utilities lies in the implementation of an efficient heat integration network. This network would be theoretically designed with the primary goal of generating steam of superior quality, ultimately reducing the overall impact of utilities on operational expenses.

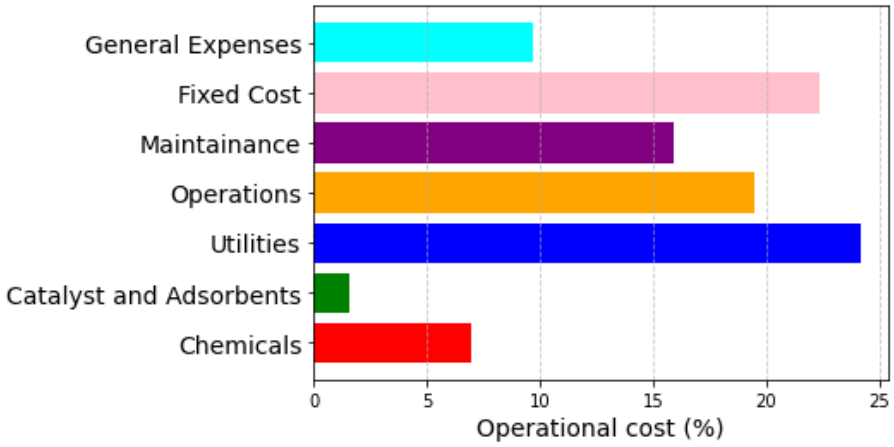

Figure 6.2: Operational expenditure cost breakdown.

A summary of the results from the operational cost calculations can be found in Table 6.2.

Table 6.2: Operational Expenditure Information.

Expenditure type	**[M$]**
Total Variable cost	39
Total Fixed cost	14.1
Total general expenses	6.1
Total Production cost	59.2

6.3. Key Performance Indicators

One cannot simply conclude if the chemical plant will be profitable by looking only at the total capital investment, total operating cost and the total sales. The profit made must be sufficient to compensate the total capital investment during the plant's lifetime. Two of these profitability measures are return on investment (ROI) and payback period (PBP). However, before these can be calculated, corporate income tax needs to be subtracted from the gross profit. The gross profit is calculated as the difference between total annual sales and total production cost, which is 19.475 M$. The Dutch corporate income tax consists of two tax brackets, 15% for a taxable amount up to 395,000 $ and 25.8% for all taxable income exceeding 395,000 $ [123]. This results in a net profit of 14.5 M$ annually, when selling the produced H_2 at a rate of 8 $/kg.

6.3.1. Profitability measures

The return on investment or ROI, is an indication of the rate at which the original capital investment can be paid back. The ROI is calculated using Equation 3.55, resulting in a value of 9.7%, meaning that annually 9.7% of the total capital investment can be paid back. This value is then compared with the equity risk premium updated for the year 2023, which represents the expected return of a stock above the risk-free rate for the Netherlands [124]. Therefore, the value of ROI found for the designed plant is above the one stated for Netherlands (5%), making it a promising business model for investors.

The payback period or PBP, indicates the time required for the net profit to equal the original investment. The PBP is calculated slightly differently than the ROI, as the total permanent investment is used instead of the total capital investment. Additionally, the annual depreciation is added to the net profit, since the 'depreciation is retained by the company' [104]. The PBP for this plant, calculated using Equation 3.56, is circa 5 years.

A summary of the profitability measures can be found in Table 6.3.

Table 6.3: Summary of the profitability measures.

Measure	Unit	Value
Gross profit	[M$/y]	19.475
Net profit	[M$/y]	14.5
ROI	[%]	9.7
PBP	[y]	5

6.3.2. Levelized cost of H_2

The Levelized cost of H_2 or $LCOH$, holds significant importance in assessing and quantifying the comprehensive process chain. It plays a key role in considering CAPEX and OPEX simultaneously. The $LCOH$ stands out as a standardize measure for the purpose of comparing distinct business models within the H_2 production sector. In this investigation, the $LCOH$ is used to answer the third research question with regards to different business models for H_2 production.

The last research question posed in Chapter 1 is repeated below for convenience.

Research Question 3

What would be the price comparison between different H_2 production routes (e.g. electrolysis, SMR, among others)?

The work of Jordan et al. [108] engages in a comparative analysis of $LCOH$ values across various sources, scales, and process methodologies. The findings of this analysis are extended to six business models, namely:

- Small scale Waste to H_2 or SmallWtH.
- Large scale WtH or LargeWtH.
- Small scale Biomass to H_2 or SmallBtH.
- Large scale BtH or LargeBtH.
- Steam Methane Reforming with Carbon Capture and Storage or SMRwCCS.
- Electrolysis

Figure 6.3 presents the adapted cost of H_2 for the six H_2 production methods.

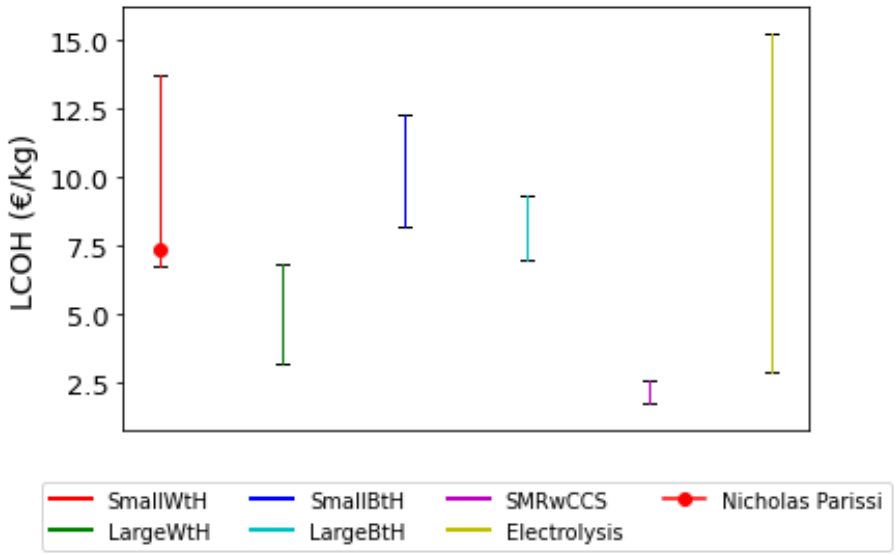

Figure 6.3: $LCOH$ for various sources, scales and process routes [108].

Notably, a $LCOH$ of 7.35 €/kg of the designed plant scenario aligns closely with the values of Waste to H_2 schemes of similar sizes. Figure 6.3 is critical to compare different H_2 production routes based on:

Economy of scale comparison

One salient observation pertains to the scale of the plants under evaluation. As anticipated, larger scale H_2 production plants exhibit a commendably lower $LCOH$. Ng et al. [21] examined the impact of economies of scale on H_2 production. The study concludes that a larger gasification to H_2 system is desirable to compete with the production cost of hydrogen derived from fossil based systems. Additionally, the study recommends the integration of multiple Material Recovery Facilities (MRF) for an economically competitive production of H_2. To delve deeper into the concept, Ng et al. [21] conducted an analysis, differentiating between two scenarios.

- Scenario 1: this scenario involved an analysis of a smaller scale configuration, providing a baseline for comparison.
- Scenario 2: this scenario examined the economies of scale of the gasification to H_2 system when the throughput of rejected materials from MRF was increased by a factor of approximately 50.

The H_2 price, when scaling up, exhibited a reduction of approximately 2.8 times less than the base case. Furthermore, a preliminary speculation suggests that a throughput of MRF rejected materials higher than 100 dry t/h is essential to be competitive with fossil fuels based H_2 production methods. This insight highlights the threshold that must be surpassed to establish H_2 production from waste materials, as a formidable contender in the energy landscape.

Comparison with the Biomass to H_2 route

The comparison can be extended between the Waste to H_2 and Biomass to H_2 business models. Specifically, the advantageous position of Waste to H_2 plants in terms of feedstock costs is analysed. As elucidated in the operational expenditure analysis, the remuneration for waste processing presents viable business opportunities. Despite the need for additional purification requirements, these opportunities are notable. To comprehensively assess the viability of Waste to H_2 plants, a scenario was considered in which gasification was exclusively performed on waste wood, utilizing the same quantity of feedstock while maintaining an identical process flowchart. Under these conditions, the estimated feedstock cost amounted to 10.7 million dollars, representing circa 15% of the total production cost. The implications of this feedstock cost alteration on the $LCOH$ were found to be significant. The consequences on the price of H_2 were drastic, reaching a value of 8.62 €/kg. This represented a notable increase, with the H_2 price being 1.2 times higher than in the previous scenario. In conclusion, the analysis revealed that the tailored solution of Waste to H_2 surpasses the use of biomass as a feedstock for H_2 production in terms of economic feasibility.

Comparison with the Steam Methane Reforming with Carbon Capture and Storage

Steam Methane Reforming with Carbon Capture and Storage maintains its cost competitiveness as it can be seen in Figure 6.3. The work of Santos et al. [125] is utilized to gain necessary insights when contrasting Bio-H_2 production process against Blue H_2 generated through steam methane reforming and autothermal reforming. The Blue H_2 life cycle assessment (LCA) model for SMR is established with a 90% carbon capture rate, with the remaining CO_2 emissions released into the atmosphere. Table 6.4 shows the values of CO_2 released and sequestered of two production processes: Bio-H_2 and SMR.

Table 6.4: Key inventory data of H_2 production processes: Bio-H_2 and Steam methane reforming (SMR) [125].

Parameter	Bio-H_2	SMR
CO_2 released [kg]	16.3	21.6
Sequestered CO_2 [kg]	516	194.4

The results unequivocally indicate that Bio-H_2 surpasses the Blue H_2 routes with regards to climate change impact and feedstock selection. It is important to note that the indicative value of CO_2 released and sequestered for the Bio-H_2 was derived from a process route different from the one originally designed

for this study. As such, it is reasonable to anticipate that a comprehensive LCA conducted on the designed plant would highlight different implications.

Comparison with Electrolysis

The $LCOH$ has emerged as a key metric in simultaneously evaluating various H_2 production routes. However, Figure 6.3 alone may not suffice for a comprehensive comparison between the Waste to H_2 process and electrolysis, primarily due to the wide price range associated with the latter. Therefore, additional qualitative insights are essential to contextualize and contrast these two routes effectively.

Waste to H_2, as a production route, presents a distinctive set of advantages. Most notably, it operates as a low carbon emission process, offering a solution to the pressing concerns associated with waste management and promoting energy security. Its success is threatened by several key factors, including feedstock variability and environmental impact. Conversely, electrolysis emerges as an entirely renewable H_2 production route, harnessing clean energy sources such as wind or solar power. One of its significant strengths lies in its capacity to generate high purity H_2, ideally suited for an array of applications, including fuel cells. Nevertheless, this route faces certain bottlenecks that warrant consideration. The cost of electrodes can pose a substantial economic challenge, and the profitability of operations is closely linked to the electricity price. Additionally, further development and optimization of electrolysis technology are essential to boost its Technology Readiness Level along the learning curve, ensuring its widespread viability and scalability.

In summary, the choice between the Waste to H_2 process and electrolysis as H_2 production routes involves a complex interplay of factors. Nevertheless, it is relevant to state that the Waste to H_2 route stands out as solution to the waste management problem, which is inevitable.

Part II

Closure

7

Conclusion and Recommendations

7.1. Closing Remarks

The present work focused on the production of H_2 through pressure swing adsorption following the gasification of pelletized waste from blends of woody biomass and RDF. A techno-economic analysis of the Waste to H_2 route revealed the following:

- The designed 7 steps process configuration introduced, resulted in a improvement of 6.1 % with respect to H_2 yield. This might be attributed to high tar and water removal during the proposed configuration process.
- When evaluating the disparities between the simulation results in Aspen Tech and industry standards, a relative error of 0.4 % in the syngas adjustment unit is observed. This minimal error could potentially be attributed to differences in the catalyst used or variations in steam injection. In the context of the syngas purification unit, the market alternative for the water scrubber, demonstrates a superior NH_3 removal efficiency, approximately 9 % higher than the proposed system. This disparity can be linked to the lower solvent temperature, which has resulted in increased vapor condensation.
- The PSA system records a H_2 recovery of 63% and purity around 99.5 vol%. The H_2's quality aligns with the requirements for use in refineries, ammonia and methanol production and for various heat-related applications. Attaining a higher purity (99.9+ vol%) is feasible by tuning critical parameters, including adsorption pressure, purge to feed ratio or cycle time.
- The ROI of the proposed design is calculated at 9.7 %, exceeding the Dutch standard of 5 %, making it attractive for investors. Meanwhile, the payback period (PBP) is estimated at 5 years.
- The final price of the proposed system is H_2 of 7.35 €/kg, expressed in terms of Levelized Cost of H_2 ($LCOH$). This price was found to be competitive with different H_2 production routes such as biomass to H_2, electrolysis and steam methane reforming with carbon capture and storage [108].

7.2. Recommendations

To enhance the study's quality, future work should consider several key aspects:

- Incorporation of a rigorous design of the bio-Diesel absorption column and the MDEA absorption and stripping unit in Aspen Plus. Aspen Tech offers simulation templates for validated demonstration and commercial process units. The use of these templates as a starting point, could significantly enhance the accuracy of simulations and the reliability of results.
- Evaluating national and international policy instruments to support a renewable process route. This project is designed within the context of the energy transition scenario, where microalgae-based bio-Diesel is chosen for the tar absorption unit. According to the International Energy Agency, the price of bio-Diesel in Europe is 1.7 times higher than conventional Diesel, underscoring the importance of seeking government incentives and concessions to fully harness the potential of this renewable process.

- Integrating profitability measures like the Net Present Value is essential to account for the value of money over time and the risk considerations associated with a business model.
- Addressing a life cycle assessment, as a standardized metric, allowing the comparison of the developed system against other H_2 production routes from an environmental standpoint.

This research study makes a substantial contribution to the field of Waste to H_2 chain by offering an extensive and practical user guideline tailored specifically for the Aspen Tech environment. The Aspen Plus package is particularly suited for simulating steady-state scenarios and is highly recommended for future researchers, especially when working on syngas purification projects. On the other hand, Aspen Adsorption posed challenges in terms of convergence and conducting sensitivity analyses. Therefore, future studies might consider exploring the implications of using alternative industry standard simulators, such as gPROMS.

To conclude, the Waste to H_2 holds great promise for promoting a sustainable approach towards waste management and energy security, carrying substantial implications within the energy transition context.

References

[1] statista. *Global waste generation - statistics and facts*. 2023. URL: https://www.statista.com/topics/4983/waste-generation-worldwide/#topicOverview (visited on 05/2023).

[2] José Carlos Escobar Palacio et al. “Municipal Solid Waste Management and Energy Recovery”. In: *Energy Conversion*. Ed. by Ibrahim H. Al-Bahadly. Rijeka: IntechOpen, 2018. Chap. 8. DOI: 10.5772/intechopen.79235. URL: https://doi.org/10.5772/intechopen.79235.

[3] statista. *Waste management in Europe*. 2020. URL: https://www-statista-com.tudelft.idm.oclc.org/study/85571/waste-management-in-europe/ (visited on 09/2023).

[4] Kim Sinnige. “ZERO WASTE TO ENERGY: Identifying opportunities for spatial intervention to address overcapacity of Waste-To-Energy plants in the Netherlands”. MA thesis. Faculty of Architecture and the Built Environment, Delft University of Technology, 2023.

[5] International Energy Agency. “Net Zero by 2050: A Roadmap for the Global Energy Sector”. In: *International Energy Agency* (2021).

[6] International Energy Agency. *Global Hydrogen Review 2022 Executive summary*. 2022. URL: https://www.iea.org/reports/global-hydrogen-review-2022/executive-summary (visited on 09/2023).

[7] IEA. *Hydrogen*. 2022. URL: https://www.iea.org/reports/hydrogen (visited on 05/2023).

[8] Marise van der Linden. “Waste prevention strategies of municipalities in the Netherlands”. MA thesis. Radboud University Nijmegen, 2021.

[9] M.de Leeuw et al. *Decarbonisation options for the Dutch waste incineration industry*. Tech. rep. © PBL Netherlands Environmental Assessment Agency; © TNO, 2022. URL: https://www.pbl.nl/en/publications/decarbonisation-options-for-the-dutch-waste-incineration-industry.

[10] Babatunde Ismail Adefeso. *Techno-Economic Analysis of a Gasification System Using Refuse-Derived Fuel From Municipal Solid Waste*. 2017.

[11] P. Bhada-Tata D. Hoornweg. “What a Waste : A Global Review of Solid Waste Management cb”. In: *World Bank* 15 (November 2014), pp. 1–2.

[12] eurostat. *Municipal waste statistics*. 2023. URL: https://ec.europa.eu/eurostat/statistics-explained/index.php?title=Municipal_waste_statistics#Municipal_waste_generation (visited on 05/2023).

[13] Mebrahtom Negash Araya. “A Review of Effective Waste Management from an EU, National, and Local Perspective and Its Influence: The Management of Biowaste and Anaerobic Digestion of Municipal Solid Waste”. In: *Journal of Environmental Protection* 09 (06 2018). DOI: 10.4236/jep.2018.96041.

[14] *DIRECTIVE 2008/98/EC OF THE EUROPEAN PARLIAMENT AND OF THE COUNCIL of 19 November 2008 on waste and repealing certain Directives*. Directive. European Union, 2008.

[15] *COMMUNICATION FROM THE COMMISSION TO THE EUROPEAN PARLIAMENT, THE COUNCIL, THE EUROPEAN ECONOMIC AND SOCIAL COMMITTEE AND THE COMMITTEE OF THE REGIONS A new Circular Economy Action Plan For a cleaner and more competitive Europe*. Action Plan. European Union, 2020.

[16] Ana Pires et al. “Solid waste management in European countries: A review of systems analysis techniques”. In: *Journal of Environmental Management* 92 (4 2011). DOI: 10.1016/j.jenvman.2010.11.024.

[17] Paulien De Jong et al. “The structure of the Dutch waste sector and impediments for waste reduction”. In: *Waste Management and Research* 15 (6 1997). DOI: 10.1006/wmre.1996.0117.

[18] Jade Lui et al. “A critical review on the principles, applications, and challenges of waste-to-hydrogen technologies”. In: *Renewable and Sustainable Energy Reviews* 134 (2020). DOI: 10.1016/j.rser.2020.110365.

[19] Harshit Srivastava. *Market Analysis and Literature Review on Refuse Derived Fuel (RDF) from Residual Waste*. Tech. rep. The university of British Columbia; City of Vancouver, 2021. URL: https://sustain.ubc.ca/about/resources/market-analysis-and-literature-review-refuse-derived-fuel-rdf-residual-waste.

[20] Giovanna Pinuccia Martignon. *Trends in the use of solid recovered fuels*. Tech. rep. IEA Bioenergy, 2020. URL: https://www.ieabioenergy.com/blog/publications/new-publication-trends-on-use-of-solid-recovered-fuels/.

[21] Kok Siew Ng et al. “Evaluating the Techno-economic Potential of an Integrated Material Recovery and Waste-to-Hydrogen System”. In: *Resources, Conservation and Recycling* 167 (2021). DOI: 10.1016/j.resconrec.2020.105392.

[22] Yan Yang et al. “Gasification of refuse-derived fuel from municipal solid waste for energy production: a review”. In: *Environmental Chemistry Letters* 19 (3 2021). DOI: 10.1007/s10311-020-01177-5.

[23] M.Shahabuddin et al. “Advances in the thermo-chemical production of hydrogen from biomass and residual wastes: Summary of recent techno-economic analyses”. In: *Bioresource Technology* (2020).

[24] Silpa Kaza et al. *What a Waste 2.0 A Global Snapshot of Solid Waste Management To 2050*. World Bank Publications, 2018. URL: https://ebookcentral-proquest-com.tudelft.idm.oclc.org/lib/delft/detail.action?docID=5614550.

[25] Marcel Weeda en Reinoud Segers. *The Dutch hydrogen balance, and the current and future representation of hydrogen in the energy statistics*. Tech. rep. TNO, 2020. URL: https://www.rijksoverheid.nl/documenten/rapporten/2020/06/24/the-dutch-hydrogen-balance-and-the-current-and-future-representation-of-hydrogen-in-the-energy-statistics.

[26] World Energy Council. *World Energy Resources | 2016*. Tech. rep. World Energy Council, 2016. URL: https://www.worldenergy.org/publications/entry/world-energy-resources-2016.

[27] RWE. *FUREC: Making hydrogen from household waste*. 2023. URL: https://benelux.rwe.com/projecten/furec/ (visited on 07/2023).

[28] ENERKEM. *ENERKEM*. 2023. URL: https://enerkem.com/ (visited on 07/2023).

[29] European Commission. *Innovation Fund Large Scale Projects - Innovative electrification in industry and hydrogen*. 2022. URL: https://ec.europa.eu/info/funding-tenders/opportunities/portal/screen/opportunities/topic-details/innovfund-2022-lsc-02-industry-elec-h2 (visited on 07/2023).

[30] Ann Gardiner Matthew Smith Tycho Smit. *Financial support for electricity generation and CHP from solid Biomass*. Tech. rep. Trinomics B.V, Rotterdam, 2019.

[31] Netherlands Enterprise Agency. *Energy Investment Allowance - EIA*. 2023. URL: https://english.rvo.nl/subsidies-programmes/energy-investment-allowance-eia (visited on 07/2023).

[32] Zhemin Du et al. “A review of hydrogen purification technologies for fuel cell vehicles”. In: *Catalysts* 11 (3 2021). DOI: 10.3390/catal11030393.

[33] Majid Saidi et al. “Hydrogen production from waste gasification followed by membrane filtration: a review”. In: *Environmental Chemistry Letters* 18 (5 2020). DOI: 10.1007/s10311-020-01030-9.

[34] Luca Riboldi et al. “Evaluating Pressure Swing Adsorption as a CO2 separation technique in coal-fired power plants”. In: *International Journal of Greenhouse Gas Control* 39 (2015). DOI: 10.1016/j.ijggc.2015.02.001.

[35] Ke Liu et al. *Hydrogen and Syngas Production and Purification Technologies*. 2009. DOI: 10.1002/9780470561256.

[36] Muhammad Sajid et al. “Gasification of municipal solid waste: Progress, challenges, and prospects”. In: *Renewable and Sustainable Energy Reviews* 168 (2022). DOI: 10.1016/j.rser.2022.112815.

[37] Roh Pin Lee et al. “An analysis of waste gasification and its contribution to China’s transition towards carbon neutrality and zero waste cities”. In: *Ranliao Huaxue Xuebao/Journal of Fuel Chemistry and Technology* 49 (8 2021). DOI: 10.1016/S1872-5813(21)60093-2.

[38] Sachindra Chamode Wijayasekera et al. “Waste-to-hydrogen technologies: A critical review of techno-economic and socio-environmental sustainability”. In: *International Journal of Hydrogen Energy* 47 (9 2022). DOI: 10.1016/j.ijhydene.2021.11.226.

[39] Muhammad Aziz et al. “Hydrogen production from biomasses and wastes: A technological review”. In: *International Journal of Hydrogen Energy* 46 (68 2021). DOI: 10.1016/j.ijhydene.2021.07.189.

[40] Wiebren De Jong et al. *Biomass as a Sustainable Energy Source for the Future: Fundamentals of Conversion Processes*. Vol. 9781118304914. 2014. DOI: 10.1002/9781118916643.

[41] Prabir Basu. *Biomass Gasification, Pyrolysis and Torrefaction: Practical Design and Theory*. 2013. DOI: 10.1016/C2011-0-07564-6.

[42] D. Toporov et al. “Gasification of low-rank coal in the High-Temperature Winkler (HTW) process”. In: *Journal of the Southern African Institute of Mining and Metallurgy* 115 (7 2015). DOI: 10.17159/2411-9717/2015/v115n7a5.

[43] Wolfgang Adlhoch et al. “High-temperature Winkler gasification of municipal solid waste”. In: *2000 Gasification Technologies Conference* (2000).

[44] Patrick J. Woolcock et al. “A review of cleaning technologies for biomass-derived syngas”. In: *Biomass and Bioenergy* 52 (2013). DOI: 10.1016/j.biombioe.2013.02.036.

[45] P. Mondal et al. “Syngas production through gasification and cleanup for downstream applications - Recent developments”. In: *Fuel Processing Technology* 92 (8 2011). DOI: 10.1016/j.fuproc.2011.03.021.

[46] Paula Costa et al. “Integration of gasification and solid oxide fuel cells (SOFCs) for combined heat and power (CHP)”. In: *Processes* 9 (2 2021). DOI: 10.3390/pr9020254.

[47] Kristina Göransson et al. “Review of syngas production via biomass DFBGs”. In: *Renewable and Sustainable Energy Reviews* 15 (1 2011). DOI: 10.1016/j.rser.2010.09.032.

[48] Mohammad Asadullah. “Biomass gasification gas cleaning for downstream applications: A comparative critical review”. In: *Renewable and Sustainable Energy Reviews* 40 (2014). DOI: 10.1016/j.rser.2014.07.132.

[49] L. Biacchi A. Pan F.M.da Silva Lemos. “Purification of a syngas stream for the production of hydrogen for fuel cell standards”. MA thesis. Instituto Superior Técnico Lisboa, 2017.

[50] Corinne Squire et al. *CATALYST HANDBOOK Second Edition Edited by Martyn V. Twigg*. 2013.

[51] D. B. Pal et al. “Performance of water gas shift reaction catalysts: A review”. In: *Renewable and Sustainable Energy Reviews* 93 (2018). DOI: 10.1016/j.rser.2018.05.003.

[52] André B. de Haan et al. *Fundamentals*. Berlin, Boston: De Gruyter, 2013. DOI: doi:10.1515/9783110306729. URL: https://doi.org/10.1515/9783110306729.

[53] L.Warren McCabe et al. *Unit Operations of Chemical Engineering : Fifth Edition*. Vol. 136. 1993.

[54] *Perry’s chemical engineers’ handbook*. Vol. 45. 2008. DOI: 10.5860/choice.45-4393.

[55] Kevin R. Wood et al. *Design, Simulation and Optimization of Adsorptive and Chromatographic Separations*. 2018. DOI: 10.1002/9783527815029.

[56] Ralph T. Yang. *Gas Separation by Adsorption Processes*. Butterworth-Heinemann, 1987, pp. 1–338. URL: sciencedirect.com/book/9780409900040/gas-separation-by-adsorption-processes#book-info.

[57] C. W. SKARSTROM. *Method and apparatus for fractionating gaseous mixtures by adsorption*. 1960.

[58] Cary T. Chiou. *Partition and Adsorption of Organic Contaminants in Environmental Systems*. 2002. DOI: 10.1002/0471264326.

[59] Kenneth B. Bischoff. “Chemical engineering kinetics, J. M. Smith, 2nd edit., McGraw-Hill, New York(1970). 612 pages.” In: *AIChE Journal* 18 (4 1972). DOI: 10.1002/aic.690180445.

[60] F. G. Helfferich. “Principles of adsorption and adsorption processes, by D. M. Ruthven, John Wiley and Sons, 1984, xxiv + 433 pp”. In: *AIChE Journal* 31 (3 1985). DOI: 10.1002/aic.690310335.

[61] K. S.W. Sing. “Reporting physisorption data for gas/solid systems”. In: *Pure and Applied Chemistry* 54 (11 1982). DOI: 10.1351/pac198254112201.

[62] G. Jägers B. Ramani W. Buijs. “Development of a dynamic multi-bed Pressure Swing Adsorption process for high purity hydrogen production from Coke Oven Gas A mathemtical modeling approach”. MA thesis. Delft University of Technology, 2016.

[63] Ayub Golmakani et al. “Investigating PSA, VSA, and TSA methods in SMR unit of refineries for hydrogen production with fuel cell specification”. In: *Separation and Purification Technology* 176 (2017), pp. 73–91. DOI: https://doi.org/10.1016/j.seppur.2016.11.030. URL: https://www.sciencedirect.com/science/article/pii/S1383586616306669.

[64] Mauro Luberti et al. “Review of Polybed pressure swing adsorption for hydrogen purification”. In: *International Journal of Hydrogen Energy* 47.20 (2022), pp. 10911–10933. DOI: https://doi.org/10.1016/j.ijhydene.2022.01.147. URL: https://www.sciencedirect.com/science/article/pii/S0360319922002877.

[65] The Linde Group. *Hydrogen Recovery by Pressure Swing Adsorption*. https://www.linde-engineering.com/en/process-plants/adsorption-and-membrane-plants/hydrogen-recovery-and-purification/index.html.

[66] S. Sircar et al. “Purification of hydrogen by pressure swing adsorption”. In: *Separation Science and Technology* 35 (5 2000). DOI: 10.1081/SS-100100183.

[67] Amna Abdeljaoued et al. “Simulation and experimental results of a PSA process for production of hydrogen used in fuel cells”. In: *Journal of Environmental Chemical Engineering* 6 (1 2018). DOI: 10.1016/j.jece.2017.12.010.

[68] IEA. *Combined Heat and Power*. 2008. URL: https://www.iea.org/reports/combined-heat-and-power (visited on 08/2023).

[69] ADG Efficiency. *Combined Heat and Power*. 2023. URL: https://adgefficiency.com/cheat-sheet-gas-engine-gas-turbine-chp-energy-basics/ (visited on 08/2023).

[70] Ftwi Yohaness Hagos et al. “Trends of syngas as a fuel in internal combustion engines”. In: *Advances in Mechanical Engineering* 2014 (2014). DOI: 10.1155/2014/401587.

[71] J. Francois et al. “Detailed process modeling of a wood gasification combined heat and power plant”. In: *Biomass and Bioenergy* 51 (2013). DOI: 10.1016/j.biombioe.2013.01.004.

[72] Panayiotis Nicolaou. “Removal utilization/separation of tar from syngas”. In: *Thesis, Delft University Techonology* (2016).

[73] Thomas A. Adams et al. *Processes and simulations for solvent-based CO2 capture and syngas cleanup*. 2014. DOI: 10.1016/B978-0-444-59566-9.00006-5.

[74] Jesper Larsson et al. “Evaluation of an Absorption Based aMDEA Process Using Aspen Plus A conceptual study of biobased carbon capture technology for a combined heat and power plant”. MA thesis. Chalmers University of Technology, 2022.

[75] Laura A. Pellegrini et al. “Design of the CO2 Removal Section for PSA Tail Gas Treatment in a Hydrogen Production Plant”. In: *Frontiers in Energy Research* 8 (2020). DOI: 10.3389/fenrg.2020.00077.

[76] Ana Gabriela Alves Verdade. “The potential of Aspen Adsorption software package to simulate pressure swing adsorption units”. MA thesis. University of Porto, 2020.

[77] Inc. Aspen Technology. *Introduction to Aspen Adsorption: AspenTech Customer Education Training Manual Course Number ES288.071.07*. Aspen Technology, Inc. 2010.

[78] Aspen Technology Inc. *Select Optimal Adsorbents and Design Better Adsorption Cycles Faster.* 2023. URL: https://www.aspentech.com/en/products/pages/aspen-adsorption (visited on 09/2023).

[79] Inc. Aspen Technology. *Aspen Adsorption and Aspen Chromatography*. 2023. URL: https://www.aspentech.com/en (visited on 08/2023).

[80] Jinsheng Xiao et al. “Machine learning–based optimization for hydrogen purification performance of layered bed pressure swing adsorption”. In: *International Journal of Energy Research* 44 (6 2020). DOI: 10.1002/er.5225.

[81] Bundit Kottititum et al. “Optimization of a six-step pressure swing adsorption process for biogas separation on a commercial scale”. In: *Applied Sciences (Switzerland)* 10 (14 2020). DOI: 10.3390/app10144692.

[82] Huiru Li et al. “Modelling and simulation of two-bed PSA process for separating H2 from methane steam reforming”. In: *Chinese Journal of Chemical Engineering* 27 (8 2019). DOI: 10.1016/j.cjche.2018.11.022.

[83] Nannan Zhang et al. “Single- and double-bed pressure swing adsorption processes for H2/CO syngas separation”. In: *International Journal of Hydrogen Energy* 44 (48 2019). DOI: 10.1016/j.ijhydene.2019.08.095.

[84] Gioele Di Marcoberardino et al. “Green hydrogen production from raw biogas: A techno-economic investigation of conventional processes using pressure swing adsorption unit”. In: *Processes* 6 (3 2018). DOI: 10.3390/pr6030019.

[85] Aspentech. *Acid Gas Cleaning in Aspen HYSYS®*. Tech. rep. 2022.

[86] Henrik Thunman Alberto Alamia et al. “Process Simulation of Dual Fluidized Bed Gasifiers Using Experimental Data”. In: *Energy and Fuels* 30 (5 2016). DOI: 10.1021/acs.energyfuels.6b00122.

[87] NORIT. *NORIT Activated Carbon*. 2023. URL: https://norit.com/ (visited on 09/2023).

[88] Chemviron. *Chemviron A Kuraray Company*. 2023. URL: https://www.chemviron.eu/ (visited on 09/2023).

[89] Fabian Rosner et al. “Water gas shift reactor modelling and new dimensionless number for thermal management/design of isothermal reactors”. In: *Applied Thermal Engineering* 173 (2020). DOI: 10.1016/j.applthermaleng.2020.115033.

[90] Yano Surya Pradana et al. “Biodiesel Production from Wet Spirulina sp. by One-Step Extraction-Transesterification”. MA thesis. 2018. DOI: 10.1051/matecconf/201815603009.

[91] Robert M. Secor. *Mass-transfer operations. Robert E. Treybal. McGraw-Hill Book Company, Inc., New York(1955). 666 pages*. Vol. 2. 1956. DOI: 10.1002/aic.690020430.

[92] Rob J Best. *Coulson and Richardson’s Chemical Engineering, Volume 6, Design, 3rd edition*. Vol. 81. 2001. DOI: 10.1016/s1385-8947(00)00184-4.

[93] ICARUS. *Chapter 8: Towers, Columns (G3)*. 1998. URL: https://pdf4pro.com/view/towers-columns-instruct-59a835.html (visited on 09/2023).

[94] INTECH GmbH. *Basic steps to compressor unit calculation and selection*. 2022. URL: https://intech-gmbh.com/compr_calc_and_selec_examples/#example3 (visited on 09/2023).

[95] Atlas Copco. *Atlas Copco*. 2023. URL: https://www.atlascopco.com/ (visited on 09/2023).

[96] Boyun Guo et al. *Petroleum Production Engineering, A Computer-Assisted Approach*. 2007. DOI: 10.1016/B978-0-7506-8270-1.X5000-2.

[97] Louis Theodore. *Air Pollution Control Equipment Calculations*. 2008. DOI: 10.1002/9780470255773.

[98] Wang Junchao et al. "Modified Dual-Site Langmuir Adsorption Equilibrium Models from A GCMC Molecular Simulation". In: *Applied Sciences* 10 (2020). DOI: 10.3390/app10041311.

[99] Qinglin Huang et al. "Simulation of Hydrogen Purification by Pressure-Swing Adsorption for Application in Fuel Cells". In: *Environanotechnology* (2010). DOI: 10.1016/B978-0-08-054820-3.00012-5.

[100] S. Jain et al. "Heuristic design of pressure swing adsorption: A preliminary study". In: *Separation and Purification Technology* 33 (1 2003). DOI: 10.1016/S1383-5866(02)00208-3.

[101] INNIO Jenbacher. *INNIO Jenbacher*. 2022. URL: https://www.innio.com/en (visited on 09/2023).

[102] Qlik. *What is a KPI?* 2023. URL: https://www.qlik.com/us/kpi (visited on 09/2023).

[103] Richard Turton. *Analysis, Synthesis, and Design of Chemical Processes Fourth Edition*. Vol. 53. 2013.

[104] Warren D. Seider et al. *Product and Process Design Principles: Synthesis, Analysis and Design*. 2018.

[105] Charles Maxwell. *Cost Indices*. 2023. URL: https://toweringskills.com/financial-analysis/cost-indices/ (visited on 09/2023).

[106] Eric C. Carlson. "Don't gamble with physical properties for simulations". In: *Chemical Engineering Progress* 92 (10 1996).

[107] Mauro Villarini et al. "Sensitivity analysis of different parameters on the performance of a CHP internal combustion engine system fed by a biomass waste gasifier". In: *Energies* 12 (4 2019). DOI: 10.3390/en12040688.

[108] John Weatherby C. Andrea Jordan et al. *Advanced Gasification Technologies – Review and Benchmarking - Technical assessment and economic analysis*. Tech. rep. 2021.

[109] Martyn V. Twigg. *Catalyst Handbook*. 2018. DOI: 10.1201/9781315138862.

[110] Parham Mobed et al. "Data reconciliation and dynamic modeling of a sour water gas shift reactor". In: *Industrial and Engineering Chemistry Research* 53 (51 2014). DOI: 10.1021/ie500739h.

[111] The Engineering Toolbox. *Ammonia - Properties at Gas-Liquid Equilibrium Conditions*. 2018. URL: https://www.engineeringtoolbox.com/ammonia-gas-liquid-equilibrium-condition-properties-temperature-pressure-boiling-curve-d_2013.html (visited on 09/2023).

[112] The Engineering Toolbox. *Benzene - Thermophysical properties*. 2018. URL: https://www.engineeringtoolbox.com/benzene-benzol-properties-d_2053.html (visited on 09/2023).

[113] The Engineering Toolbox. *Flue Gases - Dew Point Temperatures*. 2010. URL: https://www.engineeringtoolbox.com/dew-point-flue-gases-d_1583.html (visited on 09/2023).

[114] Pimnara Tonpakdee et al. "Influence of solvent temperature and type on naphthalene solubility for tar removal in a dual fluidized bed biomass gasification process". In: *Current Applied Science and Technology* 21 (4 2021).

[115] Michael Th Müller et al. "EXPERIMENTAL INVESTIGATIONS ON BIODIESEL AS AN ALTERNATIVE ABSORBENT FOR THE RECOVERY OF AROMATIC HYDROCARBONS UNDER INDUSTRIAL CONDITIONS". In: *Distillation Absorption 2010* (2010).

[116] Rita Harb et al. "Evaluating the impact of several scrubbing systems on the tar removal efficiency from producer gas". In: *Clean Technologies and Environmental Policy* 24 (1 2022). DOI: 10.1007/s10098-021-02189-7.

[117] The Engineering Toolbox. *Hydrogen sulfide - Thermophysical Properties*. 2018. URL: https://www.engineeringtoolbox.com/hydrogen-sulfide-H2S-properties-d_2034.html (visited on 09/2023).

[118] The Engineering Toolbox. *Carbon Dioxide - Thermophysical Properties*. 2018. URL: https://www.engineeringtoolbox.com/CO2-carbon-dioxide-properties-d_2017.html (visited on 09/2023).

[119] Raphael Idem et al. “Evaluation of the Performance of Various Amine Based Solvents in an Optimized Multipurpose Technology Development Pilot Plant”. In: *Energy Procedia* 1 (1 2009). DOI: 10.1016/j.egypro.2009.01.202.

[120] Jinyao Yang et al. “Process Simulations of the Direct Non-Aqueous Gas Stripping Process for CO2 Desorption”. In: *Industrial and Engineering Chemistry Research* 59 (15 2020). DOI: 10.1021/acs.iecr.9b05378.

[121] DNV GL. *HyQuality Hydrogen Quality Compatibility Assessment of Hydrogen Purity Requirements for Industiral Application*. Tech. rep. DNV GL, 2019.

[122] David Chiche et al. “Investigation of competitive COS and HCN hydrolysis reactions upon an industrial catalyst: Langmuir-Hinshelwood kinetics modeling”. In: *Applied Catalysis B: Environmental* 205 (2017). DOI: 10.1016/j.apcatb.2016.12.002.

[123] Central Governament. *Main tax changes as of January 1, 2022*. 2021. URL: https://www.rijksoverheid.nl/actueel/nieuws/2021/12/21/belangrijkste-belastingwijzigingen-per-1-januari-2022#:~:text=Belasting%20voor%20bedrijven&text=Het%20tarief%20voor%20de%20vennootschapsbelasting,%25%20naar%2025%2C8%25. (visited on 09/2023).

[124] Aswath Damodaran. *Country Default Spreads and Risk Premiums*. 2023. URL: https://pages.stern.nyu.edu/~adamodar/New_Home_Page/datafile/ctryprem.html (visited on 09/2023).

[125] Gema Amaya-Santos et al. “Biohydrogen: A life cycle assessment and comparison with alternative low-carbon production routes in UK”. In: *Journal of Cleaner Production* 319 (2021). DOI: 10.1016/j.jclepro.2021.128886.

[126] PRAKASHBHAI RAMABHAI BHOI. “WET SCRUBBING OF BIOMASS PRODUCER GAS TARS USING VEGETABLE OIL”. MA thesis. Oklahoma State University, 2014.

[127] Firman Asto Putro et al. “Absorption of Tar Content in Producer Gas using Used Cooking Oil in a Packed-bed Column”. In: *Equilibrium Journal of Chemical Engineering* 7 (1 2023). DOI: 10.20961/equilibrium.v7i1.70383.

[128] International Energy Agency. *Biodiesel and diesel prices, 2019 to April 2022*. 2022. URL: https://www.iea.org/data-and-statistics/charts/biodiesel-and-diesel-prices-2019-to-april-2022 (visited on 09/2023).

[129] Jassim Mohammed Khanjar et al. “Simulation and parametric analysis of natural gas sweetening process: A case study of Missan Oil Field in Iraq”. In: *Oil and Gas Science and Technology* 76 (2021). DOI: 10.2516/ogst/2021033.

[130] Eurostat. *Electricity price statistics*. 2023. URL: https://ec.europa.eu/eurostat/statistics-explained/index.php?title=Electricity_price_statistics#Electricity_prices_for_non-household_consumers (visited on 09/2023).

[131] Intratec. *Steam Current Costs, Historical Series and Forecasts*. 2018. URL: https://www.intratec.us/products/water-utility-costs/commodity/steam-cost (visited on 09/2023).

[132] Chemical Engineering Projects. *ESTIMATION OF OPERATING COSTS*. 2014. URL: https://chemicalprojects.wordpress.com/2014/05/11/estimation-of-operating-costs/ (visited on 09/2023).

[133] Intratec. *Oxygen Price Current and Forecast*. 2018. URL: https://www.intratec.us/chemical-markets/oxygen-price (visited on 09/2023).

A

Implications of impurities in syngas applications

In the table below, it is possible to notice different impurities contained in syngas streams and their implications.

Table A.1: Implications of impurities in syngas applications [44].

Implications	Definition and main impurities formation	Contaminant
Metallic components erosion, environmental pollution, deposition and blockage of mechanical parts.	Derive from ash, char, condensing compounds, and bed material of fluidized bed reactors.	Particulate Matter
Clogs filters and valves, metallic corrosion.	Complex mixture of mostly aromatic hydrocarbons which are condensable at ambient temperature.	Tars
Harmful pollutants (SO_x), acid corrosion of metals, catalysts de-activation.	COS, H_2S.	Sulphur
NO_x emission during combustion, catalysts de-activation.	NH_3, HCN.	Nitrogen
Metal corrosion at high-temperature due to the stripping-off of the protective oxide layer, defluidization of the bed.	Trace elements especially K and Na inherently present in biomass and vaporize under gasification temperature.	Alkali compounds
Harmful pollutants, acid corrosion of metals, catalysts de-activation.	HCl.	Chlorine

B

Methods to improve PSA performance.

The relevance of multibed systems is highlighted in a study carried out by Luberti et al. [64], in which general methods to improve H_2 PSA performance are assessed and reported in the table here below:

Table B.1: Methods to improve H_2 PSA performance [64].

Parameter	Implementation	Outcome
Cycle step sequence	Rigorously based on experience and literature. However, scheduling methods based on graphical and arithmetic approaches has shown promising results. Nevertheless, both approaches require a priori information about the step sequence, the constraints to meet and the number of beds.	Minimum number of beds required to operate the specified step sequence, the minimum number and location of idle steps to ensure alignment of coupled cycle steps.
Multi Bed System	PSA cycles are generally carried out to provide adsorption and regeneration. This is possible using a multibed system in parallel/series.	H_2 production in continuous operation. Increasing the number of beds allows a PSA unit to incorporate in the cycle more pressure equalisation, providing purge and simultaneous adsorption steps, which will increase the H_2 recovery.
Multiple pressure equalisation steps	Reduce the initial pressure of the blowdown step, thus minimising the hydrogen losses.	In case of a H_2 PSA unit designed to produce ultrapure H_2 (99.99+%) from a steam reformer syngas, the H_2 recovery could be improved from 60 to 65% with one pressure equalisation step to 70-75% with two pressure equalisation steps, and up to 80-90% with three pressure equalisation steps.
Use of providing purge step	Since the purge step is carried out at the lowest pressure of the cycle, the source of hydrogen can be taken from any other step in the cycle that are at a higher pressure, e.g. during a co-current depressurisation step at intermediate pressure. Often, the providing purge step is carried out in the cycle sequence after the final depressurising pressure equalisation step, that is to say, prior to the blowdown step.	Providing purge steps increase the H_2 recovery by avoiding the consumption of H_2 product in the purge step.
Multiple beds on adsorption step	This configuration splits the raw H_2 feed flowrate equally into more than one bed during the adsorption step, thus reducing the gas velocity along each bed.	Improving the H_2 recovery because lower gas velocities make the concentration fronts travel more sharply along the beds so that the length of unused bed (LUB) gets shorter. As a result, H_2 PSA units could benefit from this strategy by having a longer adsorption time or requiring smaller adsorption beds, leading to greater bed productivities and lower unit CAPEX.

C

Physical Catalyst Properties – Low Temperature Sour Shift Catalyst.

In the table below, the Physical CoMo Properties for the Low Temperature Sour Shift Catalyst [89].

Table C.1: Physical Catalyst Properties – Low Temperature Sour Shift Catalyst [89].

Specification	Unit	Value
Δ_P	bar	0.6
ρ	kg/m^3	5.645
ε	-	0.45
μ	Pa s	2.109e-5
d_p	m	0.003
v	m/s	0.8

D

Absorption and Stripping columns calculations

In this section the input parameters necessary to express the parameters with regards to absorption and stripping columns are tabulated (the values left in the blank space are collected from Aspen Plus). With regards to columns sizing, each one is conceived following the same logic and computed according a set of equations.

In the first set of equations, calculations are conducted to determine the column diameter. In this phase, information in the book of Mass Transfer operations [91] were necessary to evaluate the correlation between flooding and pressure drop in random packed towers. This was possible via the analysisi of Figure 6.34 of the book of Mass Transfer operations [91].

On the other hand, the second set of equations are needed to assess the column's flooding percentage through a hydraulic check as done in the book Coulson and Richardson's Chemical Engineering [92]. Figure 11.44 of [92] is necessary to assess the column cross-sectional area and diameter for the selected pressure drop.

D.1. Minimum Bio-Diesel flowrate for tar absorption

The input parameters to compute the Minimum Bio-Diesel flowrate of 1656.027 kmol/h for tar absorption are provided below.

Table D.1: Minimum Bio-Diesel Requirements for Tar Absorption

Specification	Unit	Value	Ref.
G_in	kmol/h	2760	
K_C6H6	-	0.3	[126]
K_C10H8	-	0.1	[127]
yin_C6H6	mol%	9.1e-4	
yout_C6H6	mol%	1e-8	Assumption
yin_C10H8	mol%	4.17e-5	
yout_C10H8	mol%	1e-8	Assumption
xin_C6H6	mol%	1e-7	
xin_C10H8	mol%	1e-7	

D.2. Bio-Diesel absorption column diameter

The parameters to calculate the Bio-Diesel absorption column diameter of 2.5 m are given below.

D.3. Bio-Diesel stripping column diameter

The parameters to calculate the Bio-Diesel stripping column diameter of 0.5 m are given below.

Table D.2: Specifications and Values for the Bio-Diesel absorption column diameter

Specification	Unit	Value	Ref.
$M_L + M_{\text{solute}}$	kg/s	131.5	
M_G	kg/s	64.8	
ρ_G	kg/m^3	18.67	
ρ_L	kg/m^3	848.35	
Fig. 6.34 factor	-	0.038	[91]
G'	kg/m^2 s	5.682	
K_4	-	0.75	[92]
K_4 at flood	-	1.8	[92]
F_P	-	32	[53]
μ_L	Ns/m^2	0.003	

Table D.3: Specifications and Values for the Bio-Diesel Stripping Column Diameter

Specification	Unit	Value	Ref.
$M_L + M_{\text{solute}}$	kg/s	0.462	
M_G	kg/s	0.038	
ρ_G	kg/m^3	0.011	
ρ_L	kg/m^3	859.02	
Fig. 6.34 factor	-	0.06	[91]
G'	kg/m^2 s	0.124	
K_4	-	1.2	[92]
K_4 at flood	-	5	[92]
F_P	-	65	[53]
μ_L	Ns/m^2	0.004	

D.4. Aqueous MDEA absorption column diameter

The parameters to calculate the Aqueous MDEA absorption column diameter of 2 m are given below.

D.5. Aqueous MDEA stripping column diameter

The parameters to calculate the Aqueous MDEA stripping column diameter of 1.1 m are given below.

Table D.5: Specifications and Values for the Aqueous MDEA stripping column diameter

Specification	Unit	Value	Ref.
$M_L + M_{\text{solute}}$	kg/s	100.78	
M_G	kg/s	0.22	
ρ_G	kg/m^3	0.228	
ρ_L	kg/m^3	39.98	
Fig. 6.34 factor	-	0.03	[91]
G'	kg/m^2 s	2.293	
K_4	-	1	[92]
K_4 at flood	-	6	[92]
F_P	-	65	[53]
μ_L	Ns/m^2	0.00038	

Table D.4: Specifications and Values for the Aqueous MDEA absorption column diameter

Specification	Unit	Value	Ref.
$M_L + M_{\text{solute}}$	kg/s	94	
M_G	kg/s	10.482	
ρ_G	kg/m^3	6.775	
ρ_L	kg/m^3	1024.7	
Fig. 6.34 factor	-	0.02	[91]
G'	kg/m^2 s	2.033	
K_4	-	0.425	[92]
K_4 at flood	-	0.9	[92]
F_P	-	65	[53]
μ_L	Ns/m^2	0.001	

D.6. Minimum Low pressure Steam flowrate for Bio-Diesel stripping

The input parameters to compute the Minimum Low pressure Steam flowrate for Bio-Diesel stripping of 38188.72 kg/h are provided below.

Table D.6: Minimum Low pressure Steam flowrate for Bio-Diesel stripping

Specification	Unit	Value	Ref.
L_in	kmol/h	2072.63	
K_Bio-Diesel	-	0.9	Assumption
yin_steam	mol%	0	
xin_Bio-Diesel	mol%	0.00127	
xout_Bio-Diesel	mol%	1e-4	Assumption

E

Adsorbent for Pressure Swing Adsorption system

E.1. Adsorbent characteristics for bed sizing

Data specifications with regards the working capacity at 15 bar for Activated Carbon and Zeolite 5A adsorbents for the 4 impurities present in the syngas before the pressure swing adsorption unit are provided below:

Table E.1: Working Capacity at 15 bar

Working Capacity [mol/kg]	CO2	CH4	CO	N2
Activated Carbon	7	5	4.5	1
Zeolite 5A	4.5	1.75	2	1.75

Table E.2 furnishes the necessary input specification for bed sizing. It is noteworthy to say that to the values should be re-adapted accordingly when sizing a 2, 4 and 8 PSA system.

Table E.3 presents the results of the bed sizing for a 4 and 8 beds PSA. it is noteworthy to sat that in the case of a 4 beds system the flowrate was kept to its initial value of 0.32 kmol/s. Conversely, designing a 8 beds system requires splitting the feed stream in two.

Table E.3: Bed sizing for a 4 and 8 beds PSA.

Parameter	4 beds PSA	8 beds PSA
Length [m]	5.25	3.75
Diameter [m]	2	2

In the event that the composition of the feed differs, analogous principles can be employed. Specifically, when the feed exhibits an elevated concentration of N_2, it is anticipated that the Zeolite 5A layer will possess an increased height. Similarly, a corollary trend is anticipated for CO_2 concerning the Activated Carbon layer. Nevertheless, the same logic described in Chapter 3 can be applied to find the new bed sizing.

E.2. Aspen Adsorption validation of Xiao et al. work

Figure E.1 represents the Aspen Adsorption flowsheet for the validation of the work conducted by Xiao et al. [80].

Table E.2: Input data for bed sizing calculations.

Parameter	Unit	Value
Flowrate	kmol/s	0.32
CO2	mol %	0.3
CH4	mol %	8.2
CO	mol %	16.8
H2	mol %	74.4
N2	mol %	0.3
t_{ads}	s	150
v	m/s	0.35
ρ_{AC}	kg/m^3	850
ρ_{Zeo5A}	kg/m^3	1160
Q_v	m^3/s	0.529
L/D	-	2.5

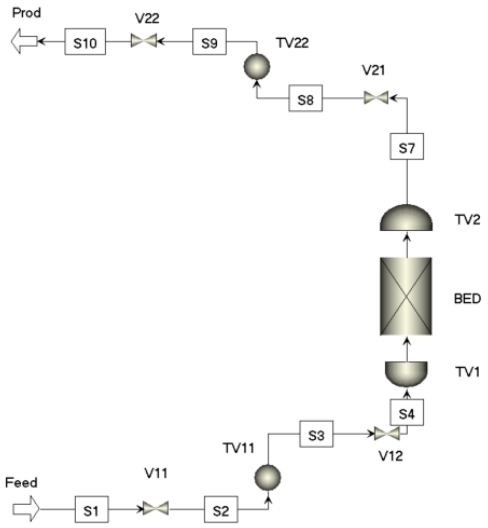

Figure E.1: Aspen Adsorption validation of Xiao et al. work [80].

The `Feed` composition is constituted by CH_4/CO/CO_2/H_2/N_2 = 1/1/50/38/10 mol%. Moreover, all the `gas_tank_void` blocks are assumed to include the compression term, to be adiabatic, and have a composition of CH_4/CO/CO_2/H_2/N_2 = 0/0/0/1/0 mol% (as well as the layers in the `gas_bed` model). The input data for the bed can be retrieved from the work of Xiao et al. [80]. The discretization method used is UDS1 assuming 40 nodes. The material balance assumes only the convection term, while the Ergun equation is selected for the momentum balance assumption. The kinetic model assumes a solid film model with lumped resistance kinetic (linear parameter) and constant mass transfer coefficient. Moreover, the isothermal conditions are maintained in the energy balance, neglecting any type of chemical reactions. The remaining values, which were omitted in that study, are presented in Table E.4.

Table E.4: Specifications to input to replicate the validation case in Aspen Adsorption.

	Active Specification	Flowrate [mol/s]	P [bar]	T [K]	Tank_Volume [m^3]
V11	3	0.0020971			
V12	1				
V21	1				
V22	1				
Feed			6.5	298.15	
Prod			1.013		
T11					1E-5
TV1					1E-5
TV2					1E-5
T22					1E-5

E.3. Algorithm for the isothermal conditions verification

Below, the Python Code for the isothermal conditions verification is presented. All the data are retrieved for a 3 m empty bed, comprising only the activated carbon layer and without the presence of N_2 in the gas given its low concentration and impact on the temperature evolution. It is noteworthy to say that all the values with regards to the heat of adsorption are expressed with the negative sign because they refer to energy release.

```
# Your Python code here
import numpy as np
import matplotlib.pyplot as plt

'''Constants for the species in the syngas'''

k_CO2 = 0.0355  # Mass transfer coefficient of CO2 (1/s)
a1_CO2 = 28.7973  # (mol/kg)
a2_CO2 = -7e-2  # (mol/K Kg)
b0_CO2 = 100e-4  # (1/bar)
b1_CO2 = 1030  # (K)
d_HCO2 = -5240 * 4.2  # Heat of adsorption CO2 (J/mol)

k_H2 = 0.7  # Mass transfer coefficient of CO2 (1/s)
a1_H2 = 16.943 # (mol/kg)
a2_H2 = -2.1e-2  # (mol/K Kg)
b0_H2 = 0.6248e-4  # (1/bar)
b1_H2 = 1229  # (K)
d_HH2 = -2880 * 4.2  # Heat of adsorption CO2 (J/mol)

k_CH4 = 0.195  # Mass transfer coefficient of CO2 (1/s)
a1_CH4= 23.86  # (mol/kg)
a2_CH4 = -5.621e-2  # (mol/K Kg)
b0_CH4 = 34.78e-4  # (1/bar)
b1_CH4 = 1159  # (K)
d_HCH4 = -4290 * 4.2  # Heat of adsorption CO2 (J/mol)

k_CO = 0.15  # Mass transfer coefficient of CO2 (1/s)
a1_CO = 33.85  # (mol/kg)
a2_CO= -9.072e-2  # (mol/K Kg)
```

```
b0_CO = 2.311e-4  # (1/bar)
b1_CO = 1751 # (K)
d_HCO = -4300 * 4.2  # Heat of adsorption CO (J/mol)


'''Partial pressure of species necessary for calculating the adsorbed
    amount'''
p_tot = 15  # Total pressure (bar)
p_CO2 = 2.25  # CO2 pressure (bar)
p_H2= 11.25 # H2 pressure (bar)
p_CH4 = 0.75  # CH4 pressure (bar)
p_CO=0.75 # CO pressure (bar)


'''Adsorbent data specifications'''
eps = 0.433  # Bed porosity
rho_g = 7.87  # Gas Density (kg/m$^3$)
cp_g = 2.283e4  # Heat capacity gas (J/kg/K)
rho_b = 482  # Bulk Density (kg/m$^3$)
C_s = 1046  # Heat capacity solid (J/kg/K)
u = 0.5  # Interstitial velocity (m/s)



'''Isothermal conditions verification using Equation in the Material and
    Methods Chapter'''
A = (eps * rho_g * cp_g + rho_b * C_s / u) + (eps * rho_g * cp_g)  #
    Constant A
B_CO2 = rho_b * d_HCO2 / u  # Constant B_CO2
B_CO = rho_b * d_HCO2 / u  # Constant B_CO
B_CH4 = rho_b * d_HCH4 / u  # Constant B_CH4
B_H2 = rho_b * d_HH2 / u  # Constant B_H2

# Define the equation for q_star = saturation concentration for the
    isotherm Extended Langmuir 3
def q_star_CO2(T):
    return (a1_CO2 + a2_CO2 * T) * b0_CO2 * np.exp(b1_CO2 / T) * p_CO2 /
        ((1 + b0_CO2 * np.exp(b1_CO2 / T) * p_CO2)+ (1 + b0_CH4 *
        np.exp(b1_CH4 / T) * p_CH4) + (1 + b0_H2 * np.exp(b1_H2 / T) *
        p_H2)+ (1 + b0_CO * np.exp(b1_CO / T) * p_CO))
def q_star_H2(T):
    return (a1_H2 + a2_H2 * T) * b0_H2 * np.exp(b1_H2 / T) * p_H2 / ((1 +
        b0_CO2 * np.exp(b1_CO2 / T) * p_CO2) + (1 + b0_CH4 * np.exp(b1_CH4 /
        T) * p_CH4) + (1 + b0_H2 * np.exp(b1_H2 / T) * p_H2) + (1 + b0_CO *
        np.exp(b1_CO / T) * p_CO))

def q_star_CH4(T):
    return (a1_CH4 + a2_CH4 * T) * b0_CH4 * np.exp(b1_CH4 / T) * p_CH4 /
        ((1 + b0_CO2 * np.exp(b1_CO2 / T) * p_CO2) + (1 + b0_CH4 *
        np.exp(b1_CH4 / T) * p_CH4) + (1 + b0_H2 * np.exp(b1_H2 / T) * p_H2)
        + (1 + b0_CO * np.exp(b1_CO / T) * p_CO))

def q_star_CO(T):
    return (a1_CO + a2_CO * T) * b0_CO * np.exp(b1_CO / T) * p_CO / ((1 +
        b0_CO2 * np.exp(b1_CO2 / T) * p_CO2) + (1 + b0_CH4 * np.exp(b1_CH4 /
        T) * p_CH4) + (1 + b0_H2 * np.exp(b1_H2 / T) * p_H2) + (1 + b0_CO *
```

```
        np.exp(b1_CO / T) * p_CO))

def dq_dtH2(T, q):
    return k_H2 * (q_star_H2(T) - q)

def dq_dtCO2(T, q):
    return k_CO2 * (q_star_CO2(T) - q)

def dq_dtCO(T, q):
    return k_CO * (q_star_CO(T) - q)

def dq_dtCH4(T, q):
    return k_CH4 * (q_star_CH4(T) - q)
''' Set up the spatial and time grid assuming:
   (i) Single adsorption step of 150 seconds
   (ii) Bed height of 3 meters for the 8 beds PSA system '''
num_z_steps = 150
num_t_steps = 150
z = np.linspace(0, 3, num_z_steps)
t = np.linspace(1, 150, num_t_steps)
dt = t[1] - t[0]
dz = z[1] - z[0]

# Initialize arrays to store results
dq_dt_values_CH4 = np.zeros((num_t_steps, num_z_steps))
dq_dt_values_H2 = np.zeros((num_t_steps, num_z_steps))
dq_dt_values_CO = np.zeros((num_t_steps, num_z_steps))
dq_dt_values_CO2 = np.zeros((num_t_steps, num_z_steps))

dT_dz_values_CO2 = np.zeros((num_t_steps, num_z_steps))
dT_dz_values_CO = np.zeros((num_t_steps, num_z_steps))
dT_dz_values_CH4 = np.zeros((num_t_steps, num_z_steps))
dT_dz_values_H2 = np.zeros((num_t_steps, num_z_steps))

T = np.zeros((num_t_steps, num_z_steps))

''' Set initial conditions:
    (i) Temperature of 298.15 K
    (ii) Empty bed with concentration (H2/CO/CO2/CH4 = 1/0/0/0) '''
T[0, :] = 298.15  # Initial temperature

# Calculate dq_dt for each time step and solve dT_dz equation
for i in range(1, num_t_steps):
    dq_dt_values_CO2[i, :] = dq_dtCO2(T[i - 1, :], 0)
    dq_dt_values_H2[i, :] = dq_dtH2(T[i - 1, :], 0)
    dq_dt_values_CO[i, :] = dq_dtCO(T[i - 1, :], 0)
    dq_dt_values_CH4[i, :] = dq_dtCH4(T[i - 1, :], 0)

    T[i, :] = T[i - 1, :] + (-(B_CO2 * dq_dt_values_CO2[i, :] + B_H2 *
        dq_dt_values_H2[i, :] + B_CO * dq_dt_values_CO[i, :] + B_CH4 *
        dq_dt_values_CH4[i, :]) / A) * dz

    dT_dz_values_CO2[i, :] = (T[i, :] - T[i - 1, :]) / dz
    dT_dz_values_CO[i, :] = (T[i, :] - T[i - 1, :]) / dz
    dT_dz_values_CH4[i, :] = (T[i, :] - T[i - 1, :]) / dz
    dT_dz_values_H2[i, :] = (T[i, :] - T[i - 1, :]) / dz
```

```
125
126 # Calculate delta temperature
127 delta_T = T - 298.15
128
129 # Plot delta temperature over time
130 plt.figure(figsize=(10, 5))
131 plt.plot(t, delta_T[:, 0], label='Position 0')
132 plt.plot(t, delta_T[:, -1], label='Position {}'.format(num_z_steps - 1))
133 plt.xlabel('Time')
134 plt.ylabel('Delta Temperature (K)')
135 plt.title('Delta Temperature over Time')
136 plt.legend()
137 plt.grid(True)
138 plt.show()
139
140
141
142 final_temperature = T[-1, -1]
143 print("Final Temperature of the Reactor: {} K".format(final_temperature))
144
145
146 # Set up the figure and axis
147 fig, ax = plt.subplots()
148
149 # Plot the temperature evolution
150 ax.plot(t, T[:, -1])
151
152 # Set the x-axis label
153 ax.set_xlabel('Time (s)')
154
155 # Set the y-axis label
156 ax.set_ylabel('Temperature (K)')
157
158 # Display the plot
159 plt.show()
```

Listing E.1: Python Code for the isothermal conditions verification.

F

Technical Datasheet by INNIO Jenbacher for the syngas composition

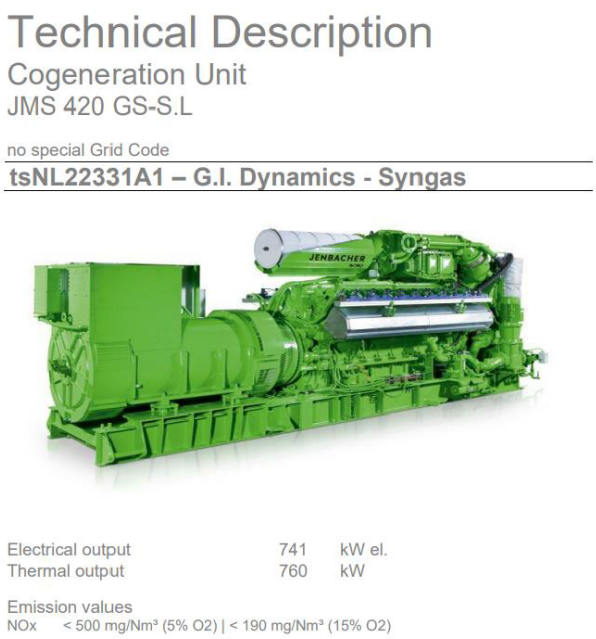

Technical Description
Cogeneration Unit
JMS 420 GS-S.L

no special Grid Code

tsNL22331A1 – G.I. Dynamics - Syngas

Electrical output	741	kW el.
Thermal output	760	kW

Emission values
NOx < 500 mg/Nm³ (5% O2) | < 190 mg/Nm³ (15% O2)

Figure F.1: Technical Datasheet by INNIO Jenbacher

JENBACHER

0.01 Technical Data (at module)

			100%	75%	min.
Power input	[2]	kW	1.906	1.495	1.421
Gas volume	*)	Nm³/h	1.589	1.246	1.184
Mechanical output	[1]	kW	764	573	538
Electrical output	[4]	kW el.	741	553	519
Recoverable thermal output					
~ Intercooler 1st stage	[9]	kW	63	10	3
~ Lube oil		kW	132	114	111
~ Jacket water		kW	227	203	199
~ Exhaust gas cooled to 180 °C		kW	338	289	278
Total recoverable thermal output	[5]	kW	760	616	591
Total output generated		kW total	1.501	1.169	1.110
Heat to be dissipated (calculated with Glykol 37%)					
~ Intercooler 2nd stage		kW	50	31	27
~ Lube oil		kW	---	---	---
~ Surface heat	ca. [7]	kW	120	~	~
Spec. fuel consumption of engine electric	[2]	kWh/kWel.h	2,57	2,70	2,74
Spec. fuel consumption of engine	[2]	kWh/kWh	2,49	2,61	2,64
Lube oil consumption	ca. [3]	kg/h	0,38	~	~
Electrical efficiency			38,9%	37,0%	36,5%
Thermal efficiency			39,8%	41,2%	41,6%
Total efficiency	[6]		78,7%	78,2%	78,1%
Hot water circuit:					
Forward temperature		°C	90,0	86,2	85,6
Return temperature		°C	70,0	70,0	70,0
Hot water flow rate		m³/h	32,6	32,6	32,6
Fuel gas LHV		kWh/Nm³	1,2		

*) approximate value for pipework dimensioning
[_] Explanations: see 0.10 - Technical parameters

All heat data is based on standard conditions according to attachment 0.10. Deviations from the standard conditions can result in a change of values within the heat balance and must be taken into consideration in the layout of the cooling circuit/equipment (intercooler; emergency cooling; ...).

Figure F.2: Technical Datasheet by INNIO Jenbacher

JENBACHER

Main dimensions and weights (at module)

Length	mm	~ 6.300
Width	mm	~ 1.800
Height	mm	~ 2.500
Weight empty	kg	~ 15.300
Weight filled	kg	~ 16.000

Connections

Hot water inlet and outlet [A/B]	DN/PN	100/10
Exhaust gas outlet [C]	DN/PN	300/10
Fuel Gas (at module) [D]	DN/PN	125/16
Water drain ISO 228	G	½"
Condensate drain	DN/PN	50/10
Safety valve - jacket water ISO 228 [G]	DN/PN	2x1½"/2,5
Safety valve - hot water	DN/PN	65/16
Lube oil replenishing (pipe) [I]	mm	28
Lube oil drain (pipe) [J]	mm	28
Jacket water - filling (flex pipe) [L]	mm	13
Intercooler water-Inlet/Outlet 1st stage	DN/PN	100/10
Intercooler water-Inlet/Outlet 2nd stage [M/N]	DN/PN	65/10

Output / fuel consumption

ISO standard fuel stop power ICFN	kW	764
Mean effe. press. at stand. power and nom. speed	bar	10,00
Fuel gas type		Syngas
Based on methane number | Min. methane number	MZ	n.a. | 45 d)
Compression ratio	Epsilon	11,8
Min./Max. fuel gas pressure at inlet to gas train	mbar	120 - 200
Max. rate of gas pressure fluctuation	mbar/sec	10
Maximum Intercooler 2nd stage inlet water temperature	°C	40
Spec. fuel consumption of engine	kWh/kWh	2,49
Specific lube oil consumption	g/kWh	0,50
Max. Oil temperature	°C	~ 85
Jacket-water temperature max.	°C	~ 95
Filling capacity lube oil (refill)	lit	~ 437

d) based on methane number calculation software AVL 3.2

Figure F.3: Technical Datasheet by INNIO Jenbacher

JENBACHER

0.02 Technical data of engine

Manufacturer		JENBACHER
Engine type		J 420 GS-D47
Working principle		4-Stroke
Configuration		V 70°
No. of cylinders		20
Bore	mm	145
Stroke	mm	185
Piston displacement	lit	61,10
Nominal speed	rpm	1.500
Mean piston speed	m/s	9,25
Length	mm	3.750
Width	mm	1.580
Height	mm	2.033
Weight dry	kg	7.200
Weight filled	kg	7.900
Moment of inertia	kgm²	11,64
Direction of rotation (from flywheel view)		left
Radio interference level to VDE 0875		N
Starter motor output	kW	13
Starter motor voltage	V	24
Thermal energy balance		
Power input	kW	1.906
Intercooler	kW	113
Lube oil	kW	132
Jacket water	kW	227
Exhaust gas cooled to 180 °C	kW	338
Exhaust gas cooled to 100 °C	kW	468
Surface heat	kW	91
Exhaust gas data		
Exhaust gas temperature at full load [8]	°C	382
Exhaust gas temperature at bmep= 7,5 [bar]	°C	~ 404
Exhaust gas temperature at bmep= 7,1 [bar]	°C	~ 408
Exhaust gas mass flow rate, wet	kg/h	5.524
Exhaust gas mass flow rate, dry	kg/h	5.281
Exhaust gas volume, wet	Nm³/h	4.219
Exhaust gas volume, dry	Nm³/h	3.917
Max.admissible exhaust back pressure after engine	mbar	60
Combustion air data		
Combustion air mass flow rate	kg/h	4.218
Combustion air volume	Nm³/h	3.264
Max. admissible pressure drop at air-intake filter	mbar	10

Figure F.4: Technical Datasheet by INNIO Jenbachern

G

Flowsheet scheme for the Syngas Adjustment Unit in Aspen Plus

G.1. Flowsheet scheme for the Syngas Adjustment Unit in Aspen Plus.

In this section, the flowsheet scheme developed for the syngas adjustment unit in Aspen Plus is provided. The raw syngas undergoes two shell and tube heat exchangers to enter the high temperature shift reactor with the adequate operating conditions.

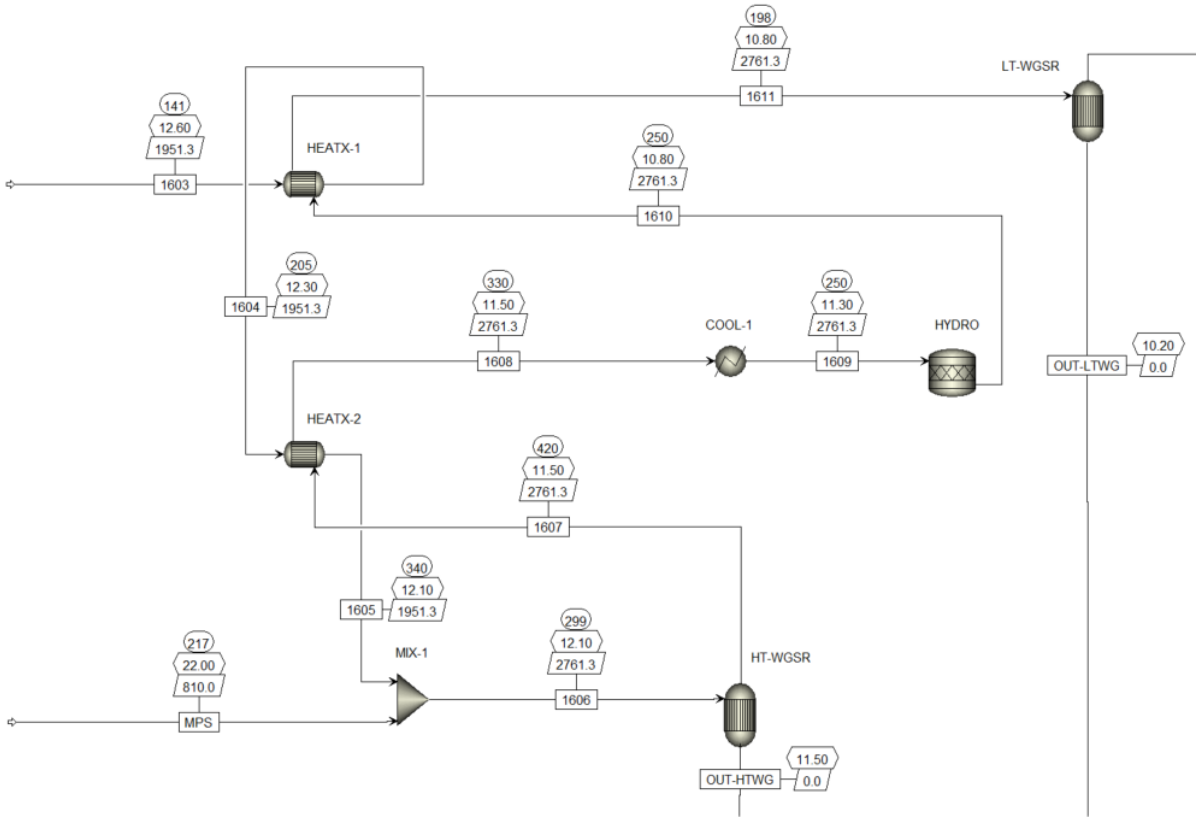

Figure G.1: Flowsheet scheme for the Syngas Adjustment Unit in Aspen Plus.

G.2. Boundary conditions for the Syngas Adjustment Unit in Aspen Plus

The equilibrium reactors, approximated by the `REquil` blocks, are chosen due to the fact that for high temperatures, the shift reaction is controlled by equilibrium. The hydrolysis reactor, approximated by the `RStoic` block, is assumed to be working under 99.99 % conversion efficiency in accordance with operational reliability proven by industry standards hydrolysis reactor.

Table G.1 reports the syngas adjustment specification for each reactor.

Table G.1: Syngas Adjustment Unit Specifications

Unit	Boundary Conditions	Stoichiometry	Assumptions
HT-WGSR	• Inlet operating T: 300 °C • Max outlet operating T increase: 150 °C • Steam/CO ratio [109]: 2.1	Equation 2.1	• Adiabatic reactor • Pressure drop: 0.6 bar
HYDRO	• Inlet operating T: 250 °C	Equation 3.2 and 3.3	• Adiabatic reactor • Pressure drop: 0.5 bar • Fractional conversion of components COS and HCN: 99.99%
LT-WGSR	• Inlet operating T: 200 °C • Max outlet operating T increase: 50 °C	Equation 2.1	• Adiabatic reactor • Pressure drop: 0.6 bar

Benzene and Ammonia phase diagrams

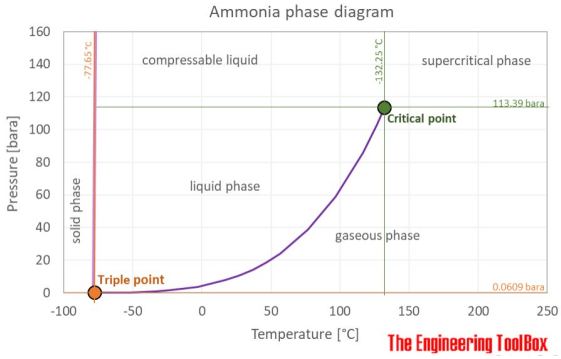

Figure H.1: Ammonia Phase diagram [111].

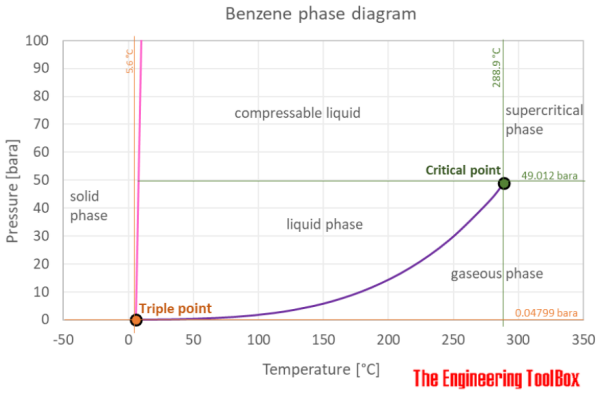

Figure H.2: Benzene phase diagram [112].

Water absorption column in Aspen Plus

The flowsheet scheme for the water absorption column in Aspen Plus is provided in Figure I.1.

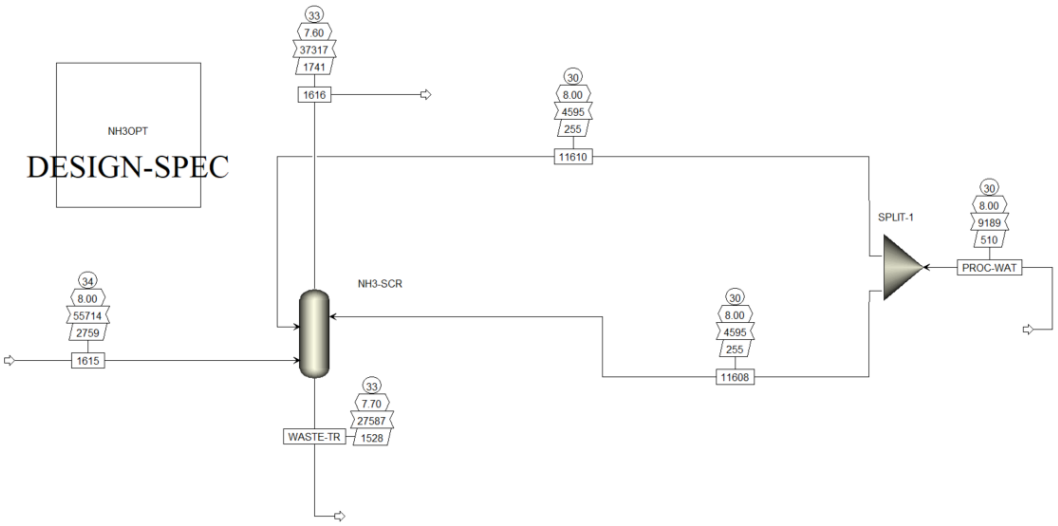

Figure I.1: Flowsheet scheme for the Water absorption column in Aspen Plus.

The summary of the water absorption columns conditions is provided in Table I.1.

Table I.1: Table summary of the Water absorption column.

Unit	Boundary Conditions	Assumptions
Water absorption column	• Gas inlet operating T: 35 °C • Process water inlet operating conditions: 30 °C, 8 bar	• Equilibrium column • Pressure drop: 0.4 bar • 2 separate fresh process water streams equally separated for the 2 column stages

J

Hydrogen Sulfide and Carbon Dioxide phase diagrams

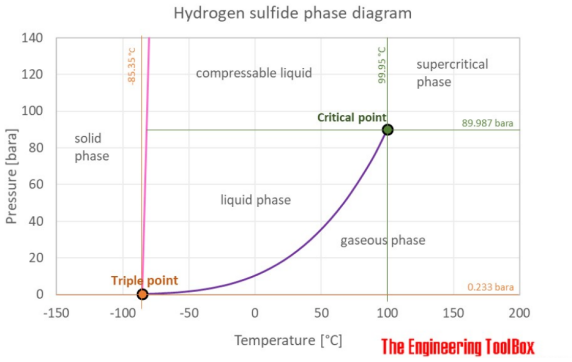

Figure J.1: Hydrogen Sulfide phase diagram [117].

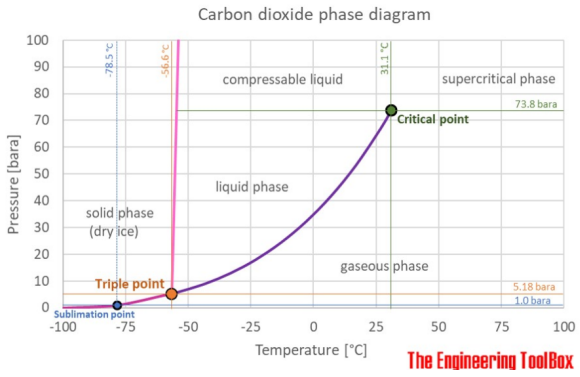

Figure J.2: Carbon Dioxide phase diagram [118].

K

Aqueous MDEA absorption and stripping columns in Aspen Plus

The complete process flow sheet simulated in Aspen Plus is given in Figure K.1.

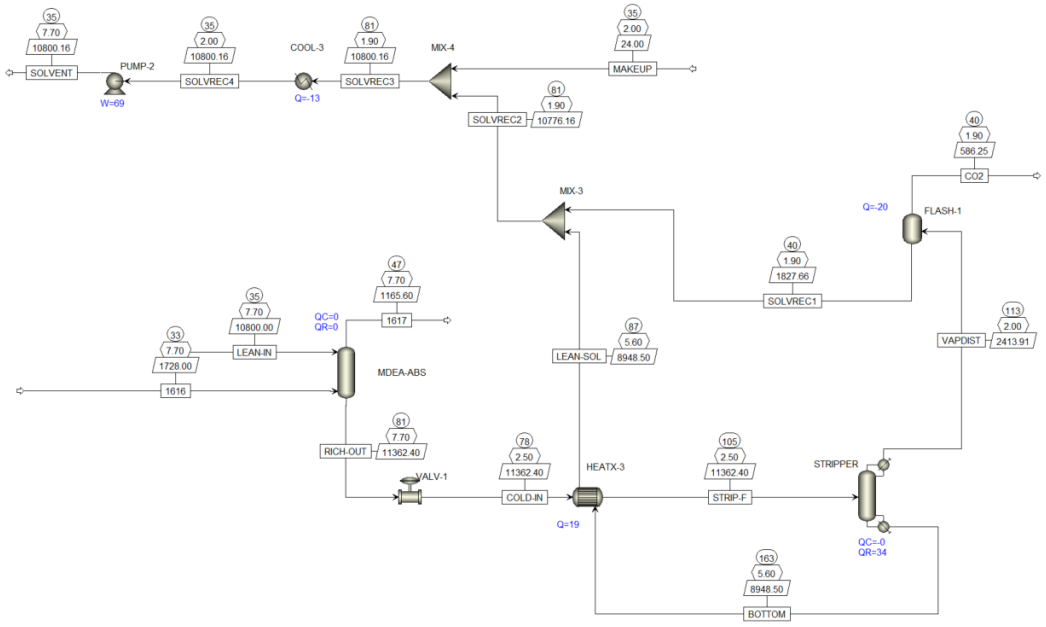

Figure K.1: Flowsheet scheme Aqueous MDEA absorption and stripping columns in Aspen Plus.

Pressure Swing Adsorption in Aspen Adsorption: Assumptions and Implementation

L.1. Assumptions and general equations

1. The gas phase is ideal.
2. One-dimensional discretization — Spatial derivatives are evaluated in axial (flow) direction only.
3. Upwind Differencing Scheme 1 (UDS1) is the preferred option due to:
   - Unconditional stability (it does not produce oscillations in the solution).
   - Decreased simulation time.
   - First-order equation accuracy

   Gives a large amount of so-called ”false” or numerical diffusion. (However, this problem decreases as the number of nodes is increased.)
4. Plug flow reactor model, in which no axial mixing occurs.
5. The system is fully mixed in the radial direction.

   As a fluid flows through a packed column, axial mixing tends to occur, reducing the efficiency of separation. Hence, it should be minimized in column design. However, if axial dispersion occurs, the model must account for its effects. In gases, three primary sources contribute to axial dispersion: wall effects, molecular diffusion or turbulent mixing effects.

   In general, the effects of molecular diffusion and turbulent mixing are additive and proportional to the second-order spatial concentration derivative. Consequently, they can be combined into a single effective dispersion coefficient, denoted as E_i. The dispersion term in the material balance is typically expressed as:

$$\frac{\partial}{\partial z}\left(\epsilon_i \frac{\partial C_k}{\partial z}\right) = -E_{zk}\frac{\partial C_k}{\partial z} \tag{L.1}$$

   Where: ϵ_i = Interparticle voidage E_{zk} = Axial dispersion coefficient of component k

   It is useful to calculate the Peclet number (Pe) using the dispersion coefficient (effective bulk diffusivity E_z), typical bed velocities (v_g), and bed height (H_b):

$$Pe = \frac{v_g H_b}{E_z} \tag{L.2}$$

   The Peclet number quantifies the degree of dispersion introduced into the system. It is dimensionless and is more convenient for this purpose than the dispersion coefficient. In the context of this study the Peclet number is assumed to be equal to infite since no axial dispersion occurs.

6. Convection-based material balance, which assumes zero dispersion. The overall mass balance in the solid phase for a multi-component gas phase is given by:

$$\varepsilon_B \cdot \frac{\delta C_j}{\delta t} + \frac{\delta (C_j v)}{\delta z} + \rho_{ads} \cdot \sum_{j=1}^{n} \frac{\delta q_j}{\delta t} = 0 \tag{L.3}$$

Where: $\varepsilon_B \cdot \frac{\delta C_j}{\delta t}$ represents the gas phase accumulation term, $\frac{\delta (C_j v)}{\delta z}$ is the convection term and $\rho_{ads} \cdot \sum_{j=1}^{n} \frac{\delta q_j}{\delta t}$ the rate of adsorption. Equation L.3 can only be solved incorporating the mass balance of the adsorption rate into an adsorbent pellet.

7. Linear Driving Force (LDF) to approximate the adsorption rate. The mass transfer driving force is expressed as a function of the solid phase loading, assuming a constant mass transfer coefficient.

Equation L.4 is repeated for all the species (indicated by the j subscript).

$$\frac{\delta q_j}{\delta t} = k_f (q_j^* - q_j) \tag{L.4}$$

In which, the information on the type of isotherm used (Extended Langmuir 3 model) is deconstructed in Equation L.5.

$$q_j^* = \frac{q_j^s b_j p_j}{1 + \sum_{j=1}^{n} b_j p_j} \tag{L.5}$$

$$q_j^s = (k_1 + k_2 T) \tag{L.6}$$

$$b_j = k_3 \exp\left(\frac{k_4}{T}\right) \tag{L.7}$$

8. Ergun equation for the momentum balance, which combines the description of pressure drops by the Karman-Kozeny equation for laminar flow and the Burke-Plummer equation for turbulent flow.

$$\frac{\delta P}{\delta z} = -\frac{150 \mu v (1 - \varepsilon_i)^2}{(D_p \phi)^2 \varepsilon_i^3} - \frac{1.75 (1 - \varepsilon_i) v^2 \rho}{\phi \varepsilon_i^3 D_p} \tag{L.8}$$

Where: ϕ is the sphericity factor, ε_i is the inter-particle voidage.

9. Isothermal energy balance. This option completely ignores the energy balance. The gas temperature and the solid temperature are held constant and equal.

L.2. Cycle scheduling for pressure swing adsorption system

Jain et al. [100] provide a guideline to conceptualize a PSA cycle. All the considerations have been adapted based on the process simulation environment. Nevertheless, a list of governing concepts and equations is listed for clarity, which reflects the information illustrated in Chapter 2.

Before running the multi-bed pressure swing adsorption system, a model based on single adsorption is build to assess:

- Best performing isotherm (Extended Langmuir 3 from Xiao et al. [80]).
- Isotherm validation (replicating the work of Xiao et al. [80]).
- Adsorption time determination for the level of pressure selected (150 s for an adsorption pressure of 15 bar) and CO_2 penetration in the Zeolite 5A layer verification.

Once this information are verified, a multi-bed pressure swing adsorption system is designed. The cycle is scheduled in Aspen Adsorption according to a fictitious two beds PSA configuration in the Unibed approach. The visual representation of the 8 steps for the Unibed approach is re-presented in Figure L.1 for clarity purposes.

The scheme presented in Figure 4.2 is used to treat the beds as black box in which mass of chemical

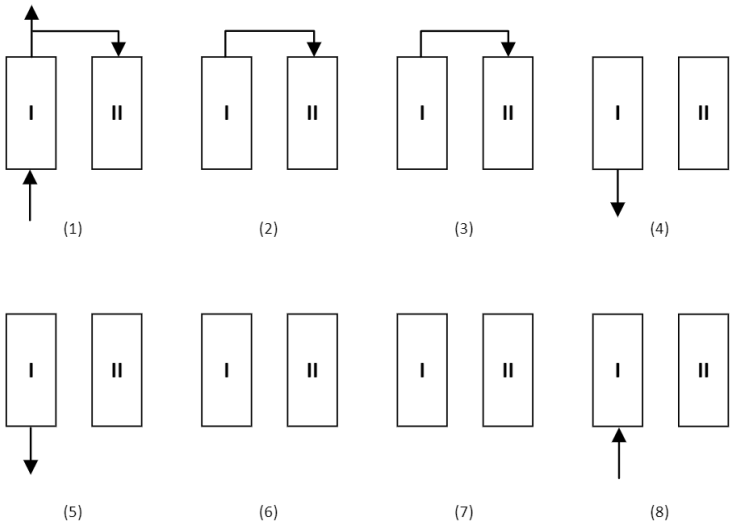

Figure L.1: Aspen Adsorption 8 steps PSA scheduling in Unibed configuration.

species can be stored. The following considerations are valid for a 4 beds pressure swing adsorption system working for a feed flowrate of 0.3 kmol/s comprising 75 mol% of H_2 and 15 mol% of impurities.

Step 1

Ideally, in a black box approach 0.225 kmol/s of H_2 will be pure raffinate ready to be sold, keeping 0.075 kmol/s of impurities retained in the bed. However, a stream of pure H_2 coming from the product line is sent to purge another bed. In this study the effect of purge-to-feed (P/F) ratio is parameterized with the value of 0.15. Figure L.2 provides the key insights in terms of flowrate for step 1 of the pressure swing adsorption system.

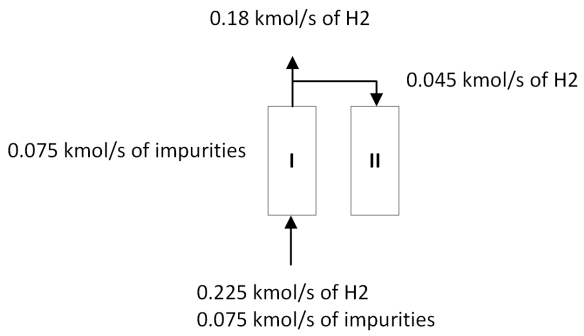

Figure L.2: Step 1 of the pressure swing adsorption system

The c_v is expressed for all the valves specification according to Equation L.9 reported below for completeness sake.

$$c_v = \frac{F}{p_{\text{in}} - p_{\text{out}}} \tag{L.9}$$

In the context of fixed flowrates,using this black box approach, the addition of the pressure difference is imperative to accurately determine the correct value of c_v as it can be seen in Table L.1.

Table L.1: Valve set up step 1.

Valve	$p_{\textbf{in}}$	$p_{\textbf{out}}$	c_v
VF	15	14.99	10
VP	15	14.5	0.36
VD	14.5	1.013	0.00325

The final remark for step 1 is that, during the adsorption step of 150 s a total amount of 11.25 kmol of impurities is ideally adsorbed.

Step 2

This step concerns a first stage of depressurization of bed I for 60 s. The same procedure can be applied, ideally depressurizing a total amount of 2.83 kmol of impurities.

Table L.2: Valve set up step 2.

Valve	$p_{\textbf{in}}$	$p_{\textbf{out}}$	c_v
VD	14.5	1.013	0.0035

Step 3

This step concerns a second stage of depressurization of bed I for 60 s until the level of equalized pressure between bed I and bed II is reached. The same procedure can be applied, ideally depressurizing a total amount of 6.75 kmol of impurities.

Table L.3: Valve set up step 3.

Valve	$p_{\textbf{in}}$	$p_{\textbf{out}}$	c_v
VD	12.5	5	0.015

Step 4

This step concerns a blow-down stage of depressurization of bed I counter-currently. The same procedure can be applied, ideally depressurizing a total amount of 0.48 kmol of impurities. A cycle variation is made from the considerations of Jain et al. [100] with regards to blow-down time. In the utilization of the Unibed approach, only 5 s were required to blowdown, corresponding to 0.033 ratio (compared with the adsorption time) instead of the 0.15 [100].

Table L.4: Valve set up step 4.

Valve	$p_{\textbf{in}}$	$p_{\textbf{out}}$	c_v
VW	7.5	1.5	0.0166

Step 5

This step concerns a purge stage of depressurization of bed I counter-currently. The same procedure can be applied, ideally depressurizing the remaining amount of 1.2 kmol of impurities. In this case it is noteworthy to say that the value of c_v was increased of 10 order of magnitude because the step time increase drastically from 5 to 150 s.

Table L.5: Valve set up step 5.

Valve	$p_{\textbf{in}}$	$p_{\textbf{out}}$	c_v
VW	1.5	1.013	0.5

Step 6

This step is replicated by Unibed and therefore is not necessary to specify anything except closing all the valves.

Step 7

This step is replicated by Unibed. However, differently from step 6, it is necessary to specify the initial pressure p_in of 13 bar before the start of the step.

Step 8

Finally, in step 8, the pressurization of bed I carried out by the feed is simulated. In this case the feed valve is opened partially, allowing the gas to flow in bed I considering a pressure difference of 0.01 bar.

M

Hydrogen specification for industrial usage

End use application	Industrial usage (mostly feedstock)							
Components	**Refinery[1]**	**Ammonia[2]**	**Methanol[3]**	**Steel production**	**Hydrogen bromide**	**Hydrogen peroxide**	**Gas turbines[4]**	**Fisher Tropsch**
Hydrogen H_2 (vol-%)	99,5	98,5 99,9	74	99,9	99,95	99,9	70	60
Total sulphur (ppb)		1	50			< 1000		< 100
Halides (ppb)		1	1				Low[5]	10
Oxygen (ppm)				ppm-level		< 10		
Carbon Monoxide (ppm)	10 – 50		20 vol-%		ppb-level	< 1		30 vol-%
Carbon Dioxide (ppm)	10 - 50					< 2		inert
Iron (ppb)			5					
Nickel (ppb)			5					
Hydrogen chloride (ppb)			2					
Water (ppm)						< 10		
Nitrogen (ppm)		reactant	0,5 vol-%			< 2000		50 ppb
Methane (ppm)	inert	inert	3 vol-%		ppb-level	< 10		inert
Argon / Helium (ppm)		inert				< 2000		inert

[1]) For crude oil desulphurisation, lower purity hydrogen (~98 vol-%) can be used

[2]) Hydrogen purity requirements differ per ammonia producer. While some producers allow for CO/CO_2 concentration up to 10.000 ppm (~ 1 vol-%), others have CO/CO2 fully removed and thus require higher purities.

[3]) Methanol can be directly made form syngas as CO/CO2 are reactants. Typical hydrogen concentrations in syngas (SMR+WGS) are ~70 vol-% or higher.

[4]) Gas turbines can be engineered using hydrogen concentrations down to 70 vol-% (the remainder being nitrogen) to lower combustion temperatures and therewith NOx emissions. Once the turbine has been designed for a certain concentration, the hydrogen purity (quality) needs to be within strict limits (typically a Wobbe-range of +/- 5%).

[5]) Low (as low as possible) typically means below 2%.

Figure M.1: General hydrogen specification for industrial usage [121].

N

Spotting differences for the best isotherm selection

The Extended Langmuir 1 isotherm model is provided below:

$$q_j^* = \frac{IP1_j p_j}{1 + \sum_{j=1}^{n} IP2_j p_j} \tag{N.1}$$

The Extended Langmuir 2 isotherm model is provided below:

$$q_j^* = \frac{IP1_j \exp\left(\frac{IP2_j}{T}\right) p_j}{1 + \sum_{j=1}^{n} IP3_j \exp\left(\frac{IP4_j}{T}\right) p_j} \tag{N.2}$$

The Extended Langmuir 3 isotherm model is provided below:

$$q_j^* = \frac{(IP1_j - IP2_j \cdot T) \cdot IP3_j \exp\left(\frac{IP4_j}{T}\right) p_j}{1 + \sum_{j=1}^{n} IP3_j \exp\left(\frac{IP4_j}{T}\right) p_j} \tag{N.3}$$

The Dual Site Langmuir isotherm model is provided below:

$$q_j^* = \frac{IP1_j \exp\left(\frac{IP2_j}{T}\right) p_j}{1 + \sum_{j=1}^{n} IP3_j \exp\left(\frac{IP4_j}{T}\right) p_j} + \frac{IP5_j \exp\left(\frac{IP6_j}{T}\right) p_j}{1 + \sum_{j=1}^{n} IP7_j \exp\left(\frac{IP8_j}{T}\right) p_j} \tag{N.4}$$

O

CAPEX calculations

O.1. Equipment list

Table O.1: Equipment list.

Unit code	Involved Equipment	Type of Equipment	Sizing base	Size	Unit
HT-WGSR	Reactor	Vessel	Flowrate	55.9	ton/h
			Volume	99.6	m^3
		Catalyst	Catalyst loading	101.6	m^3
HYDRO	Reactor	Vessel	Flowrate	55.9	ton/h
			Volume	93.1	m^3
		Catalyst	Catalyst loading	98.3	m^3
LT-WGSR	Reactor	Vessel	Flowrate	55.9	ton/h
			Volume	12.5	m^3
		Catalyst	Catalyst loading	12.75	m^3
HEX1	Heat Exchnager	Shell and Tube	Shell inlet pressure	12.6	bar
			Heat exchange area	31.07	m^2
			Duty	1471.3	kW
HEX2	Heat Exchnager	Shell and Tube	Shell inlet pressure	12.3	bar
			Heat exchange area	31.05	m^2
			Duty	2655.3	kW
HEX3	Heat Exchnager	Shell and Tube	Shell inlet pressure	2.5	bar
			Heat exchange area	983.57	m^2
			Duty	21787.3	kW

COOL-1	Cooler	Steam	Shell inlet pressure Heat exchange area Duty	8.0 31.5 2304.3	bar m^2 kW
COOL-2	Cooler	Water	Shell inlet pressure Heat exchange area Duty	2.1 422.36 15013.3	bar m^2 kW
COOL-3	Cooler	Water	Shell inlet pressure Heat exchange area Duty	1.0 637.2 14058.4	bar m^2 kW
COOL-4	Cooler	Water	Shell inlet pressure Heat exchange area Duty	1.0 18.7 119.5	bar m^2 kW
COOL-5	Cooler	Water	Shell inlet pressure Heat exchange area Duty	1.0 64 1067.8	bar m^2 kW
BIOD-W	Vessel	Vertical	Length Diameter Weight	11.25 2.5 10.06	m m ton
BIOD-STR	Vessel	Vertical	Length Diameter Weight	2.25 0.5 0.232	m m ton
MDEA-ABS	Vessel	Vertical	Length Diameter Weight	9 2 5.52	m m ton
MDEA-STR	Vessel	Vertical	Length Diameter Weight	4.95 1.1 1.11	m m ton

NH3-SCR	Vessel	Vertical	Flowrate	55.7	ton/h
COMP-1	Compressor	Centrifugal	Power	1067.4	kW
PSA	Vessel	Vertical	Length	3.75	m
			Diameter	2	m
			Weight	2.78	ton

O.2. Capital cost breakdown

The full calculations done for the capital cost estimation are discussed here. The equations and factors used are taken from Seider et al. [104], except for certain units, such as the HTW 2.0, WGS reactors, the hydrolysis reactor and the water absorption column. Their cost is estimated using data from typical industrial standards. Equations and further information about specific unit types are listed below.

Additionally, the equations listed below calculate the costs based on 2013. To convert these to 2022 pricing, the Chemical Engineering Plant Cost Index (CEPCI) is used. The CEPCI starts with a value of 100 for 1957-1959 and is updated monthly to accommodate changes in price and technology. The CEPCI for 2013 is 567, while the value for June 2022 is 832.6 [105].

Heat Exchanger and cooler

The purchase cost of a heat exchanger is expressed below:

$$CP_{\text{hex}} = F_P \cdot F_M \cdot F_L \cdot CB_{\text{hex}} \tag{O.1}$$

Where CP_{hex} is the purchase cost of the heat exchanger. F_P is the pressure factor, which is 1 below 100 psi and calculated below, with P the pressure in psi.

$$F_P = 0.9803 + 0.018\left(\frac{P}{100}\right) + 0.0017\left(\frac{P}{100}\right)^2 \tag{O.2}$$

F_M is the material factor, and is calculated below with a as 1.70 and b as 0.07 for low alloy steel shell and tube construction. F_L is the length factor, which is 1 for 20 ft tube length and 1.05 for 16 ft tube length.

$$F_M = a + \left(\frac{A}{100}\right)^b \tag{O.3}$$

CB_{hex} is calculated, with A the area in ft^2.

$$CB_{\text{hex}} = \exp\left[11.4185 - 0.9228\ln(A) + 0.09861\ln^2(A)\right] \tag{O.4}$$

Columns

The purchase cost of the absorption and stripping columns, as well as the adsorption bed for PSA, is approximated for vertical vessels constructed from stainless steel and equipped with all the necessary platforms, ladders, a nominal number of nozzles, and manholes. The purchase cost can be calculated as follows:

$$CP_{\text{flash}} = F_M \cdot CV + CPL \tag{O.5}$$

Where CP_{flash} is the purchase cost of the flash drum, F_M is 1.7 for stainless steel construction. CV is calculated below, where W is the weight in pounds of the shell and the two heads of a vertical vessel.

$$CV = \exp\left[7.1390 + 0.18255\ln(W) + 0.02297\ln^2(W)\right] \tag{O.6}$$

For vertical vessels with the boundaries $3 < Di < 21$ ft and $12 < L < 40$ ft, the cost component CPL is determined using the equation:

$$CPL = 410 \cdot (Di)^{0.73960} \cdot (L)^{0.70684} \tag{O.7}$$

Centrifugal Compressor

The purchase cost of a centrifugal compressor is expressed below:

$$CP_{\text{comp}} = F_D \cdot F_M \cdot CB_{\text{comp}} \tag{O.8}$$

Where CP_{comp} is the purchase cost of the compressor, F_D is 1 for an electric motor drive, and F_M is 2.5 for stainless steel construction. CB_{comp} is calculated below, with PC in horsepower.

$$CB_{\text{comp}} = \exp\left[9.1553 + 0.63 \ln(PC)\right] \tag{O.9}$$

Other Units

The cost of the High Temperature Winkler (HTW)-unit, is kept the same as in typical industrial plants. The cost of the remaining units, such as the WGS reactors, the hydrolysis reactor and the water absorption column is estimated using data from standard plants.

The cost of the WGSR, hydrolysis reactors and the water absorption column are calculated using , where the cost of the typical industrial units is scaled using the mass flow rates of the model versus the reference.

$$CP = \text{Reference cost} \cdot \left(\frac{\text{Flow rate model}}{\text{Flow rate reference}}\right)^{0.6} \tag{O.10}$$

With the results of these equations, the total permanent investment $(CTPI)$ and total capital investment $(CTCI)$ can be calculated. The factor 1.05 in both equations takes account for the delivery of the equipment. The Lang factors, f_{LTPI} and f_{LTCI}, are used to approximate the TPI and TCI. For a solid fluid processing plant, these factors are 4.28 and 5.03, respectively. The total capital investment $(CTCI)$ also includes the cost of land, which is taken as 2% of total permanent investment $(CTPI)$. Furthermore, the total purchase cost is first multiplied by the Investment Site Factor ($FISF$) of Western Europe as the calculations from Seider et al. [104] are based on the U.S. Gulf Coast. The $FISF$ for Western Europe is 1.20. It takes into account the difference in 'the availability of labor, the efficiency of the workforce, local rules and customs, union status, and other items'.

$$CTPI = 1.05 f_{LTPI} FISF \cdot \sum_i \left(\frac{I_{2022}}{I_{\text{base}}}\right) CP_i \tag{O.11}$$

$$CTCI = 1.05 f_{LTCI} FISF \cdot \sum_i \left(\frac{I_{2022}}{I_{\text{base}}}\right) CP_i + C_{\text{land}} \tag{O.12}$$

Table O.2 illustrates the equipment cost of the main units for the H_2 plant.

Table O.2: Equipment cost in Mln of USD.

Equipment name	CP (Mln USD)
HTW 2.0	13.57
Reactor	1.11
Cooler	0.60
Heat Exchanger	0.47
Compressor	3.38
Columns	1.03
Pumps	0.02
PSA	0.52
CHP	2.44

The capital expenditure cost breakdown is presented in Table O.3.

Table O.3: CAPEX breakdown in Mln of USD.

Cost Factor	**Cost Factor Value**	**Cost name**	**Value (Mln USD)**
		CP	23.14
Investment site (Western Europe)	1.2	$FISF$	27.76
Delivery on plant	1.05	$CTPI$ not including working capital	124.8
Lang Factor	4.28		
Land Acquisition	0.02		2.5
Delivery on plant	1.05	$CTCI$	149.15
Lang Factor	5.03		

P

OPEX calculations

The complete operational expenditure cost breakdown is given in Table P.1. The main assumptions are still listed below:

- Most of the equations and factors used for the annual cost are taken from Seider et al. [104].
- Certain costs, such as the price of catalysts and raw materials, are calculated using data based on certain vendor specifications.
- The negative numbers stands for being rewarded (e.g. by collecting the RDF or selling electricity and low pressure steam).
- 330 days of operation per year are assumed.
- Lifetime of the plant: 20 years.
- The quantity of MDEA is assumed to be as a once in the lifetime of the plant purchase given the stripping of MDEA efficiency of 99.9 %. Therefore its cost must be divided for the 20 years lifetime of the plant.
- Total depreciable capital (TDC) is equal to TPI.
- 20 operators per shift are assumed to be necessary. The direct wages and benefits (DW&B) is calculated using equation (P.1).

$$\text{DW\&B} = \frac{20 \text{ operators}}{\text{shift}} \times \frac{1}{5 \text{ shifts}} \times \frac{2080 \text{ h}}{\text{operator} \cdot y} \times \$48.89 \text{ h} \tag{P.1}$$

Table P.1: Operational expenditure cost breakdown

Category	Unit	Annual Quantity	USD/Unit	USD/Year
Variable Cost				
Raw materials				
RDF	t	130,680	-51.02	-6.67
Waste wood	t	43,560	61.22	2.67
Total raw material cost				-4.00
Chemicals Consumed				
Bio-Diesel [128]	l	558,008	1.70	0.95
MDEA [129]	kg	952,228	3.60	3.43
Total chemical cost				4.38
Catalyst Consumed				
HT-WGSR	m^3	102	397,000.87	0.40
HYDRO	m^3	98	466,491.01	0.47
LT-WGSR	m^3	13	99,690.58	0.10

Total catalyst cost				0.96
Adsorbent Consumed				
Active Carbon [67]	t	11.4	400.00	0.00
Zeolite 5A [67]	t	0.9	2,200.00	0.00
Total Adsorbent cost				0.01
Utilities				
Electricity [130]	kWh	-34,442,100	0.07	-2.41
Cooling water	t	54,675,084	0.03	1.80
LP steam [131]	t	-76,095	14.25	-1.08
MP steam	t	170,069	17.00	2.89
Superheated MP	t	54,498	17.60	0.96
HP steam	t	239,184	17.60	4.21
Instrument air [132]	Nm^3	3,423,816	0.01	0.03
MP oxygen [133]	Nm^3	50,688,000	0.15	7.65
LP nitrogen [132]	Nm^3	8,125,920	0.08	0.61
Boiler feedwater	t	538,534	0.56	0.30
Waste water treatment plant	kg	995,911	0.33	0.33
Total utilities cost				15.28
Operations				
Direct wages and benefits (DW&B)			40/operator/hr	10.17
Direct salaries and benefits			15% of DW&B	1.53
Operating supplies and benefits			6% of DW&B	0.61
Total operations cost				12.30
Maintenance				
Wages and benefits (MW&B)			3.5% of C_TDC	4.37
Salaries and benefits			25% of MW&B	1.09
Materials and services			100% of MW&B	4.37
Maintenance overhead			5% of MW&B	0.22
Total maintenance cost				10.05
Total Variable Cost				
38.98				
Fixed Cost				
Operating overhead				
General plant overhead			7.1% of M&O-SW&B	1.22
Mechanical department services			2.4% of M&O-SW&B	0.41
Property taxes and insurance			2% of C_TDC	2.50
Total operating overhead				4.13
Depreciation				
Direct plant			8% of $(C\_TDC - 1.18C\_alloc)$	9.98
Total depreciation				9.98
Total Fixed Cost				
14.11				
Cost of Manufacture (COM)				
53.09				
General Expenses				
Selling expense			3% of sales	1.59

Direct research			4.8% of sales	2.55
Allocated research			0.5% of sales	0.27
Administrative expense			2.0% of sales	1.06
Management incentive compensation			1.25% of sales	0.66
Total General Expenses				
6.13				
Total Production Cost				
59.22				

The additional informating with regards to the OPEX cost breakdown is provided below:

Table P.2: Extra cost for Operational expenditure calculation.

$CTPI$	Total permanent investment
$CTCI$	Total capital investment
C_{alloc}	Allocated costs for utility plants and related facilities
Hours of operation per year	7920
days of operation per year	330
Plant operation factor	0.904
Labor	
Number operators/shift	20
Number shifts	5
hours/operator/year	2080
Salary (USD/h)	48.89
M and O-SWB	17.15388

To compute the OPEX, the following data with regards to utilities consumption and production is necessary. It is assumed in one of the coolers (COOL-1), low pressure steam is produced internally and recirculated. Furthermore, fresh process water at the same operating conditions is assumed to circulate in:

- Remaining coolers.
- Water absorption column for NH_3 removal.
- Make up stream of the MDEA absorption column.
- Flash separator cooler.

Moreover, the waste water to be treated in the waste water treatment plant, is calculated on the quantity to be cleaned from the total flow coming from the water absorption column. Finally, the amount of boiler fee water is bought aimed at the production of low pressure steam, that will be used internally and then sold to the market.

Table P.3: Utilities.

Utility name	Unit	HTW	HT-WGSR	PUMPS	COOLERS	BIOD-W	BIOD-STR	NH3-ABS	MDEA-ABS	MDEA-STRIP	COMPR	PSA	CHP ENGINE	Total
Electricity	kW	797		71.32							1067.39		-6284.45	-4348.75
Cooling water	t/h	102			2708.74			9.218	0.414	4083.04				6903.42
LP steam	t/h				-3.488		38.18						-44.30	-9.61
MP steam	t/h	6.881	14.592											21.47
Superheated MP	t/h	6.881												6.88
HP steam	t/h	-16.9								47.1				30.20
Instrument air	Nm^3/h	432.3												432.30
MP oxygen	Nm^3/h	6400												6400
LP nitrogen	Nm^3/h	1026												1026
MP CO2	t/h	4.141												4.14
HP CO2	t/h	1.502												1.50
Boiler feedwater	t/h	20.2			3.488								44.30	68.00
Waste water treatment plant	kg/h							125.74						125.75
Caustic (20%)	kg/h	75												75.00
Bio-Diesel	l/h					558008								558008
MDEA	t/h								0.119					0.12